Preliminary Structural Design Optimization of an Aircraft Wing-Box

Sridhar Chintapalli

A thesis

in

The Department

of

Mechanical and Industrial Engineering

Presented in Partial Fulfillment of the Requirements
for the Degree of Master of Applied Science (Mechanical Engineering) at
Concordia University
Montreal, Quebec, Canada

August 2006

Your file Votre référence
ISBN: 978-0-494-20758-1
Our file Notre référence
ISBN: 978-0-494-20758-1

ABSTRACT

Preliminary Structural Design Optimization of an Aircraft Wing-Box

Sridhar Chintapalli

Structural weight has always been important in aircraft manufacturing industry. Considering that a large number of candidate material and geometric shapes are available early in the design cycle, preliminary design optimization of skin-stringer panels used to build an aircraft wing is required to obtain the best preliminary structure before the final design phase. The design of skin-stringer panels forms an important and major portion of the wing-box design. The lift generated by the wings opposes the weight of the aircraft, and thus generates bending. Depending on their location, stiffened panels that make up the wings are therefore mainly loaded in compression and tension. Upper skin-stringer panels are typically subjected to compressive load while the lower panels are subjected to tensile load. The ability to resist the compressive load is assessed through a stability study to compute the critical buckling load of the stiffened panel while the ability to withstand the tensile load is evaluated by the Damage Tolerance Analysis. Optimization routines have been developed for the design of upper and lower wing panels. The main objective here is to design a stable wing-box structure more rapidly and automatically in the most economical manner having adequate strength and stability. These optimization routines are tested on a wing section defined at a specific span wise location of a DLR-F6 aircraft. Repeating the design process at different stations along the wing span completes the preliminary design of aircraft wing-box.

ACKNOWLEDGEMENTS

I sincerely thank my academic supervisor Prof. Dr. Ramin Sedaghati for trusting my capabilities and providing me the opportunity to work in this research project. I thank him for extending his continuous intellectual guidance, encouragement and financial support during the course of this work. It has been a wonderful learning experience throughout, during this academic journey.

I am grateful to Dr. Mohammed Abdo of Bombardier Aerospace for providing good insight into the project initially. I sincerely thank him for taking out time from his busy schedules and providing valuable inputs in our regular meetings.

I wish to thank my colleagues who worked with me in this project and all my friends for their discussions, suggestions and encouragement in all times through out the research work.

This work would have been impossible without the love and encouragement I have received from my family members. I am indebted for all their sacrifices to see me successful in my academic life.

TABLE OF CONTENTS

LIST OF FIGURES

LIST OF TABLES

NOMENCLATURE

t_s - Thickness of the skin

b_s - Panel width or stringer pitch

b_e -Effective width of the skin

$b_a, t_a, b_w, t_w, b_f, t_f$ - Dimensions of the stringer

A_{sk} - Area of skin

A_{st} - Area of stringer

$A = A_{sk} + A_{st}$ - Area of panel

$SR = \frac{A_{st}}{A_{sk}}$ - Stiffening ratio

$BR = \frac{b_s}{b_e}$ - Width ratio

L- Length of the panel

E- Elastic modulus

ν - Poisson's ratio

σ_{cy} - Compression yield stress

K_I - Mode-I stress intensity

K_{IC} - Fracture Toughness

σ_{ij} - Stress tensor

ε_{ij} - Strain tensor

δ_{ij} - Kronecker delta

u_i - Displacements

t_i -tractions

U_{ij}, T_{ij} - Fundamental solutions

a- Half crack length

ΔK_e - Effective stress intensity

C_p, m_p - Paris's constants

N_{if} - Fatigue life

$C_L = \frac{L}{q_\infty S}$ - Lift coefficient

$C_D = \frac{D}{q_\infty S}$ - Drag coefficient

$C_M = \frac{M}{q_\infty S c}$ - Pitching moment coefficient

Mc- Mach number

ρ - Density of air

q_∞ - Free stream dynamic pressure

CHAPTER 1
INTRODUCTION

1.1 INTRODUCTION

Structural and Multi-disciplinary Optimizations have been gaining more attention in recent years for their contributions in the design enhancement, especially in the early stages of product development. Structural weight has always been important in aircraft manufacturing industry. When a modern full-loaded subsonic aircraft takes off, only 20% of its total weight is payload. Of the remaining 80%, roughly half is aircraft empty weight and the other half is fuel weight. Hence, any saving in structural weight can lead to a corresponding increase in payload. Alternately, for a given payload, saving in aircraft weight means reduced fuel requirements. Therefore, it is not surprising that the aircraft manufacturers are prepared to invest heavily in weight reduction. Hence, the main aim of an aircraft design engineer is to design a stable wing structure in the most economical manner having adequate strength and stability [1-10].

1.2 GENERAL LAYOUT OF WING STRUCTURE

A real commercial aircraft wing contains thousands of structural components. Creation of a detailed wing model by simultaneously incorporating all the wing features is virtually impossible. Thus, engineers rely on simplified models that provide a fairly accurate approximation of the real wing structural behaviour. Moreover, it is rare to find a design procedure that starts off with a detailed approach. Most commonly, the design is a multi-step process where the initial steps contemplate simplified configurations and each step inherits properties from the previous ones. Therefore, the importance of

obtaining initial designs is to guarantee that its best features will pass on to subsequent steps. Figure 1-1 shows the general layout of an aircraft wing structure showing its important components.

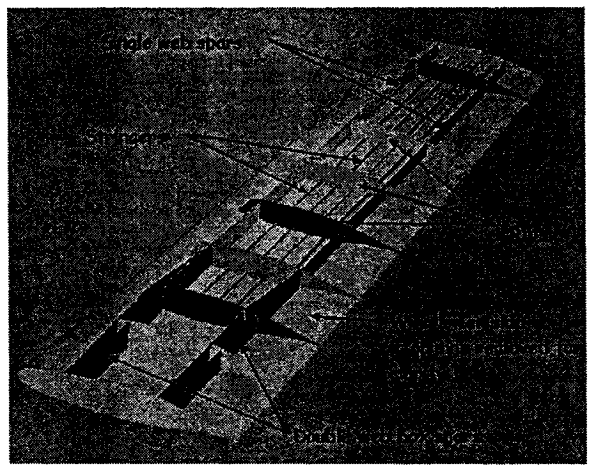

Figure 1-1: General layout of a wing structure [5]

Aircraft wing consists of a collection of basic structural elements like, the stringers running along the wing span, ribs positioned at different stations along the spanwise direction, front and rear spars and upper and lower wing skins covering these internal components. Each of these components act like a beam and a torsion member as a whole. For illustrative purpose, consider a box beam as shown in Figure 1-2.

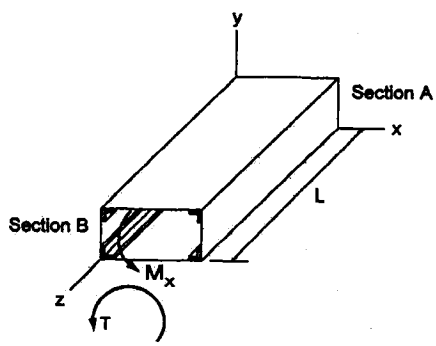

Figure 1-2: Box beam with applied loads [5]

The box beam consists of stringers (axial members) that are located at the maximum allowable distance from the neutral axis to achieve the most bending capability, and the

thin skin (shear panel), which encloses a large area to provide a large torque capability. This design would be fine if the load is directly applied in the form of global torque, T and bending moment, M_x. In reality, aircraft loads are in the form of air pressure (or suction) on the skin, concentrated loads from the landing gear, power plants, passenger seats, etc. These loads are to be collected locally and transferred to the major load carrying members. It should be done with proper care, otherwise these loads may produce excessive local deflections that are not permissible from aerodynamic considerations [5].

Using the box beam in Figure 1-2 as an example, we assume that a distributed air pressure is applied on the top and bottom surfaces of the beam. The skin (shear panel) is thin and has little bending stiffness to resist the air pressure. To avoid incurring large deflections in the skin, longitudinal stringers can be added as shown in Figure 1-3 to pick up the air loads. Figure 1-3 shows all the important elements that constitute the wing-box in cross-sectional view.

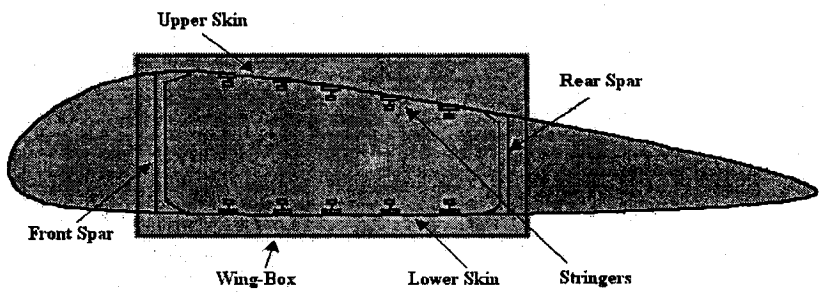

Figure 1-3: Cross-section showing wing-box elements [6]

The stiffeners are usually slender axial members with a moderate amount of bending stiffness. Therefore, the transverse loads picked up by the stiffeners must be transferred quickly to more rigid ribs or frames at Sections A and B shown in Figure 1-2 to avoid excessive deflections. The ribs collect all transverse loads from the stiffeners and transfer them to the two wide-flange beams (spars) that are designed to take transverse shear

loads. The local-to-global load transfer is thus complete. It should be noted that besides serving as a local load distributor, the stiffeners also contribute to the total bending capability of the box beam.

The main function of the wing is to pick up the air loads and transmit them to the fuselage. The wing cross-section takes the shape of an airfoil, which is designed based on aerodynamic considerations. The wing as a whole performs the combined function of a beam and a torsion member. It consists of axial members in stringers, bending members in spars and shear panels in the cover skin and webs of spars. The spar is a heavy beam running spanwise to take transverse shear loads and spanwise bending. It is usually composed of a thin shear panel (the web) with a cap or flange at the top and bottom to take bending. A typical spar construction is depicted in Figure 1-4.

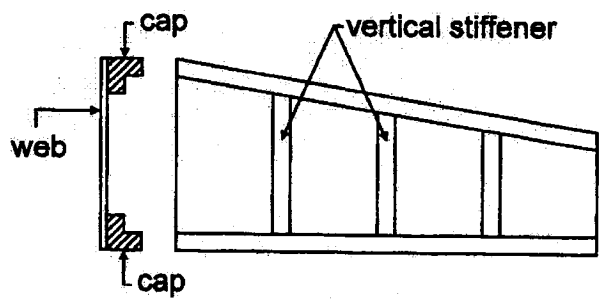

Figure 1-4: Typical spar construction [5]

Wing ribs are planar structures capable of carrying in-plane loads and are placed along the wing span. Besides serving as load redistributors, ribs also hold the skin-stringer to the desired contour shape. Ribs reduce the effective buckling length of the stringers (or the skin-stringer system) and thus increase their compressive load capability. Figure 1-5 shows the typical rib construction. It is noted that the rib is supported by spanwise spars. The cover skin of the wing together with the spar webs forms an efficient

torsion member. For subsonic airplanes, the skin can be assumed to make no contribution to bending of the wing-box. The total bending moment is taken up by spars and stringers.

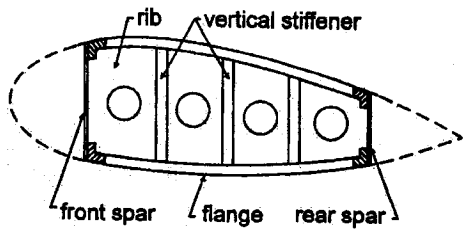

Figure 1-5: Typical rib construction [5]

Figure 1-6 presents two typical wing cross-sections for subsonic aircraft. Figure 1-6(a) consists only of spars (the concentrated flange type) to take bending. Figure 1-6(b) (the distributed flange type) uses both spars and stringers to take bending. To withstand high surface air loads and to provide additional bending capability to the wing box structure, thicker skins are often necessary. In addition, to increase structural efficiency, stiffeners can be manufactured (either by forging or machining) as integral parts of the skin [1-6].

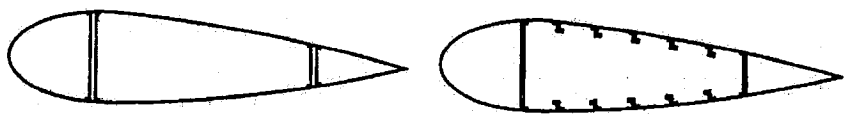

(a) (b)

Figure 1-6: Typical wing cross-sections for subsonic aircrafts [5]

1.3 STATE OF THE ART

The complexity of the structural configuration of an aircraft combined with a wide range of loading and boundary conditions requires a multilevel optimization approach. Because of its size and complexity, there is a clear need for advanced tools integrating and accelerating the design process. Multi-disciplinary Design Optimization (MDO) provides an efficient way to integrate all disciplines and determine a feasible

minimum weight design. Figure 1-7 shows the organization of the complete MDO process for designing any commercial aircraft. Within the last 20 years, several *in-house* MDO programs have been developed by aircraft industries [7-10].

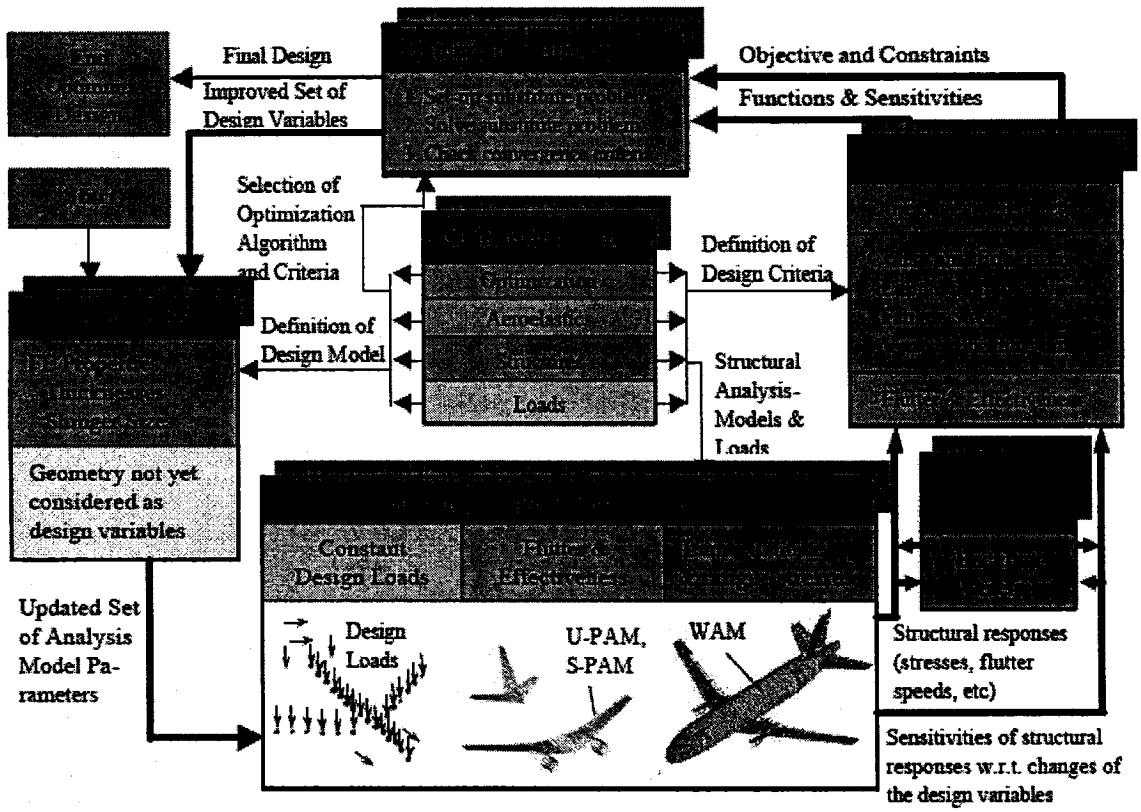

Figure 1-7: Design Process automated by Multi-Disciplinary Design Optimization Techniques [7]

The economic performance of an aircraft depends very much on its overall weight. It is important to minimize structural weight, in order to reduce fuel consumption and operating costs every time the aircraft flies. Modern aircraft design therefore utilises high performance materials with high strength to weight ratios. This when combined with efficient analysis and optimization tools, can lead to a significant increase in the strength and reliability, while reducing the structural weight of the components. Optimization of aerospace structures, such as fuselage sections and aircraft wings, however represents a

very complex task with literally hundreds of design variables. It is therefore not surprising that, despite the dramatic increase in computational power over the past twenty years, optimization is still best carried out as a multilevel process.

1.3.1 Wing-Box Design

Figure 1-8 shows the wing panels, the spars and internal ribs of the wing-box. A panel consists of a skin, stiffened by a stringer in longitudinal direction. The number of stringers decreases from inboard to outboard due to wing taper. Ribs are connected both to spars and panels. The panels and spars carry global bending and torsional loads, while the primary function of ribs is to stabilize the whole structure and transfer the local air load into the wing-box. The most important structural sizes of the wing-box comprise the skin thickness and the stringer height and thickness. For the purpose of applying buckling constraints, the upper surface of the wing is subdivided into so called wing panels. Each wing panel (stiffened panel or skin-stringer panel) is the area between two adjacent span wise ribs and middle distance between two chord wise adjacent stringers.

The mathematical objective of the optimization process is to find a minimum feasible weight for certain criteria. All relevant wing-box sizing criteria comprising limit, ultimate and fatigue stresses, buckling criteria, manufacturing criteria are applied in the form of constraints. Fatigue stress constraints are applied to all fatigue sensitive areas of the wing-box. These areas include the lower skin-stringer panels, major wing-box joints (inner and outer wing joint, lower front and rear panel joints), front spar web at the pylon attachment and rear spar web at the landing gear attachment.

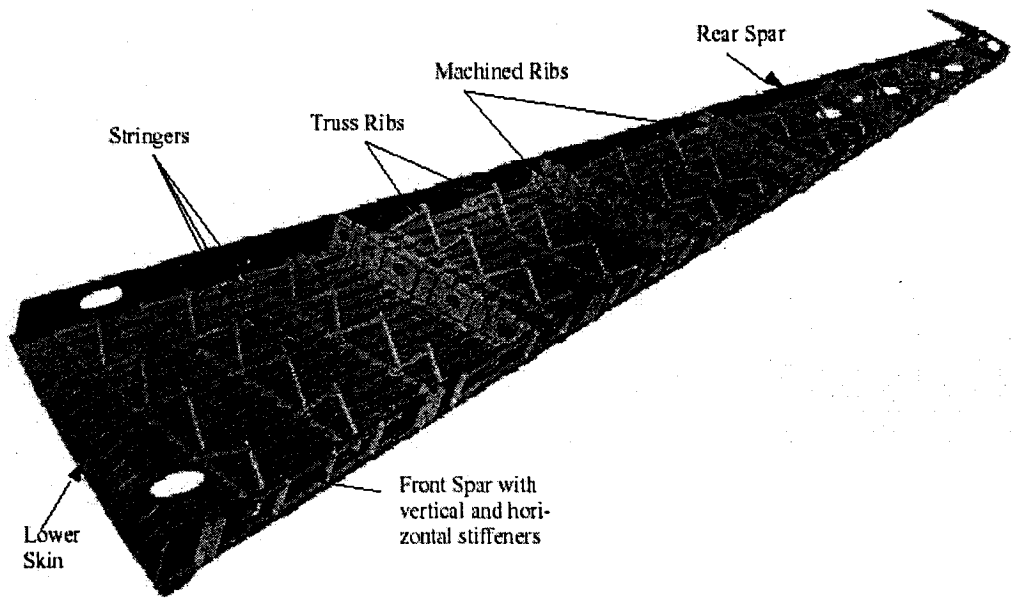

Figure 1-8: Wing-box showing internal parts (top skin removed for better view) [7]

1.3.2 Historical Development

The design of wing skin-stringer panels forms an important and major portion of the wing-box design. Depending on their location, stiffened panels that make up the wings are therefore mainly loaded in compression and tension. Upper skin-stringer panels are subjected to compressive load while the lower panels are subjected to tensile load. The ability to resist the compressive load is assessed through a stability study to compute the critical buckling load of the stiffened panel while the ability to withstand the tensile loading is evaluated mainly by the Damage Tolerance Analysis.

Buckling criteria governs the design of almost half of the structure of most commercial aircrafts. Automating this design process has been an area of widening research over the last 20 years. The initial stages of research to design the compressive structures were mostly dealt in NACA reports [11-12]. Butler and Williams [13], Butler, Tyler and Cao [14] developed a program called VICONOPT which is used to find the optimum dimensions of a range of blade-stiffened panels of composite or honeycomb

sandwich construction and a metal T-stiffened panel. VICONOPT (VICON with OPTimization) combines the analysis capability of VIPASA and VICON with a newly developed and efficient design technique to produce designs satisfying buckling and material strength constraints. Bushnell [15] developed a program called PANDA2 for minimum weight design of stiffened composite panels for locally buckled panels. Later, a software interface to design these structures was started by Butler [16,17]. He tailored a design procedure for obtaining the optimum dimensions for prismatic assemblies of laminated, composite plates which occur in advanced aerospace construction.

Veen [18,19] at Pechiney Aerospace developed a design tool called *Panel.* This tool acts as a large macro, which launches the meshing and analysis of a user defined stiffened panel configuration on a commercial finite element package of proven reliability. The development of conceptual design methodologies to integrate with MDO process was developed by Bombardier Aerospace. Abdo *et. al.* [20] developed a conceptual design methodology to design a skin-stringer compression panel. However, the developed design methodology was more an *ad hoc* optimization than a formal design optimization procedure.

Stiffened panels as explained in the previous sections are metal sheets reinforced by stringers, which can be bonded to the sheet by means of adhesive material or connected to it by means of rivets or machined as an integral part of the panel. Lower wing panels are usually designed for damage tolerance. A structural component is damage tolerant if it can sustain cracks safely until it is repaired or its economic service life has expired. Therefore, damage tolerance analysis provides information about the effect of cracks on the strength of the structure. For all the high strength materials used in

aerospace industry, damage tolerance analysis can be performed using Linear Elastic Fracture Mechanics theory (LEFM), in which case, the Stress Intensity Factor (SIF) plays a fundamental role. During the last four decades, a great deal of research has been dedicated to the calculation of SIF in cracked stiffened panels [24,25].

Finite Element Method (FEM) has been extensively used for the solution of crack problems in fracture mechanics. In the recent past, Boundary Element Method (BEM) has emerged as a powerful numerical technique for solving crack problems. Its most attractive feature is that the high stress gradients near the crack tip can be modelled more efficiently in comparison with FEM. Moreover, it has been shown that BEM produces more accurate Stress Intensity Factors than FEM [25-28].

Dowrick *et. al.* [29], Dowrick [30], and Utukuri and Cartwright [34] investigated analytically the effect of patch shape, attachment flexibility and patch stiffness on the stress intensity factor of a crack in a thin sheet. Young *et. al.* [31] and Young [32] used BEM combined with the method of compatible deformations to obtain stress intensity factor for a cracked sheet reinforced with a repair patch.

Dowrick, Cartwright and Rooke [33], Young, Rooke and Cartwright [35] used BEM to solve problems involving continuously and discretely attached stiffeners, respectively. In their work, the method of compatible deformations was used to combine the boundary integral displacement equations with stiffener displacement equation. The presence of a straight crack was implicitly considered, using special Crack Green's functions derived by Erdogan [36]. This last feature, although avoiding the need for modelling the crack geometry, restricts their application to problems involving a straight crack [28].

Salgado and Aliabadi [37] presented a formulation based on the dual boundary element method and the dual reciprocity method for the analysis of thin cracked metal sheets to which thin metal patches and stiffeners are adhesively bonded. The stress intensity factor is evaluated using the crack-tip opening displacement method after finding the solution for the system of equations formulated.

Dirgantara and Aliabadi [38] presented an extension of the dual boundary element method to analyse the crack growth in plates loaded in combined bending and tension. Stress intensity factors are computed using the *J*-integral technique. Crack growth processes are simulated with an incremental crack extension analysis based on the maximum principal stress criterion. Crack growth incremental analysis requires, regardless of the numerical method being used, remeshing at the end of each iteration. Except for simple cases, where the crack paths are known in advance, remeshing can be quite cumbersome.

1.4 MOTIVATION AND SCOPE OF THE PRESENT WORK

The MOSAIC (Multidisciplinary Optimization Standardization Approach for Integration and Configurability) project consists of development of multi-disciplinary design optimization (MDO) environment. This project is sponsored by Bombardier Aerospace through Consortium for Research and Innovation in Aerospace in Quebec (CRIAQ) to promote and perform collaborative pre-competitive industry research projects primarily at universities. The present research work is a part of the optimization module defined in MOSAIC project.

The loads coming from different flight conditions are converted into bending moment and shear force distributions. These quantities vary from wing root to tip. These

are used to size different components of an aircraft wing, like skin thickness, stringer spacing and dimensions, spars, web caps, ribs etc. The main objective of the present work is to develop efficient and accurate design optimization methodologies to design both upper and lower skin-stringer panels.

From the previous discussion, one can find pioneering applications in aerospace industry where lightweight structural components are required for either cost reductions or to increase payload. These optimizations are implemented in the early stages of MDO process to obtain robust and optimum aircraft designs.

1.5 ORGANIZATION OF THESIS

Chapter 1 explains the importance of structural optimization in designing aircraft structures. The advantages and necessity of Multi-Disciplinary Optimization in aircraft design is studied. The historical development in the design of skin-stringer panels to design upper and lower wing panels is also studied.

Chapter 2 presents an optimization routine to obtain the optimum dimensions for skin-stringer compression panels with minimum mass under six constraints namely, crippling stress, column buckling, up-bending at center span (compression in skin), down bending at supports (compression in stringer outstanding flange), inter-rivet buckling and beam column eccentricity. Results showed good agreement with existing skin-stringer panels taken from different aircrafts and also with the results of the conceptual design methodology developed by Bombardier Aerospace.

Chapter 3 explains a methodology to design lower skin-stringer panels under tensile loading using Damage Tolerance Analysis. Application of the Boundary Element Method during this analysis is explained in detail. The objective function (minimum mass

of a panel) and the design variables (thickness of skin and stringer pitch or panel width) remain same as used for designing compression panels. Optimization is performed for different skin-stringer panels and the results have been presented.

Chapter 4 presents the application of optimization process formulated in previous chapters on a test wing section of DLR-F6 aircraft. This chapter explains the procedure to generate the design curves from known values of aerodynamic coefficients. These coefficients can be obtained from either wind tunnel tests or from a complete CFD solution. The number of stringers required to support the section and the dimensions of skin-stringer panels are calculated. The optimization routines developed in previous chapters are used for designing the panels on upper and lower wing covers. Chapter 2 considered only compressive bending load (single load case) for designing a skin-stringer panel on upper wing skin. The margin of safety is modified to include the effect combined bending and torsion (multiple load case). Results are presented separately for single and multiple load cases.

Chapter 5 presents the conclusions from this current research work along with recommendations for the future work.

CHAPTER 2

OPTIMIZATION OF A COMPRESSION SKIN-STRINGER PANEL

2.1 INTRODUCTION

Considering that a large number of candidate material and geometric shapes are available early in the design cycle, preliminary design optimization of compression skin-stringer panels used in an aircraft wing is required to obtain the best preliminary structure before the final design phase. A conceptual design of skin-stringer compression panels has been developed by Bombardier Aerospace [20]. Although this conceptual design is an efficient approach, it is rather an *ad hoc* optimization procedure without explicitly minimizing the mass of the panel.

Figure 2-1 shows a skin-stringer panel, with a stringer attached to the skin. The distance between two adjacent stringers in the chord wise direction is the width of the panel (or stringer pitch) and the distance between two consecutive ribs in the span wise direction is the length of the panel.

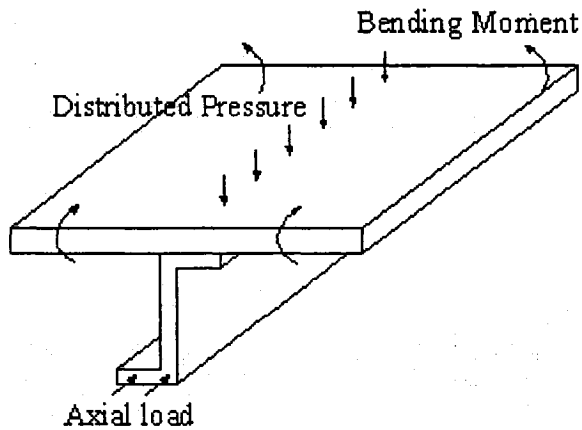

Figure 2-1: Compression Skin-Stringer panel subjected to design loads

Now, the objective is to develop a design optimization algorithm in order to minimize the mass of the panel while guarding against failures modes such as crippling stress, column buckling, up-bending at center span and compression in skin, down bending at supports and compression in stringer outstanding flange, inter-rivet buckling and beam column eccentricity.

2.2 DEFINITION OF THE OPTIMIZATION PROBLEM

Design optimization is a technique that seeks to determine an optimum design [22]. By optimum design, we mean, the one that meets all specified requirements but with a minimum expense of certain factors such as weight, surface area, volume, stress, cost, etc. Any optimization problem is defined in terms of three essential components namely, the design variables, the constraints and the objective function. Design variables are independent quantities that are varied in order to achieve the optimum design. Upper and lower limits, usually called as side constraints are specified on design variables. The constraints are dependent variables, typically the response quantities that are functions of the design variables and may have a maximum or minimum limit. The third essential component of an optimization problem, the objective function or the cost function, is also a function of the design variables. Changing the values of the design variables changes the value of the objective function. The solution of an optimization problem is a set of allowed values for the design variables for which the objective function assumes an 'optimal value'. In mathematical terms, optimization usually involves maximizing or minimizing the objective function.

Based on the above classical definition of an optimization process, the present optimization problem, minimum mass design of compression skin-stringer panel, is

formulated. Before defining the optimization problem, a typical cross-section of skin-stringer panel with important dimensions is shown in Figure 2-2. The compression surface (skin) is stabilized by a stringer attached to the skin by fasteners (rivets).

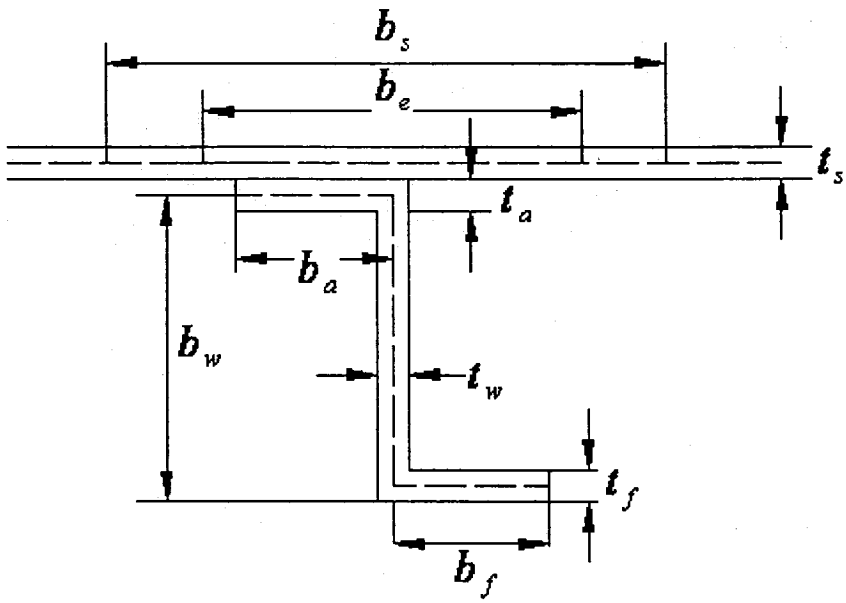

Figure 2-2: Cross-section of a typical compression skin-stringer panel

Different dimensions shown in Figure 2-2 are defined below:

t_s - thickness of the skin

b_s - panel width or stringer pitch

b_e - effective width of the skin

$b_a, t_a, b_w, t_w, b_f, t_f$ - dimensions of the stringer

Area of the panel (A) is the sum of the areas of the skin and stringer. A_{sk}, area of skin, is given by:

$$A_{sk} = t_s b_s \tag{2-1}$$

The area of the stringer is calculated from the ratio $\frac{A_{st}}{A_{sk}}$, called the stiffening ratio (SR) which is in the range of 0.5-0.7. It is usually set to 0.5 for preliminary designs. Thus,

$$A_{st} = \left[\frac{A_{st}}{A_{sk}}\right] A_{sk} \tag{2-2}$$

$$A = A_{sk} + A_{st} \tag{2-3}$$

Another important ratio that is required in the design optimization process is the width ratio (BR) defined as $\frac{b_s}{b_e}$. A suitable width ratio is set before starting the optimization.

2.2.1 Design Variables for the Optimization Problem

The two design variables for this problem are identified as t_s and b_s. Using t_s and b_s, different dimensions of the stringer (for instance J-type and Z-type stringers as shown in Figures 2-3 and 2-4) can be obtained from design practice relations or by maximizing the moment of inertia of the panel [20].

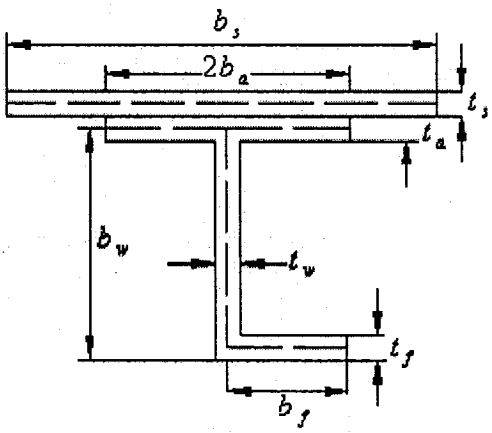

Figure 2-3: J-type stringer

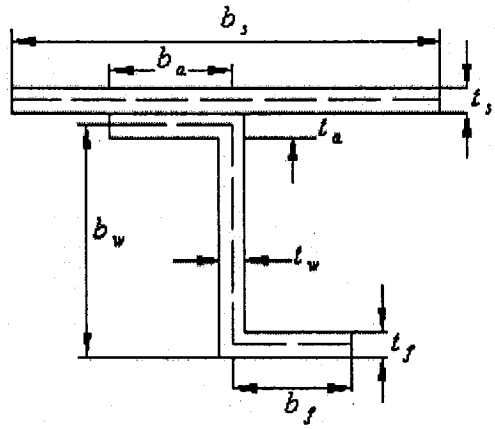

Figure 2-4: Z-type stringer

Design practice relations for J-type and Z-type stringers are given below [20]. The numerical coefficients defining these relations are optimized by maximizing the moment of inertia of the panel. The method of obtaining these coefficients by maximizing the moment of inertia is explained later in section 2.3.

J-type stringer

$b_a = 2.08t_s + 0.68$; If $t_s \le 0.3$

$b_a = 1.312$; If $t_s > 0.3$

$t_a = 0.7t_s$

$b_w = \sqrt{\frac{b_e}{t_s}(\frac{A_{st} - 2b_a t_a}{1.327})}$; $\frac{b_w}{t_w} \approx \frac{b_e}{t_s}$

$t_w = b_w\left[\frac{t_s}{b_e}\right]$

$b_f = 0.327 b_w$

$t_f \approx t_w$

Z-type stringer

$b_a = 2.08t_s + 0.68$; If $t_s \le 0.3$

$b_a = 1.312$; If $t_s > 0.3$

$t_a = 0.7t_s$

For equal flanges: $b_f = b_a$ & $t_f = t_a$

$b_w = \sqrt{\frac{b_e}{t_s}(A_{st} - 1.4 b_a t_s)}$; $t_w = b_w\left[\frac{t_s}{b_e}\right]$

For unequal flanges: $b_f \neq b_a$ & $t_f \neq t_a$

$b_w = \sqrt{\frac{b_e}{t_s}(\frac{A_{st} - 0.7 b_a t_s}{1.327})}$; $t_w = b_w\left[\frac{t_s}{b_e}\right]$

$b_f = 0.327 b_w$; $t_f \approx t_w$

It is noted that for integrally stiffened panel, $b_a = 0$ and $t_a = 0$.

2.2.2 Objective Function for the Optimization of a Skin-Stringer Panel

The objective is to minimize the mass of the compression skin-stringer panel. Mass of the panel (m_{panel}) is defined in terms of the design variables as below:

$$m_{panel}(t_s, b_s) = (A_{sk}\rho_{sk} + A_{st}\rho_{st})L \tag{2-4}$$

where L, ρ_{sk} and ρ_{st} are length of the panel, mass density of the skin and stringer materials, respectively.

2.2.3 Set of Constraints to Prevent the Failure of the Panel

The minimum of the three loads, namely, allowable buckling load of the skin-stringer panel, allowable compression load intensity for the up-bending at panel center span (compression in skin) and allowable compression load intensity for the down-bending at supports (compression in stringer outstanding flange) should be slightly less than or equal to the design load for the panel to be safe. Calculation of these loads is

explained in detail in section 2.4. Satisfying this condition results in conservative design and the chances of panel failure are minimized or even eliminated [1-3].

2.3 MAXIMIZATION OF THE MOMENT OF INERTIA

Before performing the design optimization for minimizing the mass of panel, the optimum design relations to calculate different dimensions of the stringer are obtained by maximizing the moment of inertia of the panel. To accomplish this, different dimensions of the stringer are expressed in terms of t_s and b_s using the constants k_1, k_2, k_3, k_4. For J and Z-type stringers, the design practice relations are expressed as below [20]:

For the J-type stringer as shown in Figure 2-3,

$$
\begin{aligned}
&b_a = k_1 t_s + k_2 ; && \text{If } t_s \le 0.3 \\
&b_a = k_1 (0.3) + k_2 ; && \text{If } t_s > 0.3 \\
&t_a = k_3 t_s \\
&b_W = \sqrt{\frac{b_e}{t_s}\left(\frac{A_{st} - 2b_a t_a}{1 + k_4}\right)} ; \ \frac{b_w}{t_w} \approx \frac{b_e}{t_s} \\
&t_w = b_w \left[\frac{t_s}{b_e}\right] \\
&b_f = k_4 b_w \quad ; \quad t_f = t_w
\end{aligned}
\tag{2-5}
$$

For the Z-type stringer as shown in Figure 2-4,

$$
\begin{aligned}
&b_a = k_1 t_s + k_2 ; && \text{If } t_s \le 0.3 \\
&b_a = k_1 (0.3) + k_2 ; && \text{If } t_s > 0.3 \\
&t_a = k_3 t_s \\
&b_W = \sqrt{\frac{b_e}{t_s}(A_{st} - 2b_a t_a)} ; \ \frac{b_w}{t_w} \approx \frac{b_e}{t_s} && \text{(with equal flanges)} \\
&t_w = b_w \left[\frac{t_s}{b_e}\right] \\
&b_f = b_a \ \& \ t_f = t_a
\end{aligned}
\tag{2-6}
$$

$$b_W = \sqrt{\frac{b_e}{t_s}\left(\frac{A_{st} - b_a t_a}{1 + k_4}\right)}\;;\quad \frac{b_w}{t_w} \approx \frac{b_e}{t_s} \qquad \text{(with unequal flanges)}$$

$$t_w = b_w\left[\frac{t_s}{b_e}\right]$$

$$b_f = k_4 b_w \quad ; \quad t_f = t_w$$

The numerical constants k_1, k_2, k_3, k_4 are the design variables (except for a Z-type stringer with equal flanges, which has k_1, k_2, k_3 as design variables). The initial values to start the optimization are taken as k_1=2.08, k_2=0.688, k_3=0.7 and k_4=0.327 [1,20]. Having defined all the dimensions, the moment of inertia of the panel can be evaluated. The objective here is to maximize the value of the moment of inertia while guarding against a set of important constraints. Two important constraints are identified as below [1-3]:

(a) $t_a \geq 0.7 t_s$ (To prevent forced crippling)

(b) $\frac{b_f}{b_w} = 0.4 - 0.5$ (To prevent rolling of the stringer)

The process of calculating the moment of inertia during the optimization is done using stress-strain curves of the materials used for skin and stringer. Using an iterative process, starting from the maximum allowable strain, the value of strain is decreased until the desired panel length is obtained. This procedure is practical with material stress-strain curves being a part of the entire process.

A smooth continuous stress-strain curve as shown in Figure 2-5 can be represented by using Ramberg-Osgood equation as,

$$\frac{\varepsilon E}{\sigma_n} = \frac{\sigma}{\sigma_n} + \frac{1}{m}\left[\frac{\sigma}{\sigma_n}\right]^m \qquad (2\text{-}7)$$

where ε , E, m, σ_n are strain in the material, modulus of elasticity, material characteristic number and reference stress, respectively [23].

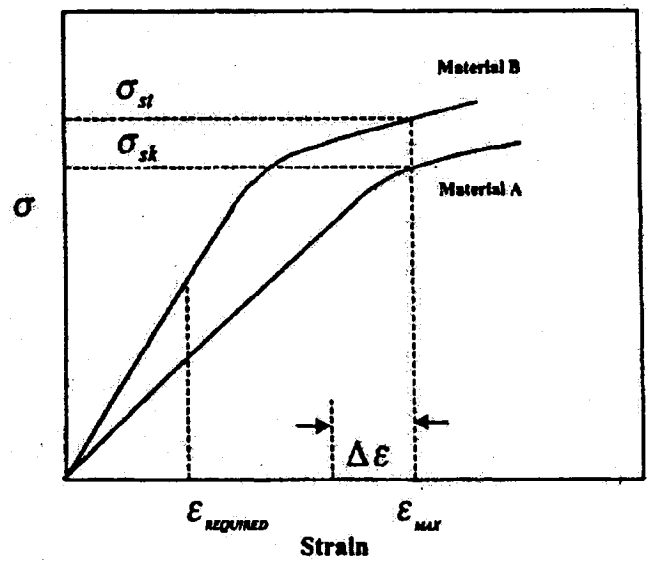

Figure 2-5: Stress-strain curves for skin and stringer materials [20]

For a known value of m, the reference stress σ_n can be calculated as,

$$\sigma_n = \sigma_R \left[\frac{m\varepsilon_R E}{\sigma_R} \right]^{-1/(m-1)} \tag{2-8}$$

where σ_R is the known stress value on the stress-strain curve of the material and ε_R is the strain corresponding to σ_R. The stress corresponding to 0.2 % strain on the stress-strain curve can be considered as the yield stress. This implies that for ε_R = 0.002, the corresponding stress is the compressive allowable yield stress of the material. Eq. (2-7) is re-arranged to calculate the tangent modulus of elasticity (E_t) corresponding to a stress σ as,

$$E_t = \frac{d\sigma}{d\varepsilon} = E[1 + (\frac{\sigma}{\sigma_n})^{m-1}]^{-1} \tag{2-9}$$

Since it is difficult to calculate the stress corresponding to a given strain by using Eq. (2-7), the equation is re-arranged as,

$$\frac{\sigma}{\sigma_n} = (\frac{\varepsilon E}{\sigma_n})[1 + \beta(|\frac{\varepsilon E}{\sigma_n}|)^k + \frac{1}{m}(|\frac{\varepsilon E}{\sigma_n}|)^{m-1}]^{-1/m} \tag{2-10}$$

where $\beta = (1+1/m)^{(m-1-k)} - (1+1/m)^{-k}$ and $k = 0.79044m - 0.06977$.

From Figure 2-5, it is observed that, for a given strain ε, the corresponding tangent modulus of elasticity E_{tsk} and the stress σ_{sk} in the skin are calculated using Eqs. (2-9) and (2-10), respectively. Similarly, E_{tst} and σ_{st} in stringer are calculated.

Consider one skin-stringer panel as shown in Figure 2-2. The load applied on the stiffened wide column under axial compression is given by:

$$Q = \sigma_{sk} A_{sk} + \sigma_{st} A_{st} \tag{2-11}$$

$$\Rightarrow \quad \frac{Q}{A_{sk}} = \sigma_{sk} + \sigma_{st}\left[\frac{A_{st}}{A_{sk}}\right] \tag{2-12}$$

The effective skin area is given as,

$$A_{sk} = t_s b_e \tag{2-13}$$

The axial load intensity on the panel is expressed as,

$$N = \frac{Q}{b_s} \tag{2-14}$$

Substituting Eq. (2-13) and Eq. (2-14) into Eq. (2-12), we obtain:

$$\frac{N b_s}{t_s b_e} = \sigma_{sk} + \sigma_{st}\left[\frac{A_{st}}{A_{sk}}\right] \tag{2-15}$$

Subsequently, the skin thickness can be obtained as,

$$t_s = \frac{N\left[\frac{b_s}{b_e}\right]}{\sigma_{sk} + \sigma_{st}\left[\frac{A_{st}}{A_{sk}}\right]} \tag{2-16}$$

It is noted that a suitable width ratio $\left[\frac{b_s}{b_e}\right]$ is set before starting the optimization process.

According to the plate theory [1-3], the stress in the skin is given by,

$$\sigma_{sk} = K\eta E(\frac{t_s}{b_e})^2 \tag{2-17}$$

where K is the buckling coefficient and $\eta = \sqrt{\frac{E_t}{E}}$, is the Plasticity correction factor. The value of K is in the range of 3.62-6.32. Effective skin width is calculated using Eq. (2-17) as,

$$b_e = t_s\sqrt{\frac{K\eta E}{\sigma_{sk}}} \tag{2-18}$$

The global buckling mode of failure given by Euler-Engesser equation can be written as,

$$\sigma_e = \frac{c\pi^2 E_{te}}{(L/\rho)^2} \tag{2-19}$$

where c, L and $\rho = \sqrt{\frac{I}{A}}$ are the end fixity coefficient, the length of the panel and radius of gyration, respectively. The panel is composed of the skin and stringer elements with different stress-strain characteristics. The tangent modulus and the value of stress in Eq. (2-19) are the effective values and can be described as below:

$$\text{Effective Stress, } \sigma_e = \frac{\sigma_{sk} + \sigma_{st}\left[\frac{A_{st}}{A_{sk}}\right]}{1+\left[\frac{A_{st}}{A_{sk}}\right]} \tag{2-20}$$

It is noted that equal strain 'ε' is experienced by both skin and stringer.

Effective Tangent Modulus of Elasticity, $E_{te} = \dfrac{E_{tsk} + E_{tst}\left[\dfrac{A_{st}}{A_{sk}}\right]}{1+\left[\dfrac{A_{st}}{A_{sk}}\right]}$ (2-21)

Substituting Eq. (2-20) and Eq. (2-21) in Eq. (2-19) and re-arranging the terms, we obtain,

$$L_{cal} = \pi\sqrt{\frac{E_{tsk} + E_{tst}(A_{st}/A_{sk})}{\sigma_{sk} + \sigma_{st}(A_{st}/A_{sk})}}\sqrt{\frac{I}{A}} \tag{2-22}$$

where I is the moment of Inertia of panel and $A = A_{sk} + A_{st}$, is the total area of the panel. From Figure 2-5, it can be observed that the strain is decremented from $\varepsilon_{\max}$ to $\varepsilon_{required}$ until the required panel length is achieved, i.e. ($L_{cal} = L$). The optimum values for the design variables k_1, k_2, k_3, k_4 obtained during this optimization are used to define the stringer dimensions.

2.4 CALCULATION OF LOADS

The axial load intensity *N*, obtained from the aerodynamic loads, is the main input to the optimization problem. The panel length (*L*), the material properties of the skin and stringer, *E*, σ_{cy} and *m* (elastic modulus, allowable compression yield stress and material characteristic index, respectively), stiffening ratio (*SR*), width ratio (*BR*) and surface load intensity w_0 are the additional inputs to the optimization problem [20,21]. For a known t_s and b_s values, the effective skin width is calculated using the width ratio as,

$$b_e = \frac{b_s}{BR} \tag{2-23}$$

The effective stress (σ_e) in the skin-stringer panel due to compressive axial load intensity N can be obtained using Eq. (2-15) and Eq. (2-20) as,

$$\sigma_e = \frac{N}{t_s(1+SR)}\left[\frac{b_s}{b_e}\right] \tag{2-24}$$

2.4.1 Calculation of Column Buckling Allowable Load of the Panel, N_{all}

Buckling allowable load of the skin-stringer compression panel is calculated as below:

(i) If the stringer is connected to the skin with standard rivets, the horizontal distance between two rivets (taken from the rivet center line) is given by:

$$B_R = 2(b_a - e_h) \tag{2-25}$$

where 'e_h' is the horizontal distance between the fastener center line and the stringer edge. Now, the total new effective width can be written as,

$$b_{e/new} = b_e + B_R \tag{2-26}$$

This new effective width $b_{e/new}$ should be greater than b_s and hence, a constraint is considered on the new effective width [20].

(ii) The crippling stress, σ_{cc} of the stringer section is calculated using the empirical equations. The entire section is broken down into individual segments. Segments with width 'b' and thickness 't' having one free edge or no free edge are identified. The allowable crippling stress for each segment 'n' is calculated using the following empirical relations [1-3] as,

(a) For segment 'n' with free edge,

$$\sigma_{ccn} = 0.6121\,\sigma_{cyn}\left[\frac{b_n}{t_t}\sqrt{\frac{\sigma_{cyn}}{E_n}}\right]^{-0.7735} \tag{2-27}$$

(b) For segment 'n' with no free edge,

$$\sigma_{ccn} = 1.1819\sigma_{cyn}\left[\frac{b_n}{t_t}\sqrt{\frac{\sigma_{cyn}}{E_n}}\right]^{-0.7882} \tag{2-28}$$

where σ_{cyn} and E_n are allowable compression yield stress and modulus of elasticity of segment 'n', respectively. The allowable crippling stress for the entire section of the stringer is computed by taking the weighted average of the allowable for each segment as,

$$\sigma_{cc} = \frac{\sum b_n t_n \sigma_{ccn}}{\sum b_n t_n} \tag{2-29}$$

The cut-off or maximum crippling stress for composite sections like J-sections and Z-sections should be limited to $0.9\sigma_{cy}$, unless test results are obtained to substantiate the use of higher crippling stresses [3]. Hence, a constraint is placed on the upper limit value of the crippling stress σ_{cc} in the optimization routine.

The allowable column buckling stress σ_{CB} is calculated using the Johnson-Euler column buckling equation as [1-3],

$$\sigma_{CB} = \sigma_{cc} - \frac{(\sigma_{cc})^2\left[\frac{L'}{\rho}\right]^2}{4\pi^2 E} \tag{2-30}$$

where I, $L' = \frac{L}{\sqrt{c}}$, c and $\rho = \sqrt{\frac{I}{A}}$ are moment of inertia of the panel, effective length between the rib supports, end fixity coefficient and radius of gyration, respectively. The column buckling allowable load of the panel is given by:

$$N_{all1} = \frac{\sigma_{CB} A}{b_s} \tag{2-31}$$

2.4.2 Calculation of Rivet Pitch to Avoid Inter-Rivet Buckling

The inter-rivet buckling theory is the same as that for buckling of a flat plate or sheet as a column with two fixed edges at each end (at rivet). Figure 2-6 shows the inter-rivet skin buckling phenomenon [1].

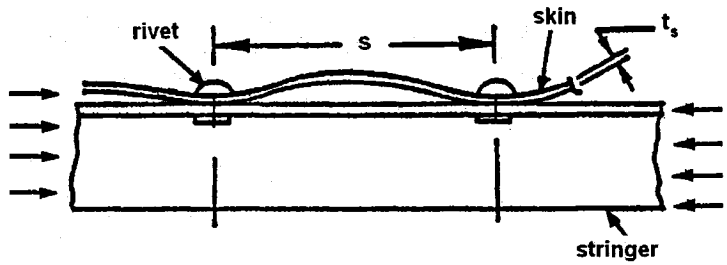

Figure 2-6: Inter-rivet skin buckling [1]

The buckling of skin between two successive rivets is eliminated by selection of suitable rivets and calculating the required rivet spacing or pitch in length direction of the panel. The inter-rivet buckling stress can be estimated using Euler equation as,

$$\sigma_{ir} = \frac{c_r \pi^2 E_t}{\left[\frac{L}{\rho}\right]^2} \tag{2-32}$$

Considering a sheet of unit width with a thickness 't'. We have,

$$I = t^3/12, A = t \text{ and } \rho = \sqrt{\frac{I}{A}} \Rightarrow \rho = 0.288t$$

$$\Rightarrow \quad \sigma_{ir} = \frac{c_r \pi^2 E_t}{\left[\frac{L}{0.288t}\right]^2} \tag{2-33}$$

Considering the distance between two successive rivets, usually referred as rivet pitch to be 's', the inter-rivet buckling stress is given by:

$$\sigma_{ir} = 0.9 c_r E_t \left[\frac{t_s}{s}\right]^2 \tag{2-34}$$

where c_r is the end fixity coefficient. By equating the inter-rivet buckling stress to crippling stress of the section (σ_{cc}), the rivet pitch 's' is calculated. Some typical values of c_r taken for different rivet heads are c_r = 4 (for flat head rivet), c_r = 3.5 (for spot welds), c_r = 3 (for Brazier type rivet) and c_r = 1 (for counter-sunk).

2.4.3 Effect of Beam Column Eccentricity

In order to incorporate the effect of beam column eccentricity in the calculation of compression bending loads N_{all2} and N_{all3} for up-bending and down-bending of the panel, it is required to calculate the Euler inelastic buckling allowable load [1-3]. It is calculated using Euler equation as,

$$N_e = \frac{\pi^2 E_{te} I}{L_e^{\,2}} \tag{2-35}$$

where E_{te} and L_e are the effective tangent modulus of the panel and the effective length of the panel, respectively. The tangent modulus is calculated using Ramberg-Osgood equation [23] as,

$$E_t = \frac{E}{1 + \frac{3}{7} m \left[\frac{\sigma_e}{\sigma_{0.7}}\right]^{m-1}} \tag{2-36}$$

where m, E and $\sigma_{0.7}$ are the material characteristic number, modulus of elasticity and stress value corresponding to the secant modulus of $0.7E$ on the stress-strain curve.

Now, using Eq. (2-21), the effective tangent modulus value for the panel is calculated as,

$$E_{te} = \frac{E_{t\,skin} + E_{t\,stringer}(SR)}{(1+SR)} \tag{2-37}$$

2.4.4 Calculation of Compression Allowable Load Intensity for Up-Bending at the Panel Center Span (Compression in Skin), N_{all2}

An iterative process is required to obtain the value of axial compression stress σ_{CU}. The iteration steps are defined as below:

(i) Initialize the value of the axial compressive stress. A recommended initial value would be the effective stress in the panel, σ_e

$$\sigma_{CU} = \sigma_e \tag{2-38}$$

(ii) Find the corresponding total axial load

$$P_{axial} = \sigma_{CU} A \tag{2-39}$$

(iii) Evaluate the tangent modulus of elasticity for the skin material under axial compressive stress using Ramberg-Osgood equation

$$E_{t\,skin} = \frac{E}{1+\frac{3}{7}m\left[\frac{\sigma_{CU}}{\sigma_{0.7}}\right]^{m-1}} \tag{2-40}$$

(iv) Obtain torsional spring parameter μ_T

$$\mu_T = \frac{P_{axial}(L)^2}{E_{t\,skin} I} \tag{2-41}$$

(v) Calculate the bending moment parameter $\overline{BM} = \frac{M}{w_0(L)^2}$ corresponding to μ_T value from the following empirical relations [2,20]:

$$\overline{BM} = 6x10^{-6}(\mu_T)^4 - 8x10^{-5}(\mu_T)^3 + 0.0007(\mu_T)^2 + 0.0032\mu_T + 0.0726$$
$$(\text{for } 0 \le \mu_T \le 11.958)$$

$$\overline{BM} = -7x10^{-5}(\mu_T)^4 + 0.0103(\mu_T)^3 - 0.346(\mu_T)^2 + 4.4262\mu_T - 19.449$$
$$(\text{for } 11.958 < \mu_T \leq 18.297)$$

$$\overline{BM} = 1.0$$
$$(\text{for } \mu_T > 18.297)$$

(vi) Find the compression bending moment

$$M_{comp} = \overline{BM} w_0 (L)^2 \tag{2-42}$$

Beam column eccentricity has a pronounced effect in the system stability of these types of structures. This can be clearly observed in Figure 2-7 which has an initial eccentricity '*e*'. The value of '*e*' is usually $\pm\frac{L}{1000}$ [3]. In this study, a sinusoidal imperfection with amplitude '*e*' has been considered. The presence of this sinusoidal imperfection increases the compressive bending moment occurring due to bending.

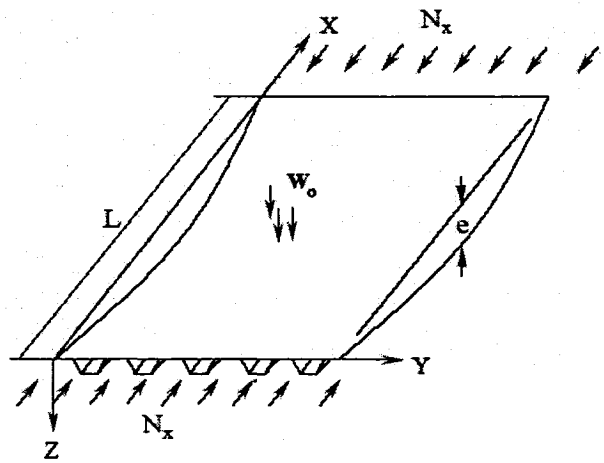

Figure 2-7: Beam column eccentricity '*e*' [3]

For a beam subjected to axial load *N* and with an initial sinusoidal eccentricity, '*e*' at the centre of the panel, the bending moment induced in the panel can be easily shown to be,

$$M_e = \frac{Ne}{1-\gamma} \tag{2-43}$$

where $\gamma = \frac{N}{N_e}$ and N_e is the Euler inelastic buckling allowable load in the column as calculated in Eq. (2-35). Now, the total compressive bending moment is given as,

$$M_{total} = M_{comp} + M_e \tag{2-44}$$

(vii) Now, calculate the corresponding bending compression stress (in skin)

$$\sigma_{b\max} = \frac{M_{total} Y}{I} \tag{2-45}$$

where Y is the vertical position of the upper skin surface from neutral axis.

(viii) Finally, calculate maximum compression stress

$$\sigma_{\max skin} = \sigma_{CU} + \sigma_{b\max} \tag{2-46}$$

Steps (i) to (viii) are repeated to make the absolute difference (ΔS) between the maximum compressive stress in skin $\sigma_{\max skin}$ and allowable column buckling stress σ_{CB} to be minimum or within a specified tolerance ($\Delta\sigma_{tol}$)

$$\Delta S = \left|\sigma_{\max skin} - \sigma_{CB}\right| \tag{2-47}$$

At the end of step (viii), if the difference ΔS is greater than $\Delta\sigma_{tol}$, steps (i) to (viii) are repeated with modified σ'_{CU} as below:

$$\sigma'_{CU} = \sigma_{CU} - 0.5\Delta S \text{ ; when } \sigma_{\max skin} > \sigma_{CB}$$

$$\sigma'_{CU} = \sigma_{CU} + 0.5\Delta S \text{ ; when } \sigma_{\max skin} < \sigma_{CB}$$

(ix) Calculate compression allowable load intensity N_{all2} for the up-bending at panel center span (compression in skin)

$$N_{all2} = \frac{\sigma_{CU} A}{b_s} \tag{2-48}$$

2.4.5 Calculation of Compression Allowable Load Intensity for Down-Bending at Supports (Compression in Stringer Outstanding Flange), N_{all3}

An iterative process is required here as well to obtain the value of axial compression stress σ_{CD}. The iteration steps are listed as below:

(i) A recommended initial value here would be the axial compressive stress σ_{CU} calculated in the previous section 2.4.4.

$$\sigma_{CD} = \sigma_{CU} \tag{2-49}$$

(ii) Find the corresponding total axial load

$$P_{axial} = \sigma_{CD} A \tag{2-50}$$

(iii) Evaluate the tangent modulus of elasticity for the skin material under axial compressive stress using Ramberg-Osgood equation

$$E_{tskin} = \frac{E}{1 + \frac{3}{7} m \left[\frac{\sigma_{CD}}{\sigma_{0.7}} \right]^{m-1}} \tag{2-51}$$

(iv) Obtain torsional spring parameter μ_{TF}

$$\mu_{TF} = \frac{P_{axial}(L)^2}{E_{tskin} I} \tag{2-52}$$

(v) Calculate the bending moment parameter $\overline{BM} = \dfrac{M}{w_0 (L)^2}$ corresponding to μ_{TF} value from the following empirical relations [2,20]:

$$\overline{BM} = 5x10^{-7}(\mu_{TF})^4 - 1x10^{-5}(\mu_{TF})^3 + 0.0002(\mu_{TF})^2 + 0.0008\mu_{TF} + 0.0779$$
$$(\text{for } 0 \le \mu_{TF} \le 17.036)$$

$$\overline{BM} = 0.0003(\mu_{TF})^3 - 0.0193(\mu_{TF})^2 + 0.4255\mu_{TF} - 3.0216$$
$$(\text{for } 17.036 < \mu_{TF} \le 29.281)$$

$$\overline{BM} = 0.4$$
$$(\text{for } \mu_{TF} > 29.281)$$

(vi) Find the compression bending moment

$$M_{comp} = \overline{BM} w_0 (L)^2 \tag{2-53}$$

Additional bending Moment induced in the panel due to sinusoidal imperfection is given by Eq. (2-43). Hence, the total compressive bending moment becomes,

$$M_{total} = M_{comp} + M_e \tag{2-54}$$

(vii) Now, calculate the corresponding bending compression stress (in stringer outstanding flange)

$$\sigma_{b\max flange} = \frac{M_{total}(t_s + b_w + t_a/2 + t_f/2 - Y)}{I} \tag{2-55}$$

(viii) Finally, calculate maximum compression stress

$$\sigma_{\max flange} = \sigma_{CD} + \sigma_{b\max flange} \tag{2-56}$$

Steps (i) to (viii) are repeated to make the absolute difference (ΔS) between the maximum compressive stress in skin $\sigma_{\max flange}$ and $\sigma_{cc/out.flange}$ to be minimum or within a specified tolerance ($\Delta\sigma_{tol}$).

$$\Delta S = \left|\sigma_{\max flange} - \sigma_{cc/out.flange}\right| \tag{2-57}$$

$\sigma_{cc/out.flange}$ is the allowable crippling stress in the stringer outstanding flange. This is calculated using Eqs. (2-27) or (2-28). At the end of step (viii), if the difference ΔS is greater than $\Delta\sigma_{tol}$, steps (i) to (viii) are repeated with modified σ'_{CF} as below:

$$\sigma'_{CD} = \sigma_{CD} - 0.5\Delta S \text{; when } \sigma_{\max flange} > \sigma_{cc/out.flange}$$

$$\sigma'_{CD} = \sigma_{CD} + 0.5\Delta S \text{; when } \sigma_{\max flange} < \sigma_{cc/out.flange}$$

(ix) Calculate the compression load intensity N_{all3} for the down-bending at supports (compression in stringer outstanding flange)

$$N_{all3} = \frac{\sigma_{CD} A}{b_s} \tag{2-58}$$

The last and important constraint in the optimization routine is that the minimum value of the 3 loads N_{all1}, N_{all2} and N_{all3} should be less than or equal to the applied axial load intensity for conservative and safe design of the panel. In other words,

$$N_{\min} = \text{Min}\,(N_{all1}, N_{all2}, N_{all3}) \leq N \tag{2-59}$$

Since the objective function is minimize the mass of the panel, it is ideal to set a value on the moment of inertia of the panel (I) greater than zero during the optimization. This constraint ensures that the optimization process does not give the best optimum result with 'zero' mass for the panel.

2.5 VALIDATION OF RESULTS AND CONCLUSIONS

The process is programmed in MATLAB [44] environment and its optimization toolbox has been employed as optimizer. The optimizer uses Sequential Quadratic Algorithm during the optimization. The results have been compared with existing skin-stringer panels taken from different jet aircrafts and also with results of the conceptual design methodology developed by Bombardier Aerospace [20,21].

(1) Table 2-1 shows the comparison of results for panel defined at bay#2 with stringer#4 of Aircraft 1 (AC1). Table 2-2 shows the comparison for panel at bay#3 with stringer #14 of AC1 and Table 2-3 shows the comparison for panel at bay#5 with stringer #11 of same aircraft, AC1. The stringers used are Z-stringers with equal flanges. The

accuracy of the optimization has been tested by repeating with different initial points. For the above 3 test panels, Figures 2-8 to 2-10 show that, the objective function converges to approximately the same optimum value for different initial points. Tables 2-1 to 2-3 show that a good agreement exists between the present results and those in literature [20]. A minimum mass of 2.1152 *lbs*, 3.0171 *lbs*, 3.1709 *lbs* has been obtained for the above 3 panels, respectively. It should be noted that the optimum values obtained for k_1, k_2, k_3 are slightly different for the 3 panels of AC1. These constant parameters provide the maximum value for the moment of inertia during the optimization.

Material Properties for Aircraft 1 (AC1) are:

For Skin: $\sigma_{cy} = 76000 psi$; $E_{sk} = 10.6e6 psi$; $m = 12$

For Stiffener: $\sigma_{cy} = 83000 psi$; $E_{st} = 10.9e6 psi$; $m = 23$

(2) Optimum results for panel#2 of Aircraft 2 (AC2), panels #3 and #4 of Aircraft 3 (AC3) are given in Tables 2-4, 2-5 and 2-6, respectively. It can be observed from these tables that a good agreement exists between the present results and those in literature. A minimum mass of 3.8751 *lbs*, 4.3950 *lbs* and 4.4652 *lbs* has been obtained for the above 3 panels, respectively. The stringers used are Z-stringers with equal flanges. Again, the optimum values for k_1, k_2, k_3 are slightly different for these 3 panels.

Material Properties for Aircraft 2 and Aircraft 3 (AC2 and AC3) are:

For Skin: $\sigma_{cy} = 68000 psi$; $E_{sk} = 10.5e6 psi$; $m = 12$

For Stiffener: $\sigma_{cy} = 75000 psi$; $E_{st} = 10.5e6 psi$; $m = 25$

(3) Optimum results for panels at bay#0-22.5, bay#106.4-127.3 and bay#274-294 of Aircraft 4 (AC4), respectively are given in Tables 2-7 to 2-9. A minimum mass of

1.7050 *lbs*, 1.9098 *lbs* and 1.4659 *lbs* has been obtained for the above 3 panels, respectively. The stringers used are Z-stringers with equal flanges. The optimum values obtained for k_1, k_2, k_3 are different for these 3 panels.

Material Properties for Aircraft 4 (AC4) are:

For Skin: $\sigma_{cy} = 75000 psi$; $E_{sk} = 10.5e6 psi$; $m = 23$

For Stiffener: $\sigma_{cy} = 75000 psi$; $E_{st} = 10.5e6 psi$; $m = 23$

Table 2-1: Comparison with Bay#2, Stringer#4 of Aircraft 1

	AC1	CD	PM
$N\,(lb/in)$	8855	8855	8855
$L\,(in)$	22.65	22.65	22.65
$b_s\,(in)$	4.88	4.7	4.3222
$t_s\,(in)$	0.15	0.173	0.1477
$I\,(in^4)$	0.436	0.440	0.3401
$A\,(in^2)$	1.279	1.132	0.9574

k_1=2.0796; k_2=0.6856; k_3=0.7

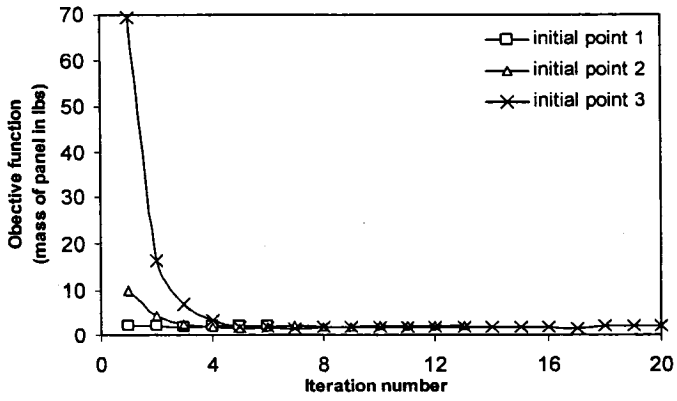

Figure 2-8: Iteration number vs objective function for different initial points for Bay#2, Stringer#4 of Aircraft 1

Table 2-2: Comparison with Bay#3, Stringer#14 of Aircraft 1

	AC1	CD	PM
$N\,(lb/in)$	10140	10140	10140
$L\,(in)$	26.7	26.7	26.7
$b_s\,(in)$	4.26	4.27	4.6424
$t_s\,(in)$	0.145	0.174	0.1664
$I\,(in^4)$	0.419	0.463	0.5534
$A\,(in^2)$	1.097	1.124	1.1584

k_1=2.0760; k_2=0.6627; k_3=0.7

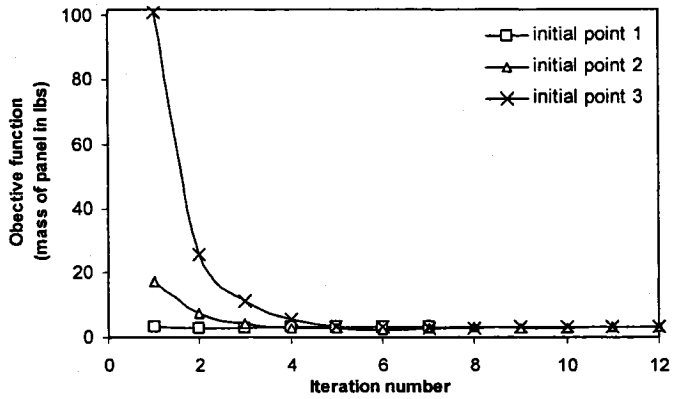

Figure 2-9: Iteration number vs objective function for different initial points for Bay#3, Stringer#14 of Aircraft 1

Table 2-3: Comparison with Bay#5, Stringer#11 of Aircraft 1

	AC1	CD	PM
$N\,(lb/in)$	10594	10594	10594
$L\,(in)$	27.1	27.1	27.1
$b_s\,(in)$	4.8	4.89	4.6791
$t_s\,(in)$	0.17	0.186	0.1709
$I\,(in^4)$	0.446	0.532	0.5943
$A\,(in^2)$	1.272	1.337	1.1995

k_1=2.0733; k_2=0.6465; k_3=0.7

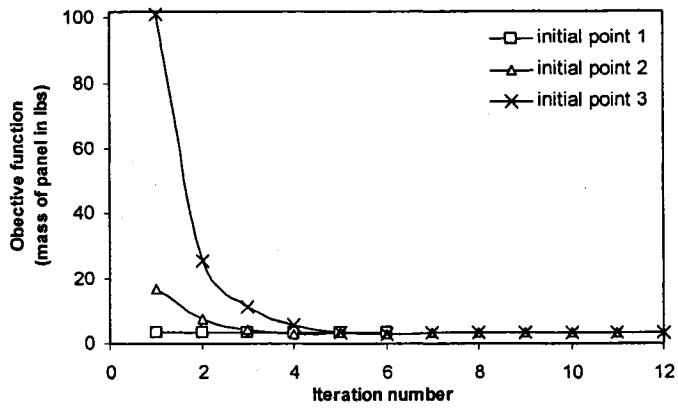

Figure 2-10: Iteration number vs objective function for different initial points for Bay#5, Stringer#11 of Aircraft 1

Table 2-4: Comparison with Test Panel#1 of Aircraft 2

	AC2	CD	PM
$N\,(lb/in)$	16200	16200	16200
$L\,(in)$	26.0	26.0	26.0
$b_s\,(in)$	5.0	4.9	4.8873
$t_s\,(in)$	0.15	0.21	0.2084
$b_a\,(in)$	1.0	1.13	0.9290
$t_a\,(in)$	0.16	0.15	0.1459
$b_w\,(in)$	2.5	2.65	2.1576
$t_w\,(in)$	0.16	0.153	0.1104

k_1=2.0383; k_2=0.5042; k_3=0.7

Table 2-5: Comparison with Test Panel#3 of Aircraft 3

	AC3	CD	PM
$N\,(lb/in)$	18600	18600	18600
$L\,(in)$	25.0	25.0	25.0
$b_s\,(in)$	5.35	5.32	5.3260
$t_s\,(in)$	0.196	0.26	0.2256
$b_a\,(in)$	1.0	1.2	0.9962
$t_a\,(in)$	0.132	0.185	0.1579
$b_w\,(in)$	2.5	2.315	2.3726
$t_w\,(in)$	0.132	0.119	0.1206

k_1=2.0428; k_2=0.5354; k_3=0.7

Table 2-6: Comparison with Test Panel#4 of Aircraft 3

	AC3	CD	PM
$N\,(lb/in)$	19000	19000	19000
$L\,(in)$	25.0	25.0	25.0
$b_s\,(in)$	5.35	5.4	5.3128
$t_s\,(in)$	0.196	0.27	0.2298
$b_a\,(in)$	1.0	1.25	0.9567
$t_a\,(in)$	0.132	0.189	0.1608
$b_w\,(in)$	2.5	2.519	2.5221
$t_w\,(in)$	0.132	0.138	0.1200

k_1=2.0331; k_2=0.4896; k_3=0.7

Table 2-7: Comparison with Bay#0-22.5 of Aircraft 4

	AC4	CD	PM
$N\,(lb/in)$	6840	6840	6840
$L\,(in)$	22.05	22.05	22.05
$b_s\,(in)$	3.64	3.89	4.0442
$t_s\,(in)$	0.12	0.13	0.1307
$A\,(in^2)$	0.796	0.77	0.7927

k_1=2.0774; k_2=0.6676; k_3=0.7

Table 2-8: Comparison with Bay#106.4-127.3 of Aircraft 4

	AC4	CD	PM
$N\,(lb/in)$	8333	8333	8333
$L\,(in)$	22.35	22.35	22.35
$b_s\,(in)$	3.73	3.23	4.0099
$t_s\,(in)$	0.14	0.15	0.1456
$A\,(in^2)$	0.781	0.754	0.8760

k_1=2.0675; k_2=0.5991; k_3=0.7

Table 2-9: Comparison with Bay#274-294 of Aircraft 4

	AC4	CD	PM
$N\,(lb/in)$	4400	4400	4400
$L\,(in)$	21.95	21.95	21.95
$b_s\,(in)$	3.64	3.42	3.5283
$t_s\,(in)$	0.1	0.115	0.1294
$A\,(in^2)$	0.638	0.58	0.6846

k_1=2.0703; k_2=0.5988; k_3=0.7

AC1- Aircraft 1
AC2, AC3- Aircraft 2, Aircraft 3
AC4- Aircraft 4
CD- Conceptual Design developed by Bombardier Aerospace
PM- Present Method

CHAPTER 3

OPTIMIZATION OF A LOWER SKIN-STRINGER PANEL BY IMPLEMENTING DAMAGE TOLERANCE ANALYSIS

3.1 IDENTIFICATION OF DESIGN METHOD

The lift generated by the wings opposes the weight of the aircraft, and thus generates bending. Depending on their location, stiffened panels that make up the wing are mainly loaded in compression and tension. The ability to resist the compressive load was studied in Chapter 2. The ability to resist the tensile load is evaluated mainly by the damage tolerance analysis.

Fracture is a potentially catastrophic failure mechanism, characterized by unstable and extremely fast crack growth and is generally the final event of a process during which the level of structural strength is gradually reduced by the presence of growing cracks. The starting point is often a small flaw in a region of stress concentration, which may later develop into a crack. If the structure is submitted to cyclic loads, then the crack grows initially at very low rates, in a process known as fatigue crack growth. Stable and slow fatigue crack growth will take place until the crack reaches a critical length. At this moment, the structure is no longer capable of withstanding the service loads and fracture occurs [24,25].

For many years, the safe-life design method is used to design a structure for these types of failures. The objective of this method is to make the time required for the initiation of the cracks longer than the operational life of the structure. However, initiation is a subjective concept. A great deal of uncertainty is associated with the

laboratory determination of the time required for the crack initiation. It is virtually impossible to ensure a crack free operational life for most structures. This lead to the introduction of a new method called the fail-safe design. In order to prevent catastrophic failure due to unexpected cracking, the structure is designed to be fail-safe. This can be achieved by utilizing redundant structural components. In the event of failure of one of the members, whether due to fracture or any other mechanism, the load is safely re-distributed to other members.

However, despite its effectiveness in the prevention of catastrophic failures, fail-safe design cannot be viewed as an evolutionary alternative to safe-life design, because it does not incorporate any new method or an idea to study the mechanics of the cracking process. The real alternative to safe-life design is the Damage Tolerance Design. The tests and analyses required to demonstrate compliance with damage tolerance principles are based on the implicit assumption of the presence of a single isolated crack. Hence, the main advantage in comparison with safe-life design is that it has a quantitative basis in the form of size of a crack as opposed to the rather subjective concept of crack initiation. Damage tolerance design also incorporates fail-safe design concepts in order to prevent catastrophic failure in the event of a crack growing undetected [25].

Fracture Mechanics is the mathematical tool used in damage tolerance analysis to study fatigue crack propagation. It studies materials and structures which contain flaws in the form of detectable or visible cracks. For all high strength materials used in airframes, Linear Elastic Fracture Mechanics (LEFM) theory can be applied [24]. The fundamental postulate of LEFM states that, a parameter called the stress intensity factor (SIF), which

is a measure of the strength of the stress singularity at a crack tip, can be used to determine the crack behaviour.

3.2 FUNDAMENTALS OF FRACTURE MECHANICS

In 1920, Griffith published the first systematic investigation of the fracture phenomenon. He studied the energy balance in a plate of elastic material submitted to a remote stress σ, containing an internal crack of size $2a$. He postulated that if crack is increased by a certain amount da, the total potential energy stored by the system decreases due to the release of elastic strain energy, as expressed by the relation [24],

$$\frac{dT}{da} = -G \tag{3-1}$$

where T is the total potential energy and G is the strain energy release rate. Conversely, he stated that for fracture to occur, a certain amount of work, denoted by S, has to be expended. According to Griffith, the energy balance of the fracture process can be expressed as,

$$\frac{dT}{da} + \frac{dS}{da} = 0 \tag{3-2}$$

where both energy terms are defined by unit thickness of the plate. In essence, the stress intensity factor serves as a scale to define the magnitude of the stress around a crack tip. It is a function of the crack size, the type of loading and the geometrical configuration of the structure. The fundamental postulate of the LEFM is that the behaviour of the crack is determined solely by the SIF. A fracture criterion based on the stress intensity factor can therefore be written as,

$$K \geq K_{IC} \tag{3-3}$$

where K is the stress intensity factor at the crack-tip and K_{IC} is a critical value, called the Fracture Toughness, which depends on material, loading and geometry. In other words, fracture will occur when the stress intensity factor reaches a critical value K_{IC}. By studying the elastic work around a crack tip, Irwin has a derived the relationship between the stress intensity factor and the energy release rate which is given as below:

$$G = \frac{K^2}{E} \qquad \begin{cases} E & \textit{for plane stress} \\ \dfrac{E}{(1-\nu^2)} & \textit{for plane strain} \end{cases} \tag{3-4}$$

where E is Young's modulus of the plate material and ν is the Poisson's Ratio. This relation is the key to LEFM. It provides the link between energy balance and crack tip stress field formulations which, in practical terms, means that if the strain energy release rate is known, the stress intensity factors can be determined. The deformation modes in a cracked structure are characterized by the relative displacements of the crack surfaces. Figure 3-1 shows three basic deformation modes.

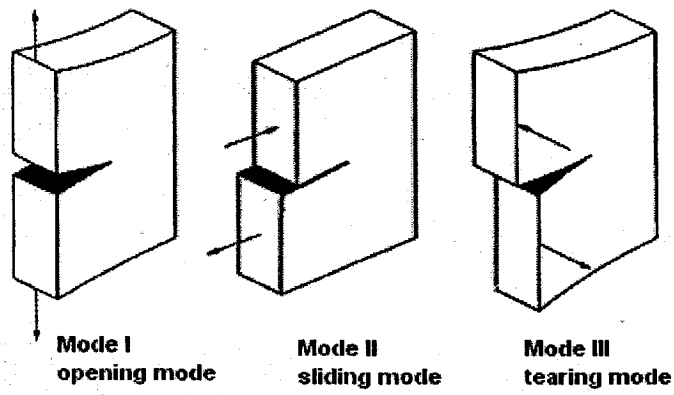

Figure 3-1: Crack opening modes [24]

Mode I is the opening mode or tensile mode where the crack surfaces move directly apart. Mode II is the sliding or in-plane shear mode where the crack surfaces slide over each other in a direction perpendicular to the crack front. Mode III is the

tearing or anti-plane shear mode, where the surfaces move away from each other and out of plane. Mode I and II are by far the most common in engineering problems. The notation for the stress intensity factor generally includes a subscript which denotes the deformation mode with which it is associated. For example, K_I is the stress intensity factor associated with deformation Mode I. Similarly, K_{II} and K_{III} denote the stress intensity factors for Mode II and Mode III, respectively [39].

3.2.1 Numerical Methods to Evaluate Stress Intensity Factor

Full scale testing is the preferred method for demonstrating compliance with damage tolerance requirements. However, it is expensive and time consuming. Numerical analysis based on Fracture Mechanics theory, has been extensively used in the aircraft industry as an alternative to full scale testing. The Finite Element Method (FEM) or the Boundary Element Method (BEM) can be used to perform numerical crack growth analysis based on LEFM concepts. Regardless of the numerical technique chosen, the design starts with creation of a complex discretized model representing the structure. Great care is required when creating such a model. Due to the presence of cracks, the model contains stress singularities at the crack tips and therefore the discrtization around the crack tips has to be fine, usually requiring a large number of elements. Moreover, the accuracy of the stiffener attachment model is very important for accuracy of the stress intensity factor predictions in stiffened panels. Finally, several iterations each simulating a different crack length has to be performed. The critical crack length corresponds to the crack size at which the stress intensity factor K at the crack-tip equals or just starts to exceed the critical value K_{IC}. Using the initial and final (or critical) crack sizes, fatigue

life of the panel is calculated. It is noted that, an initial crack is assumed to be already present in the structure during the analysis [25].

3.2.2 Advantages of using BEM over FEM

Since its introduction in the late 1960s, BEM has matured into a powerful alternative to FEM. BEM uses an analytical approach towards the solution taken by the adoption of weighting functions called fundamental solutions which satisfy the governing equation. In most cases, a formulation is obtained which does not contain integral over the problem domain and consequently does not require domain discretization. Therefore, only the boundary of the problem needs to be discretized into elements, resulting in substantial reduction in model preparation time as well as in a much smaller algebraic system of equations that needs to be solved. A fine discretization is still required near singularities. However, it is confined to the boundaries of the problem, requiring significantly fewer nodes and elements than FEM.

Another important feature of BEM is that the functions that represent essential and natural boundary conditions (displacements and stresses in elasticity theory) appear independently in the integral equation which is the basis for this method.

However, the main disadvantage of BEM is that the application to a new problem requires knowledge of the fundamental solutions of that problem. It also requires designing the procedures to perform all the integrations, a task that involves a great portion of the efforts to improve the accuracy of the method. However, moving from a certain problem to another is easy in FEM.

BEM techniques are particularly advantageous for problems involving singularities and moving boundaries such as crack propagation problems. If there is no

local problem and the interest is in the solution of the whole domain, it is typically said that the application of BEM, although feasible, would not be the best option. Since the present problem is about finding the stress intensity factor and the corresponding stress state around the crack tip, BEM is the right choice.

3.3 INTRODUCTION TO THE BOUNDARY ELEMENT METHOD

The elastic problem can be formulated through governing differential equations i.e., using equilibrium equations, compatibility equations and constitutive equations. The same can also be formulated in the integral form. To do so, several theorems which can be grouped under the generic name of reciprocity theorems are required. These theorems involve two tensional states; one corresponds to the actual problem and the other corresponds to an auxiliary state that can be taken in a convenient form in order to simplify the formulation of the actual problem under consideration. The theorem of virtual work and the second theorem of Betti are the most interesting of these general reciprocity theorems, because they lead to the two most effective numerical methods, the Finite Element Method and the Boundary Element Method. BEM is the area of interest in the present problem.

Consider an isotropic elastic body in space, with domain Ω and boundary Γ, geometrically defined in terms of Cartesian coordinate system $(x_i, i = 1,2,3)$. The body is subjected to volumetric forces acting within the domain. Rigid body movements are prevented by the application of displacement constraints at portions of the boundary. Under these conditions, any cubic element within the body domain is strained and stressed to certain extent. The state of stress in an element is defined by the stress tensor σ_{ij}. The static equilibrium equation for any such element of the body is expressed as,

$$\sigma_{ij,j} + b_i = 0 \tag{3-5}$$

where the first suffix in σ_{ij} indicates the direction of the normal to the plane on which the stress acts and the second suffix indicates the direction in which the stress acts and b_i is the applied body force per unit volume. The state of strain in any element can be expressed by Cauchy's infinitesimal strain tensor ε_{ij} as,

$$\varepsilon_{ij} = \frac{1}{2}(u_{i,j} + u_{j,i}) \tag{3-6}$$

where u_i are the displacements which are assumed to be small, such that the squares and products of their partial derivatives with respect to the cartesian axis can be neglected. The state of stress and strain is related through stress-strain or constitutive equations of the material as,

$$\sigma_{ij} = \lambda \delta_{ij} \varepsilon_{kk} + 2\mu \varepsilon_{ij} \tag{3-7}$$

where δ_{ij} is the Kronecker delta whose properties are,

$$\delta_{ij} = \begin{cases} 0 & i \neq j \\ 1 & i = j \end{cases} \tag{3-8}$$

λ and μ are known as Lame's constants. They can be expressed in terms of the material Young's modulus E and Poisson's ratio ν as,

$$\lambda = \frac{\nu E}{(1+\nu)(1-2\nu)} \tag{3-9}$$

$$\mu = \frac{E}{2(1+\nu)} \tag{3-10}$$

It is noted that the repeated suffixes are summed. Eq. (3-7) is sometimes referred to as the generalized Hooke's law. Differentiating Eq. (3-7) and re-substituting it into Eq. (3-5)

and replacing the strain components by their displacement derivatives using Eq. (3-6), gives the well known Navier's equation as given below:

$$\frac{1}{(1-2\nu)}u_{i,ij}+u_{j,ii}+\frac{1}{\mu}b_j=0 \tag{3-11}$$

Navier's equation is the governing differential equation of elasticity. It enforces static equilibrium and is expressed in terms of displacements. It is particularly convenient for the analysis of problems in which displacement boundary conditions are to be imposed. Frequently, however, boundary conditions in terms of stresses at the boundary have to be specified. Tractions, denoted by t_i, are stresses across a boundary surface. They can be expressed as,

$$t_i=\sigma_{ij}n_j \tag{3-12}$$

where n_j is a vector normal to the portion of the boundary surface where the tractions are being evaluated. Tractions and Displacements are the primary variables in the direct boundary element formulation [25,27].

3.3.1 The Boundary Integral Formulation for Elasticity

The direct boundary integral formulation for elasticity can be derived using one of the reciprocity theorems mentioned earlier. The second theorem of Betti is used here. It is stated as below:

Let an elastic body occupy a domain Ω with boundary Γ. If two distinct self-equilibrated states, (u_i,t_i,b_i) and (u_i^*,t_i^*,b_i^*) exist for the body, then the work done by the boundary tractions and body forces of the second state (*) on the displacements produced by the first is equal to the work done by the boundary tractions and body forces

of the first state on the displacements produced by the second. The theorem can be proved using the divergence theorem and can be written as,

$$\int_{\Gamma} u_i t_i^* d\Gamma + \int_{\Omega} u_i b_i^* d\Omega = \int_{\Gamma} u_i^* t_i d\Gamma + \int_{\Omega} u_i^* b_i d\Omega \tag{3-13}$$

The above equation is re-arranged in the form of generalized Green's formula as,

$$\int_{\Omega} (u_i b_i^* - u_i^* b_i) d\Omega = \int_{\Gamma} (u_i^* t_i - u_i t_i^*) d\Gamma \tag{3-14}$$

Let us consider that the domain Ω is contained within a general region Ω^*, with the same elastic properties and bounded at infinity by Γ^* as illustrated in Figure 3-2.

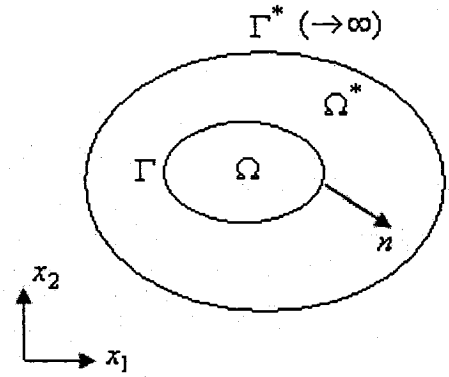

Figure 3-2: A domain within a general region bounded at infinity [25]

The displacements u_i^* and tractions t_i^* are chosen to satisfy the governing Navier's equation given in Eq. (3-11) for the special case of a body force b_i^* corresponding to a unit point body force such that,

$$\frac{1}{(1-2\nu)} u_{i,ij}^* + u_{j,ii}^* + \frac{1}{\mu} b_j^* = 0 \tag{3-15}$$

A unit point body force can be conveniently defined as,

$$b_i^* = \Delta(X - X') e_i \tag{3-16}$$

where $\Delta(X - X')$ is the Dirac delta function, $X' \in \Omega^*$ is the point where the unit load is applied, $X \in \Omega^*$ is any field point and e_i is the unit vector component corresponding to a unit point force in the direction i applied at X'. The definition properly represents a unit point force applied to a point in the domain Ω^*, because the Dirac delta function has the following property,

$$\int_{\Omega^*} g(X)\Delta(X - X')d\Omega^*(X) = g(X') \tag{3-17}$$

The displacements and traction fields, corresponding to the fundamental solutions can be written as,

$$u_i^* = u_j^*\delta_{ij} = U_{ij}(X, X')\delta_{ij}e_i \tag{3-18}$$

$$t_i^* = t_j^*\delta_{ij} = T_{ij}(X, X')\delta_{ij}e_i \tag{3-19}$$

where $U_{ij}(X, X')$ and $T_{ij}(X, X')$ represent the displacements and tractions in the j direction at a field point X, corresponding to a unit point force acting in the i direction applied at the source point X'. $U_{ij}(X, X')$ and $T_{ij}(X, X')$ are known functions, called Fundamental Solutions.

Eq. (3-14) can now be re-written by substituting b_i^* by the Dirac delta representation as in Eq. (3-16), u_i^* and t_i^* by their fundamental solutions represented by Eqs. (3-18) and (3-19) and defining $X \in \Omega$ and $x \in \Gamma$ to be the integration variables as,

$$\int_{\Omega}[u_i(X)\Delta(X - X') - U_{ij}(X, X')b_j]d\Omega(X) = \int_{\Gamma}[U_{ij}(x, X')t_j(x) - T_{ij}(x, X')u_j(x)]d\Gamma(x) \tag{3-20}$$

which corresponds to a unit point force acting in the i direction. Rearranging and using the properties of the Dirac delta function, Eq. (3-20) becomes,

$$u_i(X') = \int_{\Gamma} U_{ij}(x,X')t_j(x)d\Gamma(x) - \int_{\Gamma} T_{ij}(x,X')u_j(x)d\Gamma(x) + \int_{\Omega} U_{ij}(X,X')b_j(X)d\Omega(X) \tag{3-21}$$

The above Eq. (3-21) is a well known Somigliana's identity. It provides a continuous integral representation for the displacements at any interior point X' in the domain Ω. The strains at any interior point can be obtained by differentiating the displacements in above Eq. (3-21) with respect to the source point X' to give,

$$u_{i,k}(X') = -\int_{\Gamma} U_{ij,k}(x,X')t_j(x)d\Gamma(x) + \int_{\Gamma} T_{ij,k}(x,X')u_j(x)d\Gamma(x) - \int_{\Omega} U_{ij,k}(X,X')b_j(X)d\Omega(X) \tag{3-22}$$

where the derivatives of the fundamental fields $U_{ij,k}$ and $T_{ij,k}$ are taken with respect to the field point. Finally, Somigliana's identity for stresses can be obtained by substituting Eq. (3-22) into Hooke's law [Eq. (3-7)] resulting in the following integral equation,

$$\sigma_{ij}(X') = \int_{\Gamma} D_{kij}(x,X')t_k(x)d\Gamma(x) - \int_{\Gamma} S_{kij}(x,X')u_k(x)d\Gamma(x) + \int_{\Omega} D_{kij}(X,X')b_k(X)d\Omega(X) \tag{3-23}$$

where D_{kij} and S_{kij} contain several derivatives of $U_{ij,k}$ and $T_{ij,k}$ respectively, in addition to elastic constants.

The point force fundamental solutions used in the preceding equations are known as Kelvin's solutions. For an isotropic homogeneous material under plane strain conditions, fundamental solutions as given by Cruse [25-28] are,

$$U_{ij}(x,x') = -\frac{1+\nu}{4\pi E(1-\nu)}\left\{(3-4\nu)\delta_{ij}\ln(r) - r_{,i}r_{,j}\right\} \tag{3-24}$$

$$T_{ij}(x,x') = -\frac{1}{4\pi(1-\nu)}\frac{1}{r}\left\{[(1-2\nu)\delta_{ij} + 2r_{,i}r_{,j}]r_{,k}n_{,k} - (1-2\nu)[n_j r_{,i} - n_i r_{,j}]\right\} \tag{3-25}$$

where x' is the source point, x is the field point, n is the unit outward normal to the boundary at the field point x, and $r(x,x')$ represents the distance between the source point x' and the field point x.

$$r(x,x') = \sqrt{r_i r_i} \tag{3-26}$$

$$r_i = x_i(x) - x_i(x') \tag{3-27}$$

The derivative of r with respect to the field point can be evaluated as,

$$r_{,i} = \frac{r_i}{r} \tag{3-28}$$

The fundamental fields D_{kij} and S_{kij} are given by,

$$D_{kij}(x,x') = \frac{1}{4\pi(1-\nu)}\frac{1}{r}\left\{(1-2\nu)(\delta_{ij}r_{,k} + \delta_{ki}r_{,j} - \delta_{jk}r_{,i}) + 2r_{,i}r_{,j}r_{,k}\right\} \tag{3-29}$$

$$S_{kij}(x,x') = \frac{E}{4\pi(1-\nu^2)}\frac{1}{r^2}\left\{\begin{array}{l} 2\dfrac{\partial r}{\partial n}[(1-2\nu)\delta_{ij}r_{,k} + \nu(\delta_{ik}r_{,j} + \delta_{jk}r_{,i}) - 4r_{,i}r_{,j}r_{,k}] \\ +2\nu(n_i r_{,j}r_{,k} + n_j r_{,i}r_{,k}) \\ +(1-2\nu)(2n_k r_{,i}r_{,j} + n_j\delta_{ik} + n_i\delta_{jk}) - (1-4\nu)n_k\delta_{ij}) \end{array}\right\} \tag{3-30}$$

The fundamental solutions for plane stress can be obtained by introducing the modified Poisson's coefficient ν^* and Young's modulus E^* as defined below:

$$\nu^* = \frac{1}{1+\nu};\ E^* = E(1+\nu^2)$$

Somigliana's identity is valid for any source point within the domain Ω. In order to obtain a solution for the posed boundary value problem with the boundary element method, it is necessary to apply the equation for a source point $x' \in \Gamma$. However, when $x' \in \Gamma$, the boundary integrals in equation has a singularity, because the fundamental solutions U_{ij} and T_{ij} given in Eqs. (3-24) and (3-25) are singular when $r(x',x) \to 0$. The same does not happen with the domain integrals which are not singular because for source points at the boundary, $r(x',X) \neq 0$. The boundary displacement equation for source point on the boundary can be written as [25-27],

$$c_{ij}u_i(x') = \int_\Gamma U_{ij}(x,x')t_j(x)d\Gamma(x) - \int_\Gamma T_{ij}(x,x')u_j(x)d\Gamma(x) + \int_\Omega U_{ij}(X,x')b_j(X)d\Omega(X) \tag{3-31}$$

where the coefficient c_{ij} depends on the geometry of the surface. For a smooth surface,

$$c_{ij} = \frac{1}{2}\delta_{ij} \tag{3-32}$$

3.3.2 Numerical Solution of the Problem

In order to solve the integral equations numerically, the boundary is discretized into a series of elements over which displacements and tractions are written at a series of nodal points. Writing the discretized form of Boundary Integral Equation at every nodal point, a system of linear algebraic equations is obtained. Once the boundary conditions are applied in known values of tractions and displacements, the system is solved to obtain the unknown values of tractions and displacements. Isoparametric continuous quadratic elements are used to discrtise the boundary as shown in Figure 3-3. Considering that

body forces are absent for simplicity, the displacement and tractions which apply over each element j are defined as,

$$\mathbf{u} = \phi u^j \; ; \; \mathbf{t} = \phi t^j \tag{3-33}$$

where u^j and t^j are the element nodal displacements and tractions, respectively.

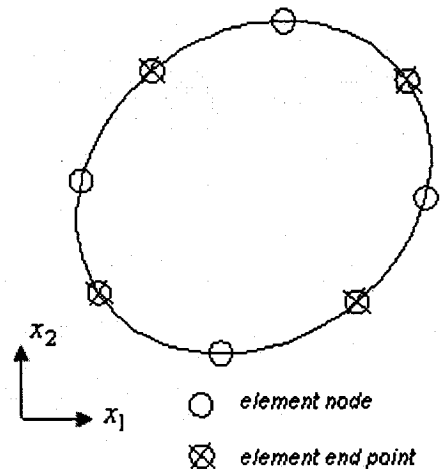

Figure 3-3: Discretization of boundary using continuous quadratic elements

A 3-node continuous quadratic element as shown in Figure 3-4 is considered to vary from -1 to +1 so that Gaussian Quadrature can be used while solving the integrals. Special Gaussian Quadrature is used for evaluating the integrals with singularity [40].

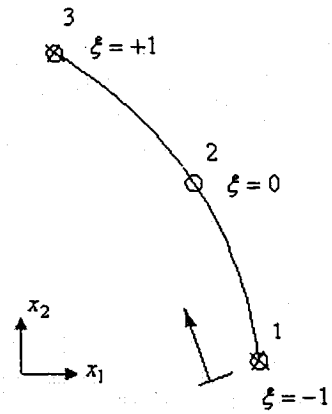

Figure 3-4: Three-noded continuous quadratic element

The shape functions for a continuous quadratic element are given as,

$$\phi_1 = \frac{1}{2}\xi(\xi - 1)$$

$$\phi_2 = (1 - \xi^2) \tag{3-34}$$

$$\phi_3 = \frac{1}{2}\xi(\xi + 1)$$

The displacements and tractions **u** and **t** are now represented as,

$$\mathbf{u} = \begin{bmatrix} \phi_1 & 0 & \phi_2 & 0 & \phi_3 & 0 \\ 0 & \phi_1 & 0 & \phi_2 & 0 & \phi_3 \end{bmatrix} \begin{Bmatrix} u_1^1 \\ u_2^1 \\ u_1^2 \\ u_2^2 \\ u_1^3 \\ u_2^3 \end{Bmatrix} \tag{3-35}$$

$$\mathbf{t} = \begin{bmatrix} \phi_1 & 0 & \phi_2 & 0 & \phi_3 & 0 \\ 0 & \phi_1 & 0 & \phi_2 & 0 & \phi_3 \end{bmatrix} \begin{Bmatrix} t_1^1 \\ t_2^1 \\ t_1^2 \\ t_2^2 \\ t_1^3 \\ t_2^3 \end{Bmatrix} \tag{3-36}$$

Discretizing the boundary and substituting Eq. (3-35) and (3-36) into Eq. (3-31), the following equation is obtained at any nodal point on the boundary:

$$c^i u^i + \sum_{j=1}^{NE} \left(\int_{\Gamma_j} T_{ij}\, \phi \, d\Gamma \right) \mathbf{u}^j = \sum_{j=1}^{NE} \left(\int_{\Gamma_j} U_{ij}\, \phi \, d\Gamma \right) \mathbf{t}^j \tag{3-37}$$

Note that the summation for $j = 1$ *to* NE indicates summation over all the NE elements on the boundary and Γ_j is the boundary of jth element. $\mathbf{u}^j$ and $\mathbf{t}^j$ are the nodal displacements and tractions in element j.

The integrals are solved numerically, since it is difficult to integrate analytically, particularly if the elements are curved. The interpolation functions ϕ_1, ϕ_2, ϕ_3 are expressed in a homogeneous system of coordinates as shown in Figure 3-4 with ξ as the local coordinate. The coordinates need to be transformed from Cartesian coordinates of the boundary to the nodal coordinates to define curved elements and this transformation involves a Jacobian defined as,

$$d\Gamma = \left\{ \sqrt{\left(\frac{dx_1}{d\xi}\right)^2 + \left(\frac{dx_2}{d\xi}\right)^2} \right\} d\xi = |J| d\xi \tag{3-38}$$

where J is called the Jacobian.

The system of equations can now be represented in compact form as,

$$c^i u^i + \sum_{j=1}^{N} \overline{H}^{ij} \mathbf{u}^j = \sum_{j=1}^{N} G^{ij} \mathbf{t}^j \tag{3-39}$$

$$\sum_{j=1}^{N} H^{ij} \mathbf{u}^j = \sum_{j=1}^{N} G^{ij} \mathbf{t}^j \tag{3-40}$$

where N is the number of nodes. The influence matrices H and G are defined as,

$$\overline{H}^{ij} = \sum_{j} \int_{\Gamma_j} T_{ij} \phi J \tag{3-41}$$

$$\begin{aligned} H^{ij} &= \overline{H}^{ij} && \text{if } i \neq j \\ H^{ij} &= \overline{H}^{ij} + c^i && \text{if } i = j \end{aligned} \tag{3-42}$$

$$G^{ij} = \sum_{j} \int_{\Gamma_j} U_{ij} \phi J \tag{3-43}$$

The contribution for all i nodes can now be written in a matrix form to give the global system of equations as,

$$H\ \mathbf{u} = G\ \mathbf{t} \tag{3-44}$$

The coefficients c^i can be obtained by rigid body considerations and the vectors **u** and **t** represent the values of displacements and tractions before applying the boundary conditions. The boundary conditions can be introduced by rearranging the columns in H and G, by passing all unknown displacements and tractions to a vector Y on the left hand side. This gives final system of equation as,

$$AY = F \tag{3-45}$$

where A is called the coefficient matrix, Y is the unknown vector containing the unknown displacements and tractions on the boundary and F is the constant vector. On solving the above system of equations, all the boundary unknown values are determined. Using Eq. (3-21) and (3-23), displacements and stresses for any point inside the body can be obtained using the complete solution of the boundary.

3.3.3 Numerical Example to Verify BEM Formulation

BEM formulation is implemented on a simple plate with unit thickness subjected to tensile load of $\sigma = 1000\,kg/cm^2$ at both the ends. The length of the plate is $L = 40\,cm$ and width is $W = 20\,cm$. The value of Elastic Modulus is $E = 2.1e6\,kg/cm^2$ and the Poisson's ratio is $\nu = 0.25$. The boundary of the plate is divided into 8 elements. To avoid rigid body motions, atleast 3 displacement boundary conditions should be applied for the structure. The meshing and boundary conditions are shown in Figure 3-5.

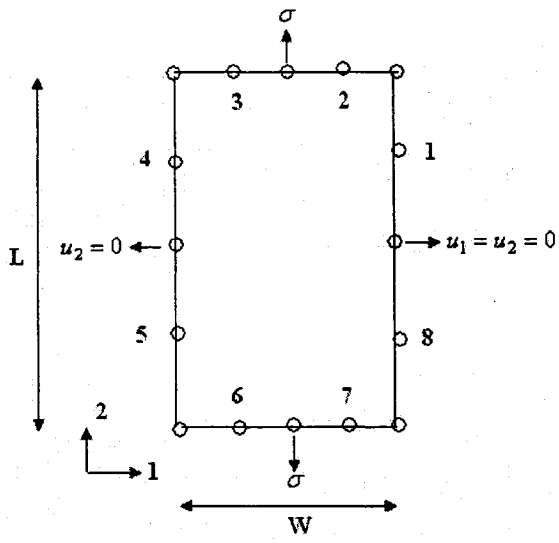

Figure 3-5: Boundary discretization and applied boundary conditions

Solving the system of equations, the maximum displacement at extreme nodes was obtained as 0.009592 *cm*. This result is in good agreement with FEM result, which was found to be 0.00982 *cm*. Figure 3-6 shows the maximum displacement in the plate obtained using PATRAN [45].

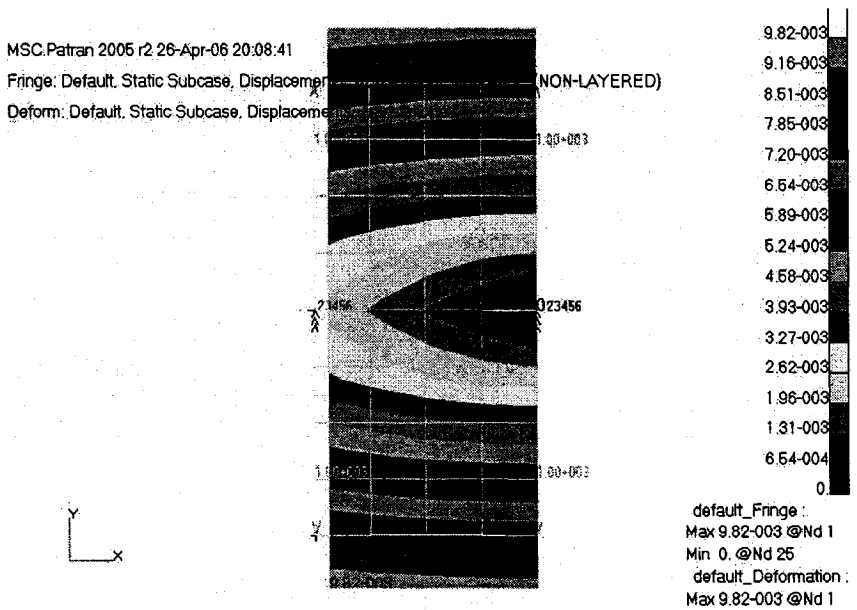

Figure 3-6: Displacements for a plate under tensile load at both ends

3.4 APPLICATION OF BEM TO SKIN-STRINGER PANELS

Most of the cracks in aerospace structures occur in high stress concentration regions like cutouts, edges or fasteners. Thin sheets of fuselage and wing structures usually incorporate stiffeners to reinforce their strength. It is therefore desirable to include the influence of these stiffeners when theoretically analyzing cracked panels if the results are to be applied for practical structural configurations. The Boundary Element Method is combined with the method of compatibility deformations to analyze the stress distributions in cracked finite sheets reinforced by bonded stiffeners [24-38].

3.4.1 Derivation of Governing Equations

Let us define a set of rectangular Cartesian coordinates x_1, x_2, x_3. Consider a flat isotropic sheet with a boundary described by the contour Γ in $\mathbf{x} \equiv (x_1, x_2)$ plane. The contour Γ is directed such that the interior of the sheet is to its left-hand side. Tractions (i.e. forces per unit thickness, per unit arc length) $t_j(\mathbf{x})$, where $(j = 1, 2)$ corresponds to the directions of x_1, x_2 on the boundary Γ and the sheet is loaded internally with force per unit arc length $f_j(\mathbf{x})$ from the stiffener attachment over a line, L_{st}. These loading conditions are accompanied by a displacement field $u_j(\mathbf{x})$ at points on the boundary Γ. The variables t_j, u_j and f_j $(j = 1, 2)$ in the configuration satisfying the integral equation based on Somigliana's identity of Eq. (3-31) is written as [35],

$$c_{ji}(\mathbf{x}_0)u_i(\mathbf{x}_0) = \int_{\Gamma} U_{ji}(\mathbf{x},\mathbf{x}_0)t_i(\mathbf{x})\,\mathrm{ds}(\mathbf{x}) - \int_{\Gamma} T_{ji}(\mathbf{x},\mathbf{x}_0)u_i(\mathbf{x})\,\mathrm{ds}(\mathbf{x})$$

$$+\frac{1}{t_s}\int_{L_{st}} U_{ji}(\mathbf{x},\mathbf{x}_0)f_i(\mathbf{x})\,\mathrm{ds}(\mathbf{x}) \qquad (3\text{-}46)$$

The coefficients $c_{ji}(\mathbf{x}_0)$ of the free term on the left hand side of Eq. (3-46) represent the contribution due to the concentrated force itself.

Expressions for the fundamental displacement solution $U_{ji}(\mathbf{x},\mathbf{x}_0)$ and the corresponding traction distribution $T_{ji}(\mathbf{x},\mathbf{x}_0)$ may be obtained from infinite sheet solutions. Eqs. (3-24) and (3-25) represent the fundamental solutions for displacement and traction respectively, obtained for a concentrated force in an intact infinite sheet, also known as the Kelvin's solutions [25-28]. Alternately, a fundamental solution derived by Erdogan [36] for a concentrated force in an infinite cracked sheet may be used. If the finite sheet to be modelled has a crack at the same location, then the conditions of $T_{ji}(\mathbf{x},\mathbf{x}_0)=0=t_i(\mathbf{x})$ on the crack locus makes the contribution from the crack itself identically zero to the boundary integral in Eq. (3-46). In this case, the crack need not be included as part of the boundary Γ and the solution of Eq. (3-46) will implicitly include the presence of the crack, along with the associated singular stress field at each crack tip. This integral equation will be used to represent a cracked sheet, using the Erdogan fundamental solutions as given in the Appendix.

Consider the following reinforced sheet configuration shown in Figure 3-7. An isotropic sheet of thickness t_s and tensile modulus E_{sk} and Poisson's ratio ν having a straight crack located at $\{-a \le x_1 \le +a, x_2 = 0\}$ and has distributions of traction $t_j(\mathbf{x})$ and displacement $u_j(\mathbf{x})$ on its boundary Γ. A stiffener is bonded to the sheet over the locus L_{st}. The stiffener exerts a line distribution of force per unit arc length $f_j(\mathbf{x})$, $(j = 1, 2)$ on the corresponding locus L_{st} on the sheet, and itself experiences an equal and opposite reaction force $-f_j(\mathbf{x})$ along its length.

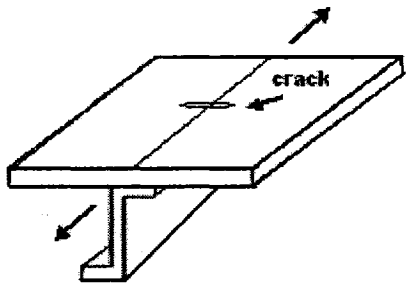

Figure 3-7: A skin-stringer panel reinforced by Z-type stringer with a crack subjected to tensile load

The material and structural parameters of the stiffener are as follows; L_{st} is the length of the stiffener, A_{st} is the cross-sectional area, I_{st} is second moment of area, E_{st} is the tensile modulus, G_{st} is the shear modulus and $D_{st} = E_{st} I_{st}$ is the transverse flexural rigidity. The conditions that the displacements of the sheet $u_j(\mathbf{x})$ and the stiffener $u_j^{st}(\mathbf{x})$ are compatible with shear deflection of the adhesive layer of thickness h_a and shear modulus G_a glued over a width w_a is given in terms of f_j, the interaction force per unit length as [35,37],

$$[u_j^{st}(\mathbf{x}') - u_j^{st}(\mathbf{x}'')] - [u_j(\mathbf{x}') - u_j(\mathbf{x}'')] = \frac{1}{w_a}\frac{h_a}{G_a}[f_j(\mathbf{x}') - f_j(\mathbf{x}'')] \qquad (3\text{-}47)$$

where $\mathbf{x}'$ and $\mathbf{x}''$ are distinct points on the stiffener locus L_{st}. The quantity $f_j(\mathbf{x})/w_a$ in the above equation corresponds to the shear stress in the adhesive layer. Combining Eqs. (3-46) and (3-47) gives the compatibility equation for points $\mathbf{x}'$ and $\mathbf{x}''$ on the stiffener locus L_{st} as,

$$[u_j^{st}(\mathbf{x}') - u_j^{st}(\mathbf{x}'')] - \int_{\Gamma}[\Delta U_{ji}\, t_i(\mathbf{x}) - \Delta T_{ji}\, u_i(\mathbf{x})]\,\mathrm{ds}(\mathbf{x})$$

$$= \frac{1}{t_s}\int_{L_{st}} \Delta U_{ji}\, f_i(\mathbf{x})\,\mathrm{ds}(\mathbf{x}) + \frac{h_a}{w_a G_a}[f_j(\mathbf{x}') - f_j(\mathbf{x}'')] \qquad (3\text{-}48)$$

The displacements u_j^{st} of the stiffener in the above Eq. (3-48) are most easily expressed in terms of an arc length parameter y measured in the longitudinal direction from one end as shown in Figure 3-8. The relative displacements of a thin stiffener due to a body force distribution $-f_i(y)$ per unit length ($0 < y \le L_{st}$) are given by,

$$u_1(y) - u_1(0) = [v_1(y) - v_1(0)]\cos\varphi - [v_2(y) - v_2(0)]\sin\varphi \tag{3-49}$$

$$u_2(y) - u_2(0) = [v_1(y) - v_1(0)]\sin\varphi + [v_2(y) - v_2(0)]\cos\varphi \tag{3-50}$$

where φ is the angle of orientation of the stiffener with respect to the x_2-direction, and the displacements v_1 and v_2 of the stiffener in its own transverse and longitudinal directions, respectively are in the form of,

$$\begin{aligned} v_1(y) - v_2(0) = {} & \frac{1}{A_{st}G_{st}}\left\{ yT_1(0) + \int_0^y (y-\eta) f_1(\eta)\, d\eta \right\} \\ & - \frac{1}{D_{st}}\left\{ \frac{1}{2}y^2 M(0) + \frac{1}{6}y^3 T_1(0) + \int_0^y \frac{1}{6}(y-\eta)^3 f_1(\eta)\, d\eta \right\} - y\beta_{21}(0) \end{aligned} \tag{3-51}$$

$$v_2(y) - v_2(0) = \frac{1}{A_{st}E_{st}}\left\{ yT_2(0) + \int_0^y (y-\eta) f_2(\eta)\, d\eta \right\} \tag{3-52}$$

where $T_1(y)$, $T_2(y)$ and $M(y)$ represent the internal forces and moment acting over the stiffener cross-section as shown in Figure 3-8 and $\beta_{21}(0)$ is the rigid body rotation consider at the stiffener starting point corresponding to y = 0. In addition, the conditions that the stiffener is in equilibrium under the action of the body forces $-f_j$ (y) and the end loads $T_1(0)$, $T_1(L_{st})$, $T_2(0)$, $T_2(L_{st})$ and moments $M(0)$, $M(L_{st})$ are given by,

$$\int_0^{L_{st}} f_1(y)\, dy = T_1(L_{st}) - T_1(0) \tag{3-53}$$

$$\int_0^{L_{st}} f_2(y)dy = T_2(L_{st}) - T_2(0) \tag{3-54}$$

$$\int_0^{L_{st}} (L_{st} - y) f_1(y)dy = M(L_{st}) - M(0) - L_{st}T_1(0) \tag{3-55}$$

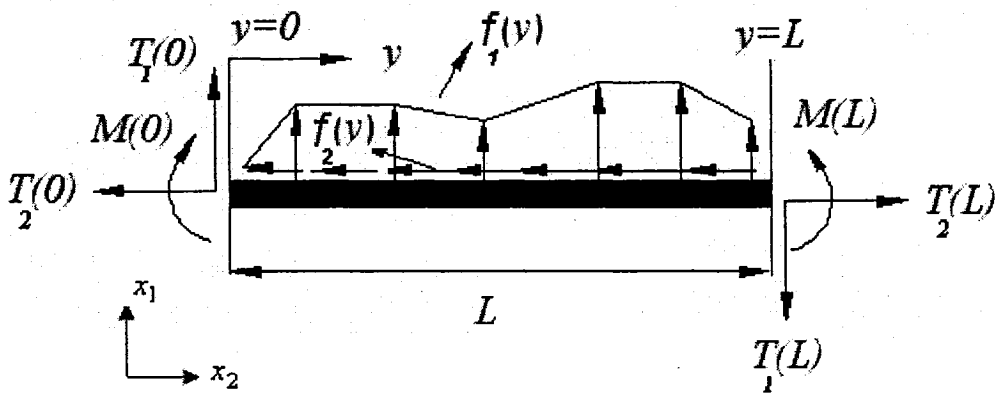

Figure 3-8: Isolated stiffener model

The end loads in above Eqs. (3-53), (3-54), (3-55) correspond to the boundary conditions for the stiffener. Setting all six values to zero will represent a stiffener with free ends.

3.4.2 Discretization and Numerical Solution of the Problem

For a given loading constraint on the reinforced sheet configuration, it is possible to determine the complete solution for the tractions and displacements on the boundaries of the sheet and the reaction force distribution due to the stiffener. In order to use the equations derived in the previous section, the problem is discritized so that the integral equations may be reduced to a set of simultaneous linear equations. The boundary Γ of the sheet is subdivided using continuous quadratic elements, each containing three nodes, one at each end and one at the centre of the element. Hence, the boundary integrals in Eqs. (3-46) and (3-48) reduce to linear combinations of the nodal values of traction and displacement. The coefficients of the nodal boundary values are in the form of integrals,

which are evaluated numerically by Gaussian quadrature. The integrals involving the stiffener forces $f_j(\mathbf{x})$ in Eqs. (3-46) and (3-48) may be treated similarly to those involving the boundary tractions $t_j(\mathbf{x})$. The locus of the stiffener reinforcement is subdivided into quadratic elements and the integrals occurring similarly reduce to linear sums of the nodal values of stiffener.

If the sheet boundary Γ incorporates N nodes and the stiffener locus incorporates Ns nodes, then the simultaneous linear equations will involve $(2N+2Ns+1)$ unknowns comprising the following: two unknowns out of t_1, t_2, u_1, u_2 at each node of the sheet boundary Γ, two unknowns of the attachment forces f_1, f_2 at each node on the stiffener locus and one end condition $\beta_{21}(0)$ of the stiffener. Hence, the required number of equations is generated as follows:

(a) Eq. (3-46) gives $2N$ simultaneous linear equations by taking the source point (collocation point) $\mathbf{x}_0$ at each of the N nodes on Γ and the unit force fundamental solution to be in the $j=1$ or $j=2$ direction.

(b) Eq. (3-48) gives $2(Ns-1)$ simultaneous linear equations by fixing the source point $\mathbf{x}''$ at one end ($y=0$) of the stiffener in turn taking the other source point $\mathbf{x}'$ to be at each of the remaining nodes in the stiffener locus in $j=1$ or $j=2$ direction.

(c) Eqs. (3-53), (3-54) and (3-55) give three simultaneous linear equations for force and moment equilibrium of the stiffener.

3.4.3 Evaluation of Stress Intensity Factor

Solving the system of equations formulated using the above set of equations, the complete solution of displacements and tractions on the boundary and distributions of

attachment forces on the stiffener are determined. Thus, the values of stress at any internal point of the sheet can be obtained. Using Hooke's Law and the linear elastic strain displacement definitions, components of stress σ_{jk} $(j,k=1,2)$ may be expressed as linear combinations of the partial derivatives of displacement evaluated at the internal point, say $\mathbf{X}$ as,

$$\sigma_{jk}(\mathbf{X}) = \frac{E}{(1+\nu)}\left[\frac{1}{2}\left\{\frac{\partial u_j}{\partial x_{0k}}(\mathbf{X}) + \frac{\partial u_j}{\partial x_{0k}}(\mathbf{X})\right\} + \frac{\nu}{(1-\nu)}\frac{\partial u_m}{\partial x_{0m}}(\mathbf{X})\,\delta_{jk}\right] \qquad (3\text{-}56)$$

where m denotes the summation of indices.

The derivatives are obtained from Eq. (3-46), and take the form of an integral formula given by the right-hand side of Eq. (3-46) with kernals $U_{ji}(\mathbf{x},\mathbf{x}_0)$ and $T_{ji}(\mathbf{x},\mathbf{x}_0)$ replaced by their derivatives, $G_{kji}(\mathbf{x},\mathbf{X})$ and $H_{kji}(\mathbf{x},\mathbf{X})$, with respect to the spatial coordinate x_{0k} $(i,j,k=1,2)$.

$$\frac{\partial u_i}{\partial x_{0k}}(\mathbf{X}) = \int_{\Gamma} G_{kji}(\mathbf{x},\mathbf{X})\,t_i(\mathbf{x})\,\mathrm{ds}(\mathbf{x}) - \int_{\Gamma} H_{kji}(\mathbf{x},\mathbf{X})\,u_i(\mathbf{x})\,\mathrm{ds}(\mathbf{x})$$

$$+\frac{1}{t_s}\int_{L_{st}} G_{kji}(\mathbf{x},\mathbf{X})\,f_i(\mathbf{x})\,\mathrm{ds}(\mathbf{x}) \qquad (3\text{-}57)$$

where $\mathbf{X}$ is an internal point, $\mathbf{x}\in\Gamma$, $i,j,k=1,2$ and

$$G_{kji}(\mathbf{x},\mathbf{X}) = \frac{\partial}{\partial x_{0k}} U_{ji}(\mathbf{x},\mathbf{X}) \text{ and } H_{kji}(\mathbf{x},\mathbf{X}) = \frac{\partial}{\partial x_{0k}} T_{ji}(\mathbf{x},\mathbf{X}) \qquad (3\text{-}58)$$

When the cracked sheet fundamental solution is used, the stress is infinite at the tips of the crack. By taking a series expansion of the differentiated kernels about either crack tip, $\mathbf{X}=(\pm a,0)$, the kernels $G_{kji}(\mathbf{x},\mathbf{X})$ and $H_{kji}(\mathbf{x},\mathbf{X})$ depend locally on the inverse

square root of the distance from **X** to the tip (Appendix). The Stress Intensity Factor can be defined as,

$$K_I = \lim_{\substack{r\to 0 \\ \phi=0}} \sqrt{2\pi r}\,\sigma_{22}(\mathbf{X}) \tag{3-59}$$

r,ϕ are polar coordinates centered at the crack tip, such that $\mathbf{X} = (\pm a \pm r\cos\phi, r\sin\phi)$. Kernel functions, G^*_{kji} and H^*_{kji}, for the stress intensity factor may be analytically extracted from the singular leading terms in the series expansions of G_{kji} and H_{kji} about the crack tip, i.e.

$$G^*_{kji}(\mathbf{x},\pm a) = \lim_{\substack{r\to 0 \\ \phi=0}} \sqrt{2\pi r}\,G_{kji}(\mathbf{x},\mathbf{X}) \tag{3-60}$$

$$H^*_{kji}(\mathbf{x},\pm a) = \lim_{\substack{r\to 0 \\ \phi=0}} \sqrt{2\pi r}\,H_{kji}(\mathbf{x},\mathbf{X}) \tag{3-61}$$

From the same procedure as that used to obtain the internal stresses from Eq. (3-56), the stress intensity factor can be obtained by replacing G_{kji} and H_{kji} by G^*_{kji} and H^*_{kji} in Eq. (3-57). Thus, the stress intensity can be calculated directly from the boundary and attachment force solution. The integrals in Eq. (3-57) are reduced to linear expressions in terms of the nodal values from the solution in the same way as described previously. Since the point **X**, is always interior to the boundary Γ, the boundary integrals in Eq. (3-57) require no special treatment and may be evaluated using Gaussian quadrature. Provided **X** does not lie on one of the stiffener loci, the same approach may be used to evaluate the integrals over L_{st} in Eq. (3-57).

3.4.4 Additional Considerations

Some of the practical aspects of this method are mentioned below. These additional considerations should be strictly followed to apply this method.

(a) When considering crack problems, nodes may not be positioned on the crack itself. The cracked sheet fundamental solution is discontinuous across the crack locus and any crack line nodes must lie at a small distance on one side or the other.

(b) In some configurations, stiffener locus L_{st} or boundary Γ may overlap. On such an intersection, all nodes of Γ and L_{st} must coincide exactly.

(c) Integrals involving functions $T_{ji}(\mathbf{x},\mathbf{x}_0)$ and $H_{kji}(\mathbf{x},\mathbf{x}_0)$ in equations may be handled more easily in terms of the functions $Y_{ji}(\mathbf{x},\mathbf{x}_0)$ and $Z_{kji}(\mathbf{x},\mathbf{x}_0)$ defined by,

$$Y_{ji}(\mathbf{x},\mathbf{x}_0) \equiv \frac{d}{ds(x)} Y_{ji}(\mathbf{x},\mathbf{x}_0) \tag{3-62}$$

$$H_{kji}(\mathbf{x},\mathbf{x}_0) \equiv \frac{d}{ds(x)} Z_{kji}(\mathbf{x},\mathbf{x}_0) \tag{3-63}$$

A function $Z^*_{kji}(\mathbf{x},\mathbf{x}_0)$ may be similarly defined from $H^*_{kji}(\mathbf{x},\mathbf{x}_0)$ for calculating the stress intensity factor. Integrating by parts, the result looks as,

$$\int_\Gamma T_{ji}(\mathbf{x},\mathbf{x}_0) u_i(\mathbf{x})\, \mathrm{ds}(\mathbf{x}) = [Y_{ji}(\mathbf{x},\mathbf{x}_0) u_i(\mathbf{x})]_\Gamma - \int_\Gamma Y_{ji}(\mathbf{x},\mathbf{x}_0) \frac{du_i(x)}{d\gamma} d\gamma \tag{3-64}$$

$$\int_\Gamma H_{kji}(\mathbf{x},\mathbf{x}_0) u_i(\mathbf{x})\, \mathrm{ds}(\mathbf{x}) = [Z_{kji}(\mathbf{x},\mathbf{x}_0) u_i(\mathbf{x})]_\Gamma - \int_\Gamma Z_{kji}(\mathbf{x},\mathbf{x}_0) \frac{du_i(x)}{d\gamma} d\gamma \tag{3-65}$$

where γ is a parameter which varies continuously along each element on the boundary Γ. Choosing γ to be local parameter in the elemental isoparametric transform (for which

$u_i(\mathbf{x})$ is quadratic in γ), the derivatives $\frac{du_i(x)}{d\gamma}$ in equations may be expressed in terms of the nodal displacements and linear derivatives of the shape functions. The forms of functions $Y_{ji}(\mathbf{x},\mathbf{x}_0)$ and $Z_{kji}(\mathbf{x},\mathbf{x}_0)$ are simpler to the corresponding $T_{ji}(\mathbf{x},\mathbf{x}_0)$ and $H_{kji}(\mathbf{x},\mathbf{x}_0)$, and are less expensive to evaluate. Details of this are given in the appendix, It can be observed that $Y_{ji}(\mathbf{x},\mathbf{x}_0)$ is of the similar form to the displacement function $U_{ji}(\mathbf{x},\mathbf{x}_0)$.

3.4.5 Calculation of Fatigue Life of the Panel

Using the analysis in section 3.4.3, stress intensity factor for skin-stringer panel is evaluated at the crack tip corresponding to the initial crack length a_i. This process is repeated by incrementing the crack length by a small amount (say Δa), until the critical crack length (a_c or final crack length a_f) is obtained. Critical crack length corresponds to the crack length at which the crack tip stress intensity factor equals or just starts to exceed the Fracture Toughness (K_{IC}) of the material of the skin. A general relationship between the rate of crack propagation and the range of the stress intensity factor was first made by P. C. Paris as part of his research work, universally known as the Paris's Law [24,25]. The fatigue life of the panel is determined using Paris's Law as,

$$N_{if} = \frac{1}{C_p} \int_{a_i}^{a_c = a_f} \frac{1}{[\Delta K_e]^{m_p}} da \tag{3-66}$$

where C_p and m_p are called Paris's constants and ΔK_e is the effective stress intensity factor. The effective stress intensity factor can be written as,

$$\Delta K_e = S\Delta\sigma\sqrt{\pi a} \tag{3-67}$$

where S is a numeric constant which depends on the geometry on the crack and $\Delta\sigma$ is the tension stress range for constant amplitude loading. Substituting Eq. (3-66) and integrating, we obtain a closed form solution to calculate the fatigue life of the panel as,

$$N_{if} = \frac{a_f^{1-mp/2} - a_i^{1-mp/2}}{C_p(S\Delta\sigma\sqrt{\pi})^{mp}(1-m_p/2)} \tag{3-68}$$

It should be noted that the above equation is valid only for constant amplitude loading.

3.5 DESIGN OPTIMIZATION OF SKIN-STRINGER PANEL

In order to formulate the above analysis into a general design optimization problem for a skin-stringer panel with a straight crack on the skin, the boundary discretization of skin as well as stringer is parameterized in terms of b_s and length of the stiffener (L_{st}). Once the number of elements required to discretize the skin and stringer boundaries is decided, it is very easy to define the coordinates of all the nodes in terms of b_s and L_{st} as shown in Figure 3-9. Considering an initial crack of length $2a$ at $-a \le x_1 \le +a, x_2 = 0$, the origin is considered at the center of the crack to define the coordinates of the nodes. Since the center of the crack and center of the panel coincide here, it is now easy to define the location of all the nodes on skin and stiffener. It is to be noted that the optimization is done for constant amplitude tensile loading and hence stress is assumed to vary from 0 to a maximum value of the stress. An initial crack of length $2a_i$ is assumed to be present in the skin. The objective is to minimize the mass of the panel with fatigue life of the panel as constraint to obtain optimum values for design variables t_s and b_s.

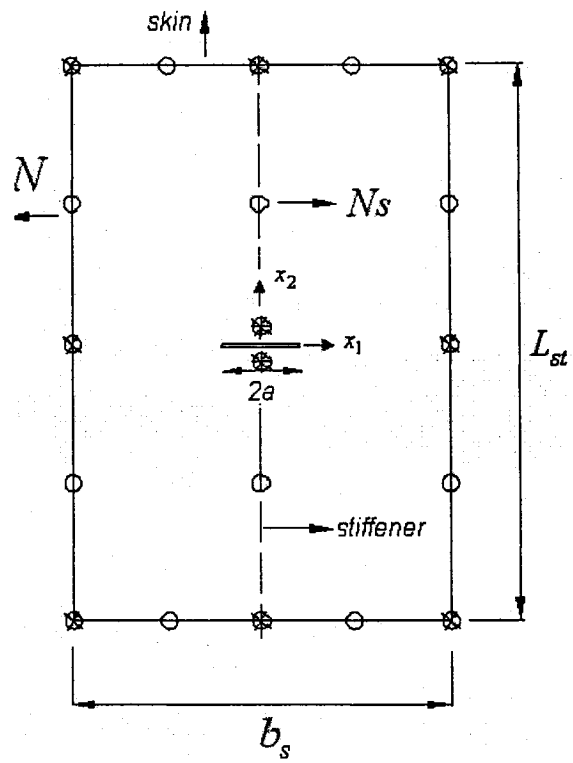

Figure 3-9: Parametric discretization of skin-stringer panel

3.6 VALIDATION OF RESULTS

(A) The above methodology is tested on a stiffened sheet with an edge crack as demonstrated in the work of Young *et. al.* [35]. The structure is shown in Figure 3-10 and details are given below:

The rectangular sheet of thickness $0.15mm$ has dimensions of $0 \le x_1 \le 90\,mm$ and $-90 \le x_2 \le +90\,mm$ and contains an edge-crack of length $a = 14.99\,mm$ located at $0 \le x_1 \le a, x_2 = 0$. The left hand tip of the crack in the fundamental solution is located outside the boundary of the sheet and does not affect the solution. The sheet is uniaxially loaded with values of traction $t_2 = \pm\sigma$ ($\sigma = 1$GPa) on the edges at $x_2 = \pm 90\,mm$ and all other tractions on the boundary are zero. A stiffener of length L_{st}=$120mm$ parallel to x_2-direction is bonded to sheet at position $x_1 = 15\,mm,\ -60 \le x_2 \le +60\,mm$. An adhesive

layer of thickness $0.15mm$ is attached over a width of $3mm$ on to the stiffener. The cross-sectional area of the stiffener used is 6 mm^2 and the ends of the stiffener at y=0 and y=$120mm$ (corresponding to $x_2 = -60mm$, $x_2 = 60mm$ respectively) are loaded with $T_2(0) = T_2(L_{st}) = \sigma A_{st} E_{st} / E_{sk}$, so that locally the ends automatically deform with the sheet.

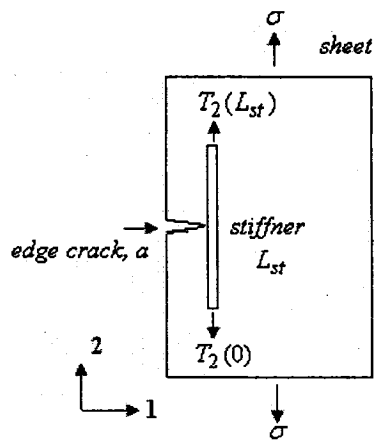

Figure 3-10: Stiffened Sheet with edge crack configuration

Material properties of Sheet: Modulus of Elasticity = 70GPa; Poisson's ratio = 0.3.

Material properties of Adhesive Bond: Shear Modulus = 0.6GPa.

Material properties of Stiffener: Modulus of Elasticity =70GPa; Shear Modulus=27GPa; Transverse Flexural Rigidity=175 GPa/mm^{-4}.

The boundary of the sheet is discretized using 16 quadratic elements and the stiffener is discretized with 8 quadratic elements. The value of the normalized stress intensity factor ($\frac{K_I}{\sigma\sqrt{\pi a}}$, where K_I is the stress intensity factor at the crack tip), obtained at the crack tip is 0.973. It is noted that the normalized stress intensity factor obtained by Young *et. al.* [35] is 1.090.

(B) Now, the analysis is used to verify the accuracy of the optimization process on different lower wing skin-stringer panels. Since there are no existing values to compare, the optimization is tested on the same compression panels designed for Aircraft-2 and 3 in Chapter 2. If the values of the design variables for lower panels are approximately around the same values of the compression panels, the optimization process can be taken to be converging to the required solution.

The value of stiffening ratio is taken as, SR = 0.5, while the width ratio is taken as, BR = 1 allowing he skin to be fully effective. The effective stress acting on the panel is calculated easily from the load intensity, N using Eq. (2-24). This value of stress is taken as the effective tensile stress acting on the lower wing panel to carry out the design optimization with fatigue life as constraint. In actual practice, the value of stress acting on a compressive panel is more than in tension panel.

All the panels are assumed to have an initial half crack of length $a_i = 0.025 in$ at the center of the skin. The values for Paris's constants are taken as C_p=1e-12 and m_p=3. Modulus of Elasticity in tension for both skin and stringer material is taken as $E = 10.3e6 psi$ with a Poisson's ratio of $\nu = 0.3$. Fracture toughness for aluminum is taken as, $K_{IC} = 26 ksi - in^{1/2}$. An adhesive material of thickness equal to the thickness of the skin (t_s), over a width of stringer upper flange (b_a) is used to attach the stringer to the skin. The shear modulus of adhesive used is 87000psi. The type of stringer considered in all the 3 panels is Z-type with equal flanges.

(a) For panel#1, a constant amplitude fatigue load with a peak value of 51823 psi is applied. The optimum dimensions for design variables obtained after the optimization

are $0.202in$ and $5.973in$ for thickness of skin and width of panel, respectively. The final half crack length is found to be $a_f = 0.0801in$. The fatigue life obtained is 4361 *cycles*. Table 3-1 shows the optimum dimensions for design variables for Compressive Design (CD) as well as Fatigue Design (FD).

(b) For panel#3, a constant amplitude fatigue load with a peak value of 47692 *psi* is applied. The optimum dimensions for design variables obtained after the optimization are $0.24in$ and $5.89in$ for thickness of skin and width of panel, respectively. The final half crack length is found to be $a_f = 0.0946in$. The fatigue life obtained is 6160 *cycles*. Table 3-2 shows the optimum dimensions for design variables for Compressive Design (CD) as well as Fatigue Design (FD).

(c) For panel#4, a constant amplitude fatigue load with a peak value of 46914 *psi* is applied. The optimum dimensions for design variables obtained after the optimization are $0.23in$ and $5.82in$ for thickness of skin and width of panel, respectively. The final half crack length is found to be $a_f = 0.0977in$. The fatigue life obtained is 6582 *cycles*. Table 3 shows the optimum dimensions for design variables for Compressive Design (CD) as well as Fatigue Design (FD).

It can be observed from Tables 3-1 to 3-3 that the values for the design variables obtained for Fatigue Design are in the same range of the Compressive Design. Hence, it can be concluded that the optimization routine developed gives appropriate results.

Table 3-1: Test Panel #1 of Aircraft 2

	AC2 compressive axial load (16200 *lb/in*)	CD compressive axial load (16200 *lb/in*)	FD traction on skin (51823 *psi*)
L (*in*)	26.0	26.0	26.0
b_s (*in*)	5.0	4.8873	5.973
t_s (*in*)	0.15	0.2084	0.202

Table 3-2: Test Panel #3 of Aircraft 3

	AC2 compressive axial load (18600 *lb/in*)	CD compressive axial load (18600 *lb/in*)	FD traction on skin (47692 *psi*)
L (*in*)	25.0	25.0	25.0
b_s (*in*)	5.350	5.32	5.89
t_s (*in*)	0.196	0.26	0.24

Table 3-3: Test Panel #4 of Aircraft 3

	AC2 compressive axial load (19000 *lb/in*)	CD compressive axial load (19000 *lb/in*)	FD traction on skin (46914 *psi*)
L (*in*)	25.0	25.0	25.0
b_s (*in*)	5.350	5.40	5.82
t_s (*in*)	0.196	0.27	0.23

AC2, AC3- Aircraft 2, Aircraft 3
CD- Compressive Design using the Present Method (Refer to section 2.5 of Chapter 2)
FD- Fatigue Design

3.7 CONCLUSIONS AND LIMITATIONS

(a) Boundary Element Method has been used to model thin, cracked, finite sheet reinforced by bonded stiffener. It is assumed that the reinforced structure undergoes plane deformation only.

(b) The fundamental solution used in the boundary integral equation for the sheet avoids the need to satisfy the boundary conditions on the crack surface and leads to an exact modeling of the crack-tip singularities.

(c) Solutions are obtained numerically by subdividing the domains of integrations into quadratic isoparametric elements, giving a system of simultaneous linear equations in terms of nodal values of traction and displacement on the boundary and attachment force over the reinforced regions. Values of stress intensity factors of the crack are subsequently calculated numerically from integral formulae.

(d) The geometry of the configurations which may be studied is limited to cases where the crack can be described by a single straight line and must lie at the center of the sheet.

(e) It is noted that the entire structure does not bend out of plane and it is linearly elastic.

CHAPTER 4

DESIGN OPTIMIZATION OF A WING SECTION

4.1 DLR-F6 WING GEOMETRY

In order to test the optimization routines (developed in Chapters 2 and 3 for upper and lower wing panels, respectively), a test wing section is taken from DLR-F6 aircraft [41]. The actual wind tunnel model geometry of the aircraft is shown in Figure 4-1.

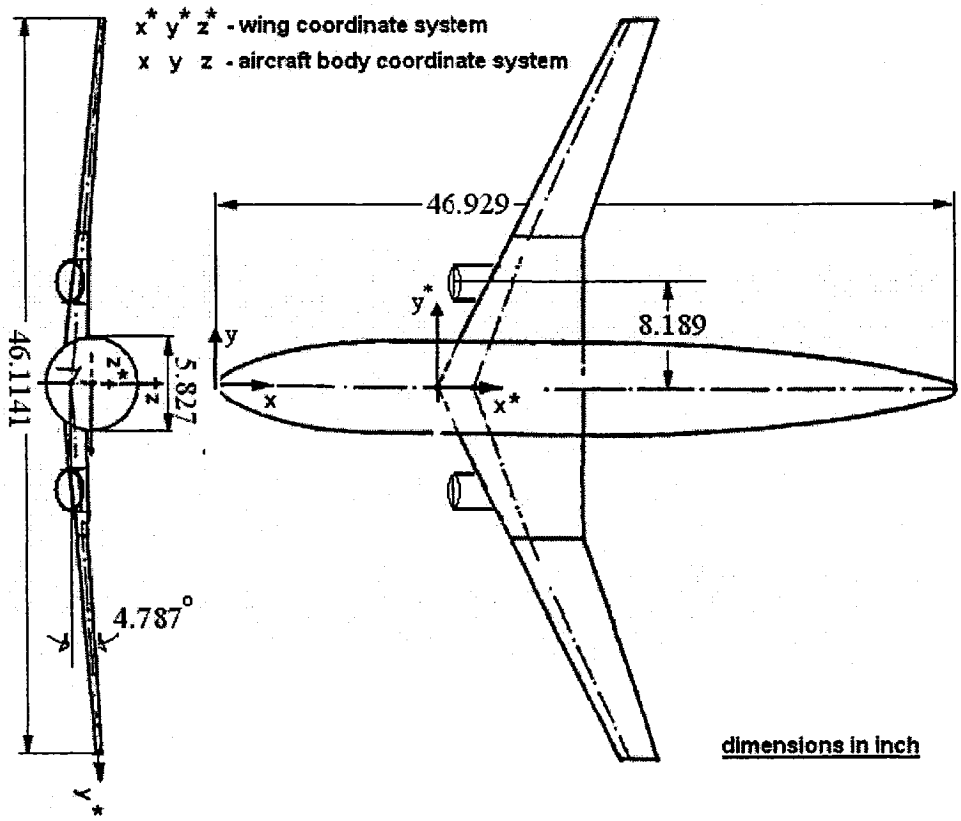

Figure 4-1: DLR-F6 Wind Tunnel Model Geometry [41]

Axes x, y, z denote the aircraft coordinate system and axes x^*, y^*, z^* refer to the wing coordinate system. Nacelles are located at 8.189 *in* from wing's origin on either side of the fuselage. The projected wing semi-span is 23.0571 *in*. The wing is defined by a number of airfoil sections at different stations along the wing semi-span as shown in

Figure 4-2, where η is the normalized coordinate, defined as $\eta = \frac{y^*}{s^*}$. The shape of the airfoil section at each station is designed according to the aerodynamic considerations.

In order to test the design optimization routines, the wind tunnel model geometry in Figure 4-1 is scaled by a factor of $\lambda = 20$ to build an approximately realistic aircraft. The wing reference area for the scaled model is $S = 90148\ in^2$ and the semi-span in wing coordinate system is $s^* = 463.3\ in$. The average chord length of the wing is $C_{av} = 97.746\ in$ and the mean aerodynamic chord length is $C_{mac} = 111.18\ in$.

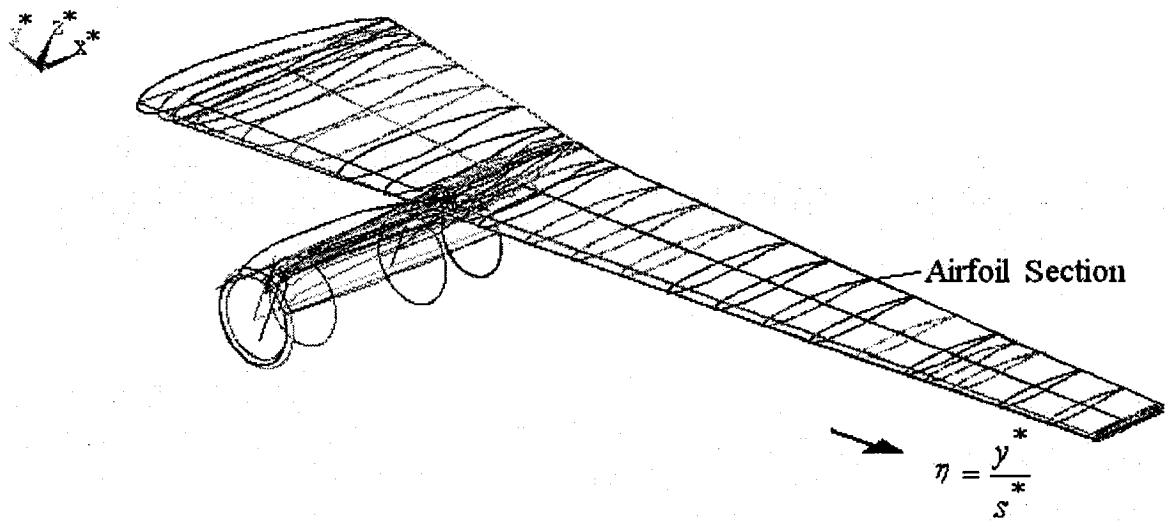

Figure 4-2: DLR-F6 Wing showing different airfoil sections [41]

A test wing section defined by connecting two airfoil sections defined at stations $\eta = 0.6854$ and $\eta = 0.7304$ is selected. The length of the panel (distance between these two stations) is $L = 20.8153 in$. The airfoil section shapes at stations $\eta = 0.6854$ and $\eta = 0.7304$ are plotted as shown in Figure 4-3 and Figure 4-4, respectively. The front

spar is positioned at 15% of chord and the rear spar at 65% of chord [1-3]. The enclosed area between the spars is called the wing-box.

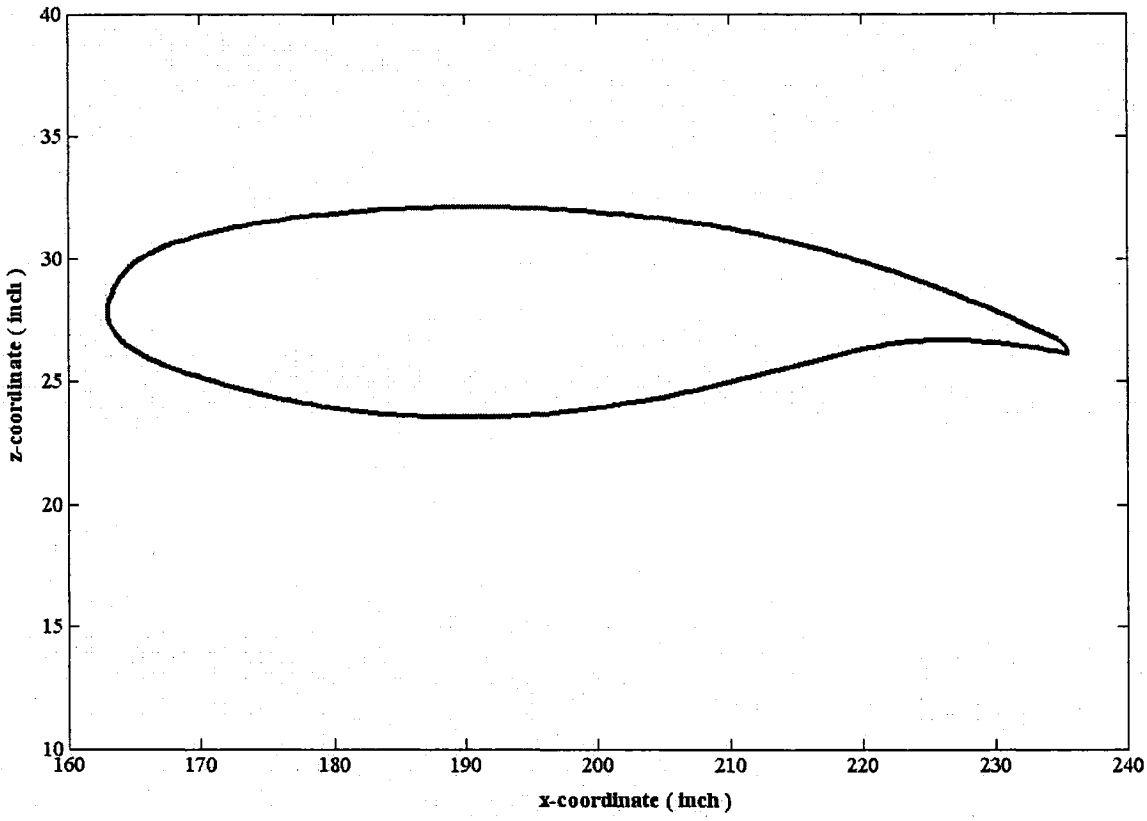

Figure 4-3: DLR-F6 Airfoil section geometry defined at station $\eta = 0.6854$

Figure 4-5 shows the test wing section defined between the two stations $\eta = 0.6854$ and $\eta = 0.7304$. The important dimensions of this tapered wing section are essentially the dimensions of skin-stringer panels that make up the wing-box. However, obtaining the optimum web thickness value for the front and rear spars and also the dimensions of their corresponding upper and lower web caps are not considered in this work. Therefore, suitable approximate dimensions are assumed for them during the analysis.

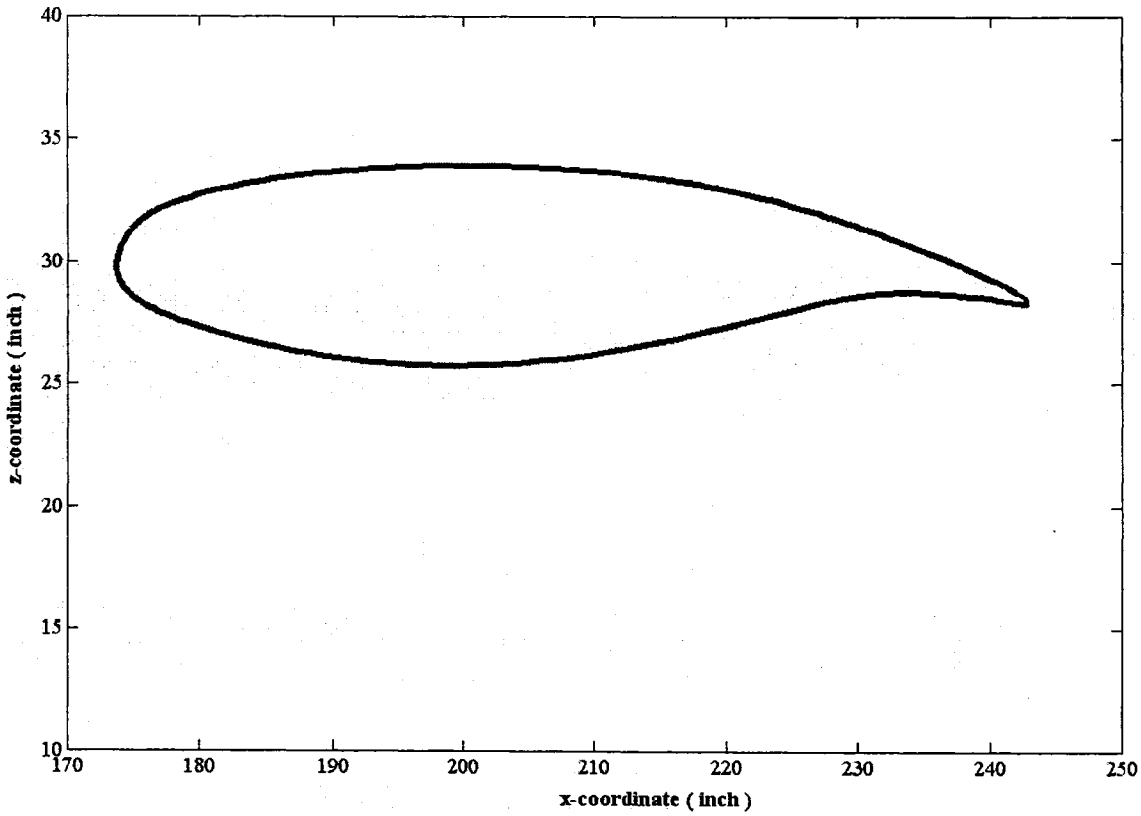

Figure 4-4: DLR-F6 Airfoil section geometry defined at station $\eta = 0.7304$

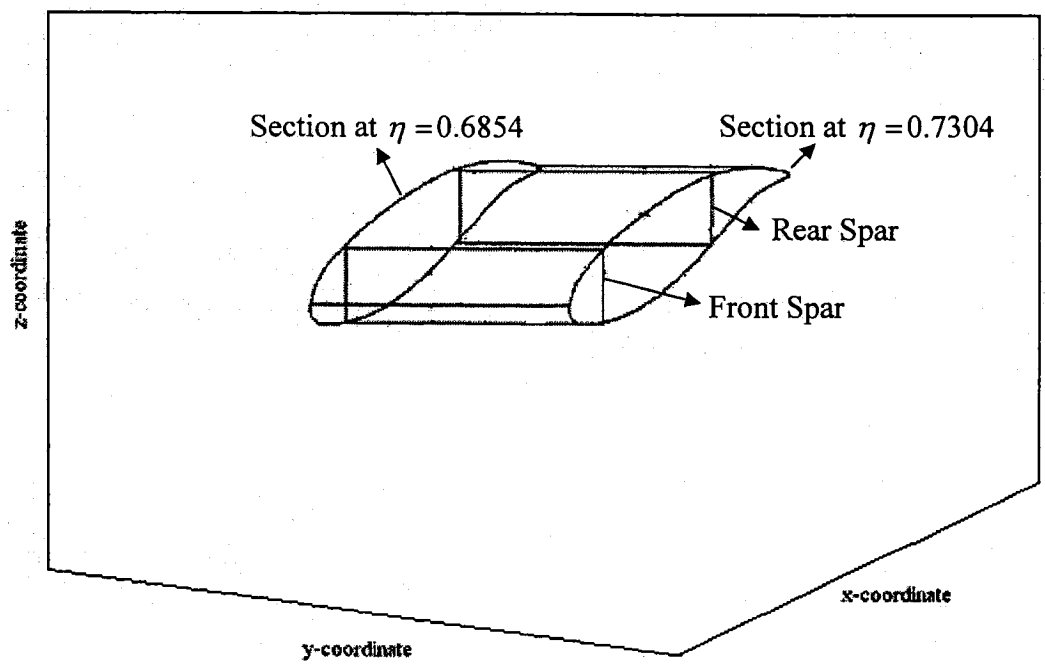

Figure 4-5. DLR-F6 wing section defined between the stations at $\eta = 0.6854$ and $\eta = 0.7304$

4.2 AIRCRAFT AERODYNAMICS AND GENERATION OF DESIGN LOADS

An aircraft flying in air is subjected to aerodynamic loads [42,43]. The lift produced by the aircraft balances its weight and the drag force balances the thrust produced by the aircraft as shown in Figure 4-6.

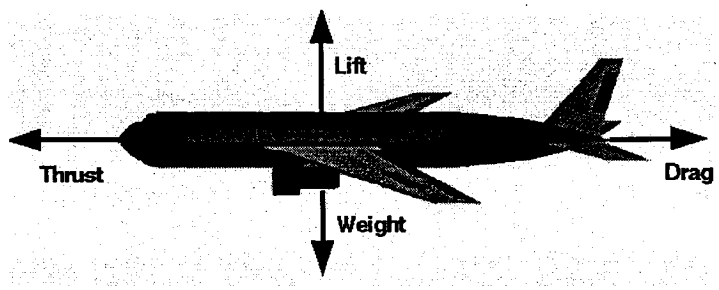

Figure 4-6: Lift & Weight and Drag & Thrust balancing the Aircraft [42]

Figure 4-7 shows different rotational motions exhibited by aircraft. Pitching moment is expressed about the center of gravity of the aircraft.

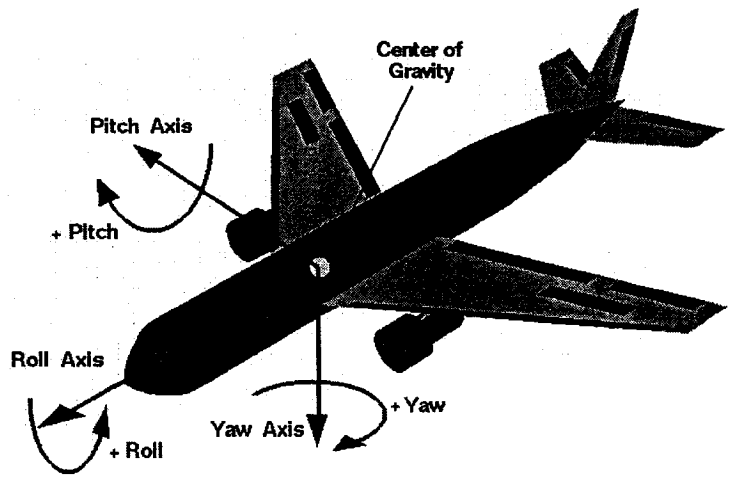

Figure 4-7: Pitch, Yaw and Roll motions of an Aircraft [42]

The loads experienced by an aircraft wing are usually expressed in terms of aerodynamic coefficients [3,42], namely, the lift coefficient (C_L), the drag coefficient (C_D), the pitching moment coefficient (C_M), the normal force coefficient (C_N) and the tangential

force coefficient (C_T). All these coefficients are usually calculated by wind tunnel tests since testing an actual aircraft is quite cumbersome and expensive. Alternately, a complete CFD solution using commercial softwares may be used for generating these coefficients. The above coefficients are defined as below:

$$\text{Lift coefficient, } C_L = \frac{L}{q_\infty S} \tag{4-1}$$

$$\text{Drag coefficient, } C_D = \frac{D}{q_\infty S} \tag{4-2}$$

$$\text{Pitching moment coefficient, } C_M = \frac{M}{q_\infty S c} \tag{4-3}$$

$$\text{Normal force coefficient, } C_N = \frac{N}{q_\infty S} \tag{4-4}$$

$$\text{Tangential force coefficient, } C_T = \frac{T}{q_\infty S} \tag{4-5}$$

where S is the wing reference area and q_∞ is called the free stream dynamic pressure calculated as,

$$q_\infty = \frac{1}{2}\rho V^2 \tag{4-6}$$

where ρ and V are the density of the air and speed of the aircraft (calculated from Mach number, *Mc*), respectively. Since the speed of sound varies with the density of air (or any material it is transmitted through), one needs to determine the density of air through which the aircraft is flying. To compute this, we use the chart shown in Table 4-1, called the International Civil Aviation Organization Table (ICAO) [3]. It can be noticed from Table 4-1 that as the altitude increases, the density of air decreases and so does the speed of sound.

Table 4-1: Variation of density of air and speed of sound with altitude

Altitude (*feet*)	Density of Air (kg/m^3)	Speed of Sound (*m/s*)
0	1.2249	340.4076
1000	1.1894	339.2758
2000	1.1548	338.0926
3000	1.1208	336.9094
4000	1.0878	335.7262
5000	1.0554	334.5429
6000	1.0239	333.3083
7000	0.9930	332.1250
8000	0.9626	330.9418
9000	0.9332	329.7072
10000	0.9044	328.5239
15000	0.7709	322.4021
20000	0.6524	316.1773
25000	0.5488	309.7982
30000	0.4581	303.2647
35000	0.3798	296.6284
40000	0.3015	295.1880
45000	0.2370	295.1880
50000	0.1865	295.1880
55000	0.1469	295.1880

The CFD solution results for wing-body-pylon-engine (wing-mounted engine) case for a DLR-F6 aircraft wing at test conditions of Mach number, $Mc = 0.75$; CL = 0.5 (CL is the overall lift coefficient), angle of attack, $\alpha = -0.0111^{\circ}$ and Reynolds number, $Re = 0.300e7$ are given in Tables 4-2 and 4-3. Table 4-2 provides the values of local lift coefficient at different stations along the wing semi-span. For the scaled model, the local chord length, c is also given in this table. The variation of $\frac{C_L c}{C_{av}}$ along the wing span is plotted in Figure 4-8. Figure 4-9 shows the variation of C_L along the wing span.

Table 4-2: Variation of Lift Coefficient (vs) η

$\eta = \frac{y^*}{s^*}$	$\frac{C_L c}{C_{av}}$	C_L	c
0.1274	0.7034	0.4328	158.8756
0.1651	0.7026	0.4580	149.9319
0.2029	0.6900	0.4784	140.9653
0.2409	0.6626	0.4908	131.9525
0.2793	0.6192	0.4926	122.8697
0.3180	0.5657	0.4864	113.6916
0.3572	0.5491	0.5141	104.3917
0.3971	0.5325	0.5483	94.9413
0.4377	0.5327	0.5698	91.3885
0.4792	0.5320	0.5899	88.1641
0.5219	0.5268	0.6068	84.8560
0.5657	0.5176	0.6212	81.4495
0.6111	0.5055	0.6340	77.9280
0.6582	0.4893	0.6439	74.2717
0.7074	0.4687	0.6502	70.4573
0.7589	0.4455	0.6553	66.4566
0.8133	0.4141	0.6504	62.2348
0.8711	0.3753	0.6353	57.7487
0.9330	0.3175	0.5861	52.9427
1.0000	0.2360	0.4832	47.7443

Table 4-3 gives the values of pitching moment coefficient about the local quarter chord point (C_{Mqc}) along the wing semi-span and is plotted in Figure 4-10. Figure 4-11 shows the variation of the lift force per unit length along the semi-span calculated using Eq. (4-1). Integration of these values gives the variation of shear force along the semi-span as plotted in Figure 4-12.

Table 4-3: Pitching Moment Coefficient about Local Quarter Chord Point (vs) η

$\eta = \frac{y^*}{s^*}$	C_{Mqc}
0.1274	-0.0958
0.1651	-0.0929
0.2029	-0.0939
0.2409	-0.0987
0.2793	-0.1071
0.3180	-0.1201
0.3572	-0.1374
0.3971	-0.1461
0.4377	-0.1381
0.4792	-0.1325
0.5219	-0.1280
0.5657	-0.1249
0.6111	-0.1231
0.6582	-0.1221
0.7074	-0.1228
0.7589	-0.1222
0.8133	-0.1203
0.8711	-0.1165
0.9330	-0.1128
1.0000	-0.1093

The shear force values are then integrated to obtain the bending moment distribution along the semi-span as shown in Figure 4-13. As expected, the shear force and bending moment values are maximum at the wing root and minimum at the wing tip, similar to a cantilever beam.

Subsequently, the pitching moment values about quarter chord per unit length are calculated using Eq. (4-3). These values are integrated to obtain the actual pitching moment values along the semi-span. It is noted that the value of parameter c in Eq. (4-3) is taken from Table 4-2 corresponding to that station. Figure 4-14 shows the variation of

pitching moment about quarter chord point along semi-span. It is noted that the values plotted in Figures 4-11 to 4-14 are the values for cruise condition.

The loads generated here are still not the actual DESIGN loads. They need to be scaled up by applying suitable scaling factors as these loads are too small to be used for sizing the wing-box. The conditions of Mach = 0.75; CL=0.5 and *Re* = 0.300E7 is considered as cruise condition. Here, a design case of 2.5g maneuver is considered. These loads are multiplied by a factor 2.5 to make them design loads [3,20]. Also an additional safety factor of 1.5 is applied over these loads. Optimization is started with these Design Loads considering the scaled wing geometry as defined earlier.

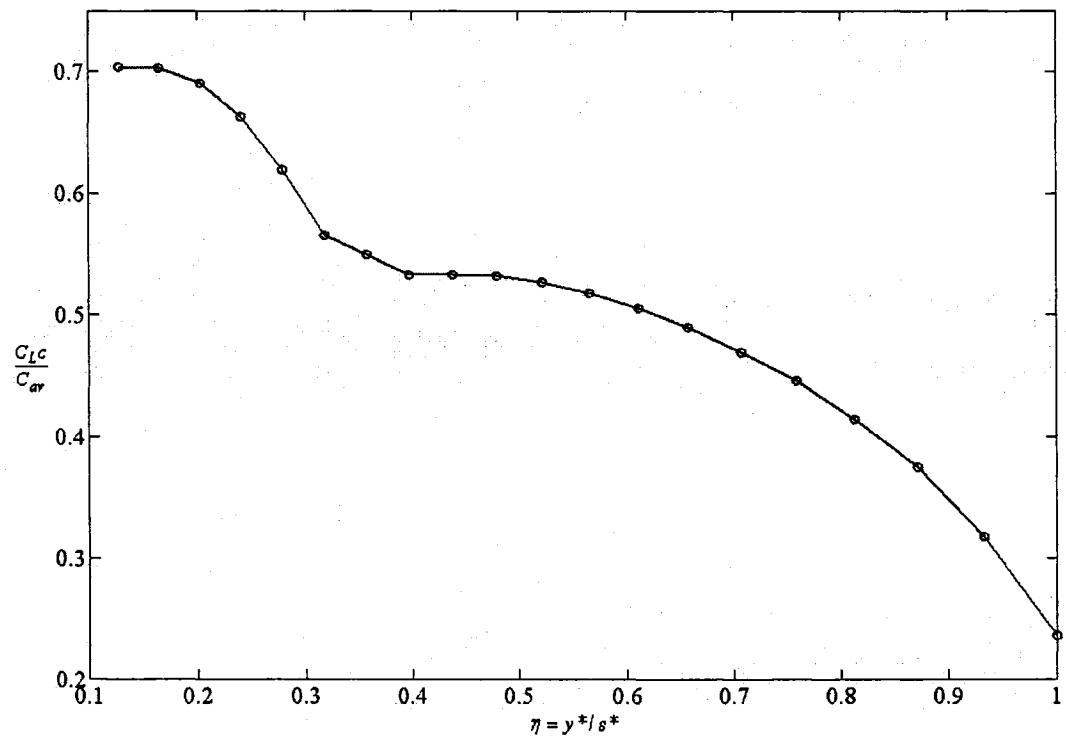

Figure 4-8: $C_L c / C_{av}$ **(vs)** η

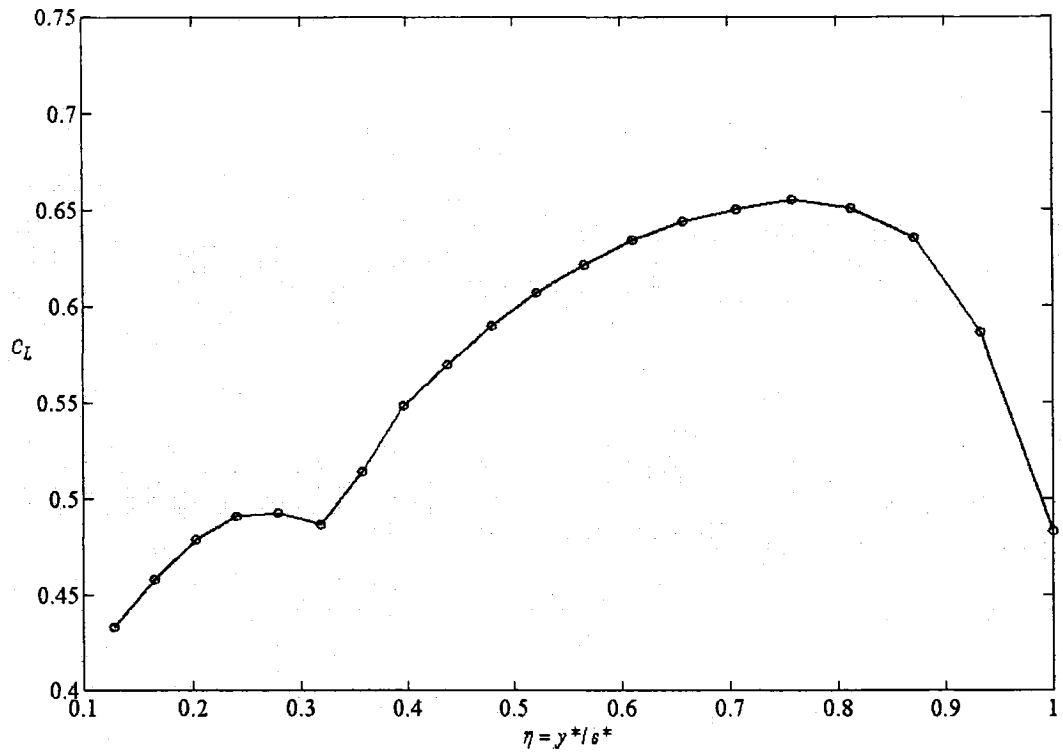

Figure 4-9: C_L **(vs)** η

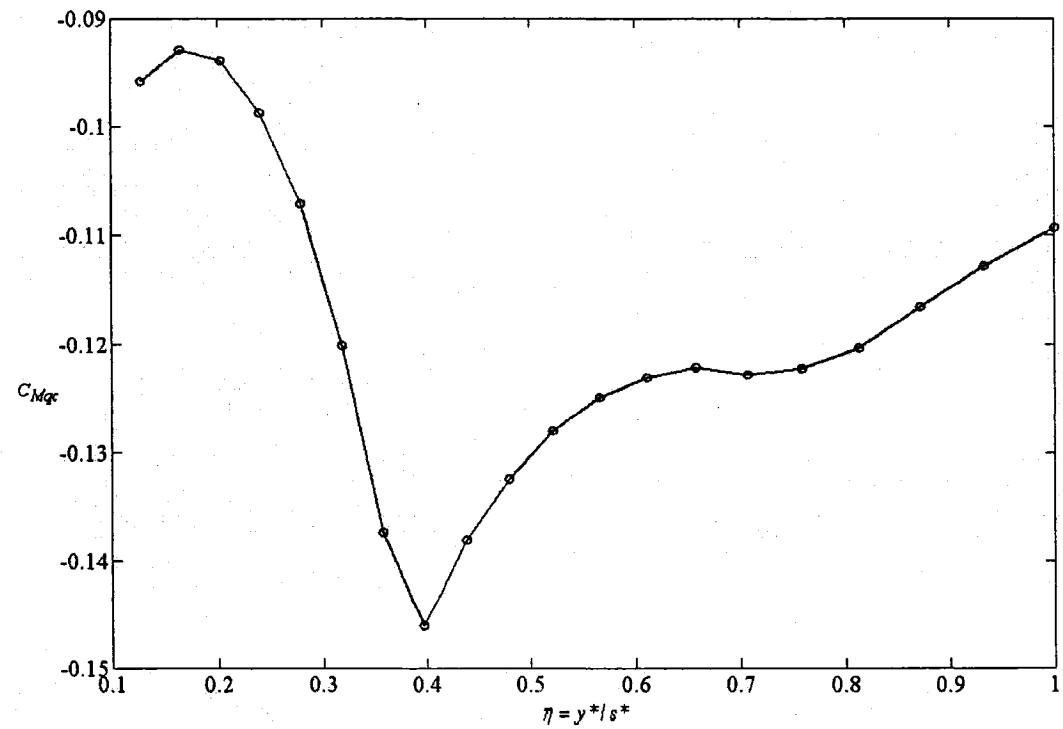

Figure 4-10: C_{Mqc} **(vs)** η

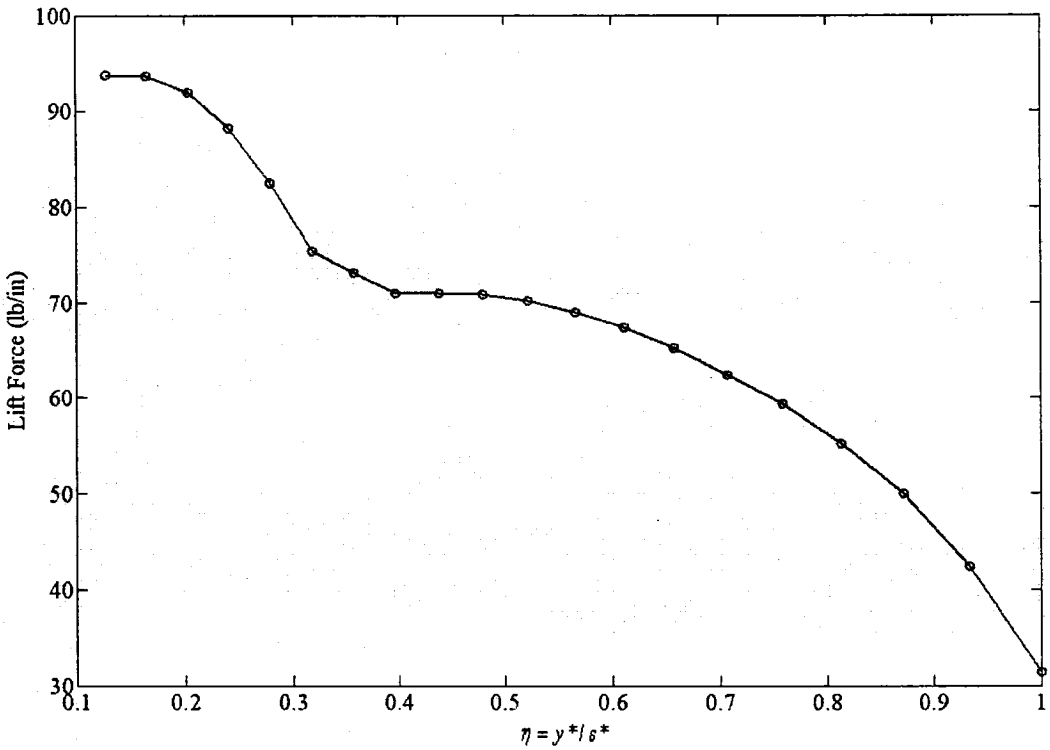

Figure 4-11: Lift Force per unit length (vs) η

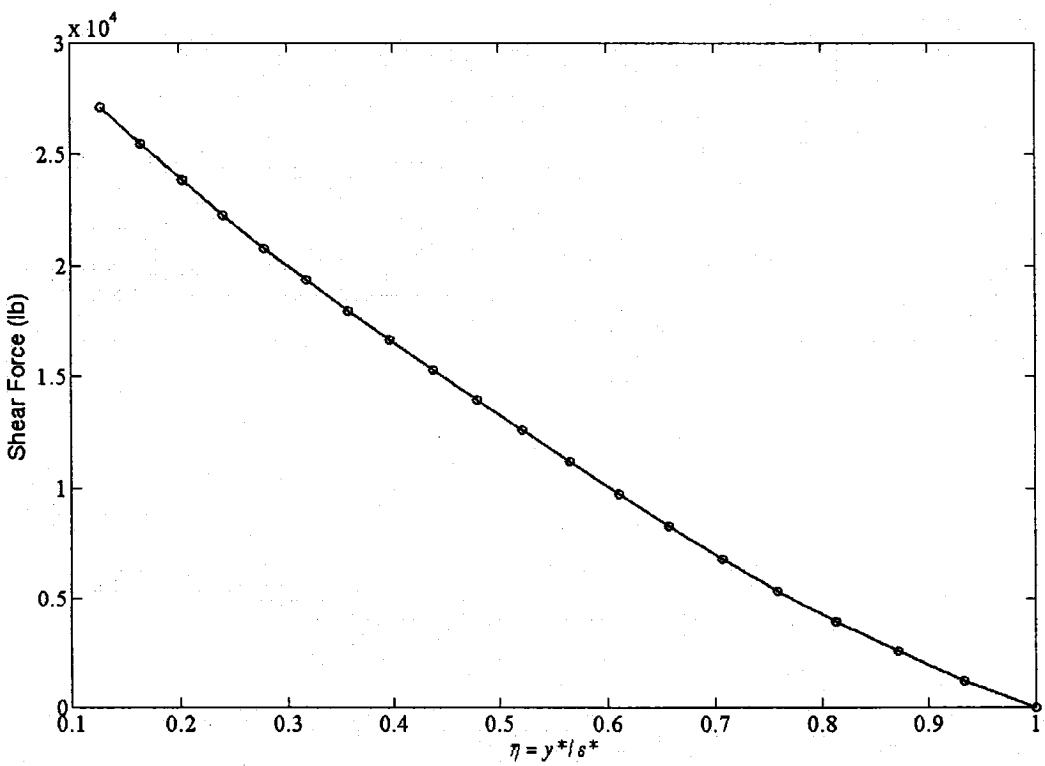

Figure 4-12: Shear Force (vs) η

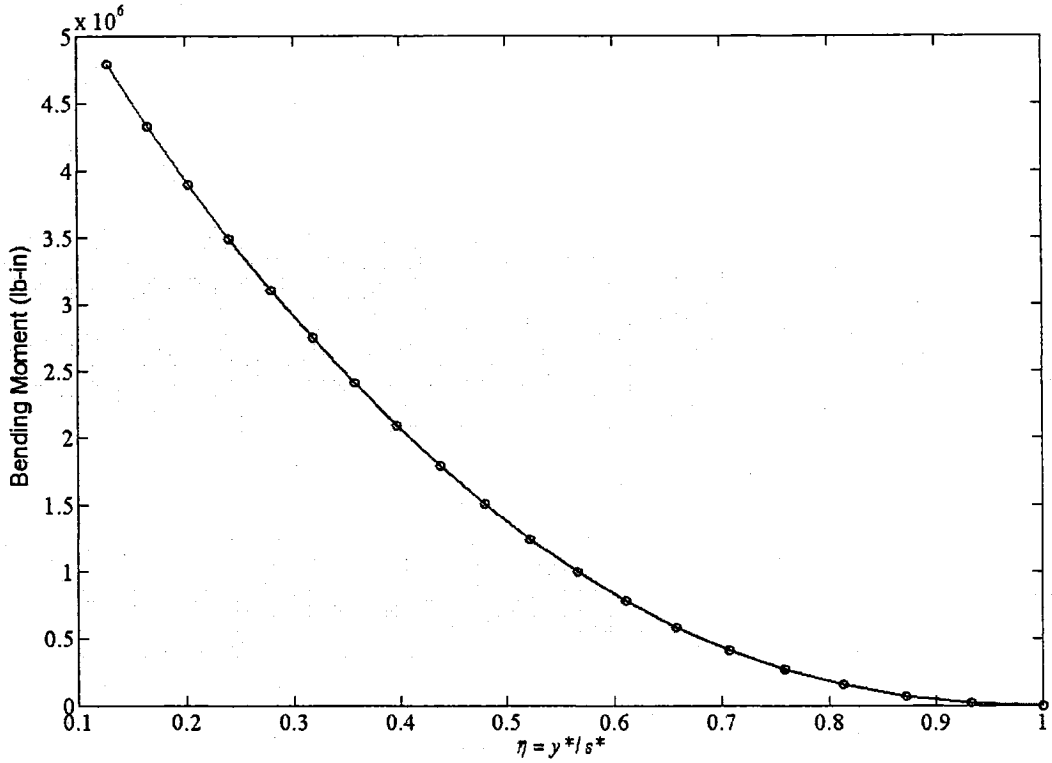

Figure 4-13: Bending Moment (vs) η

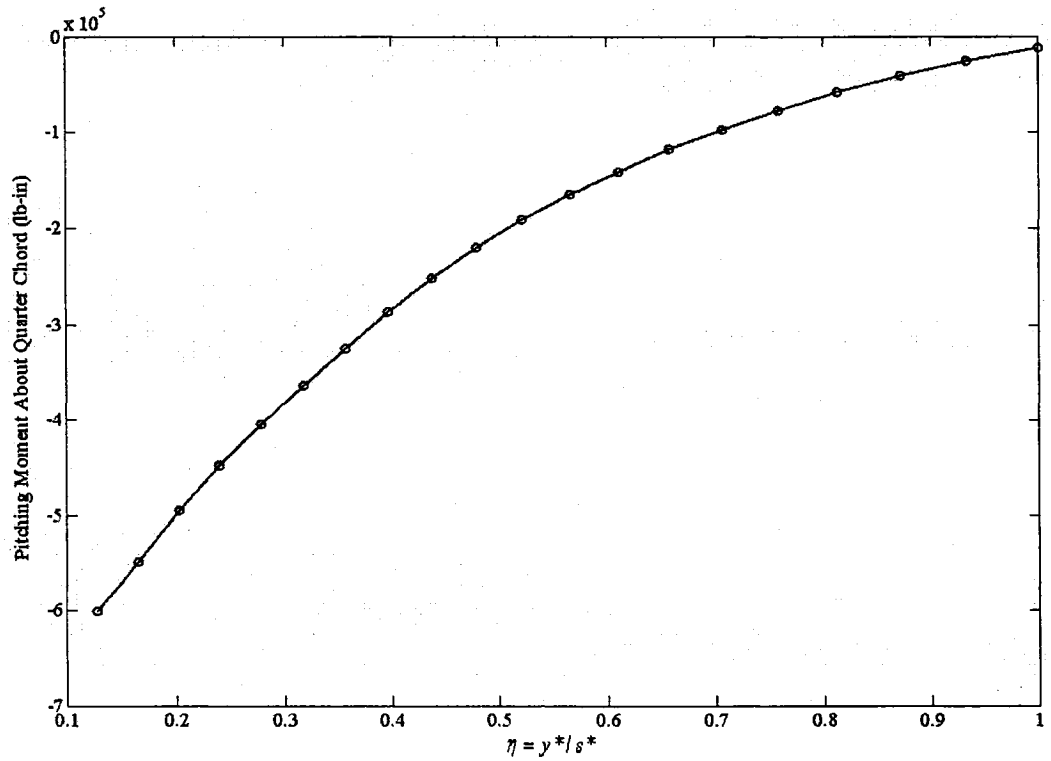

Figure 4-14: Pitching Moment about Quarter Chord Point (vs) η

4.3 DESIGN OPTIMIZATION OF A WING SECTION

In order to simplify the complete design optimization of a wing section, the process is divided into two stages. From Chapter 2, it is clear that the input design load for optimizing a compression skin-stringer panel is N (axial load intensity). And from Chapter 3, the axial tensile stress (σ_t) acting on the wing panel is the required input for design optimization. Considering the test section as defined in Figure 4-5, for easy reference, let the section at station $\eta = 0.6854$ be named as Section A and the one at $\eta = 0.7304$ be Section B. The two sections are named such that the values of shear force and bending moment at Section A are greater than the values at Section B.

4.3.1 Initial design of wing-box: Stage-I

At a specific station along the wing semi-span, the value of the bending moment (M) is obtained from Figure 4-13. The axial compressive load intensity acting on a panel is calculated as [2,20],

$$N = \frac{M}{c_S h_S} \tag{4-7}$$

where c_S, h_S are the width and average thickness of the wing box, respectively as shown in Figure 4-3. This value of N will be the same for any panel placed on the upper wing cover along the chord direction. As mentioned in Chapter 2, thickness of skin (t_s) and panel width or stringer pitch (b_s) are the design variables and mass of the panel (m_p) is the objective function in the optimization process. The same constraints are used here as explained in Chapter 2. Once the optimum values for design variables are obtained, the number of stringers (n_u) required to support the upper skin of the wing-box is calculated as,

$$n_u = \frac{c_s}{b_s} \tag{4-8}$$

The value of n_u is rounded to the nearest integer. The first stringer is placed at a $0.5b_s$ distance from the front spar and continued with a stringer pitch of b_s to arrange the remaining stringers. It should be noted that the thickness of skin on all these panels remains the same, i.e. t_s. Now, in order to find the optimum dimensions for a lower skin-stringer panel, the effective tensile stress acting on the lower panel is calculated using Eq. (2-24) as,

$$\sigma_t = \frac{N(BR)}{[t_s(1+SR)]} \tag{4-9}$$

where SR is called stiffening ratio and BR is called width ratio as explained in Chapter 2. The value of stiffening ratio is usually taken as SR =0.5, while the width ratio is taken as BR =1 for lower panels. Optimization of skin-stringer panels on lower wing cover is done using the procedure explained in Chapter 3. The number of stringers n_l required to support the lower skin of the wing-box is calculated as,

$$n_l = \frac{c_s}{b_s} \tag{4-10}$$

This value of n_l is rounded to the nearest integer. These n_l stringers are arranged on lower wing skin in a similar fashion as done on upper wing skin. This completes Stage-I and the initial design of the wing-box.

4.3.2 Final design of wing-box: Stage-II

To refine the design obtained in Stage-I, another iteration is performed by calculating the re-distributed load acting on the panels arranged in the wing-box. Each

panel will experience a different load intensity, N and tensile stress, σ_t depending on its relative location with respect to the centriodal axes of the section. In Stage-II, the optimization process is repeated with actual value of the load acting on each panel (N for upper panel and σ_t for lower panel).

4.4 CALCULATION OF RE-DISTRIBUTED LOAD ACTING ON WING PANELS

In order to calculate the actual load (compressive or tensile) acting on each panel, the calculation of geometric properties of the section such as area moment of inertia and product of inertia are necessary. Unsymmetrical beam cross-sections are very common in aircraft structure, airfoil section being one of them. The general procedure is to find the area moment of inertia about a set of rectangular axes (say, reference axes) and transfer them to other inclined axes of interest [3].

4.4.1 Equation to Calculate the Bending Stress at a Point on the Section

Consider a beam having an arbitrary cross-section shown in Figure 4-15(a) [4]. The beam supports bending moments M_x and M_y and bends about some axis in its cross-section which is therefore an axis of zero stress or a neutral axis (NA). Let the origin of axes coincide with the centriod C of the cross section and that the neural axis is a distance p from C. The direct stress σ_z on an element of area δA at a point (x, y) and a distance ξ from the neutral axis is,

$$\sigma_z = E\varepsilon_z \tag{4-11}$$

If the beam is bent to a radius of curvature ρ about the neutral axis at this particular section then, since plane sections remain plane after bending, we have,

$$\varepsilon_z = \frac{\xi}{\rho} \tag{4-12}$$

Substituting for ε_z in Eq. (4-11) we have,

$$\sigma_z = \frac{E\xi}{\rho} \tag{4-13}$$

The beam supports pure bending moments so that the resultant normal load on any section must be zero. Hence,

$$\int_A \sigma_z dA = 0 \tag{4-14}$$

Replacing σ_z in this equation by Eq. (4-13) and cancelling the constant terms we get,

$$\int_A \xi \, dA = 0 \tag{4-15}$$

i.e. the first moment of area of the cross-section of the beam about the neutral axis is zero. It follows that the neutral axis passes through the centroid of the cross-section as shown in Figure 4-15(b).

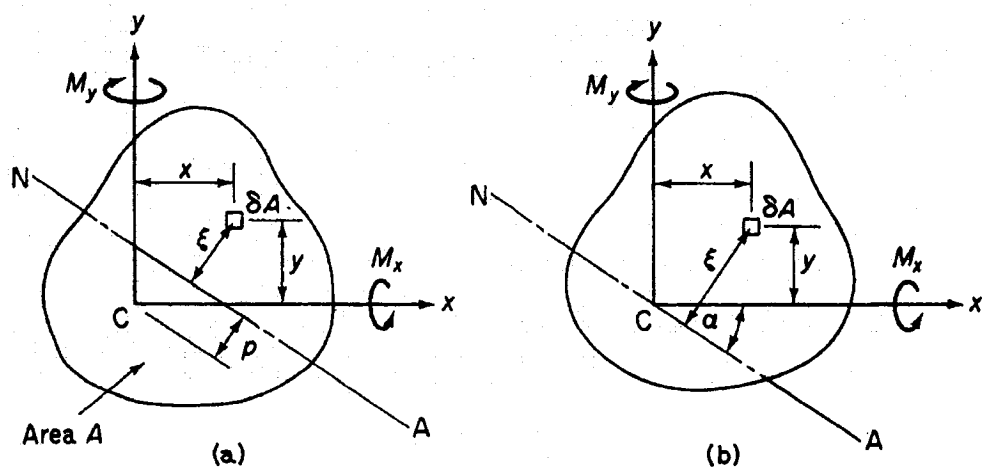

Figure 4-15: Arbitrary beam cross-section [4]

Let the inclination of the neutral axis to Cx is α (measured clockwise from Cx), then

$$\xi = x\sin\alpha + y\cos\alpha \tag{4-16}$$

From Eq. (4-13),

$$\sigma_z = \frac{E}{\rho}(x\sin\alpha + y\cos\alpha) \tag{4-17}$$

The moment resultants of the internal direct stress distribution have the same sense as the applied moments M_x and M_y. Thus,

$$M_x = \int_A \sigma_z\, y\, dA \text{ and } M_y = \int_A \sigma_z\, x\, dA \tag{4-18}$$

Substituting for σ_z from Eq. (4-17) into Eq. (4-18) yields,

$$M_x = \frac{E\sin\alpha}{\rho} I_{xy} + \frac{E\cos\alpha}{\rho} I_{xx} \tag{4-19}$$

$$M_y = \frac{E\sin\alpha}{\rho} I_{yy} + \frac{E\cos\alpha}{\rho} I_{xy} \tag{4-20}$$

where the second moments of area of the section about Cx and Cy axes are defined as,

$$I_{xx} = \int_A y^2 dA,\ I_{yy} = \int_A x^2 dA,\ I_{xy} = \int_A xy\, dA \tag{4-21}$$

Arranging Eqs. (4-19) and (4-20) in matrix form as,

$$\begin{Bmatrix} M_x \\ M_y \end{Bmatrix} = \frac{E}{\rho}\begin{bmatrix} I_{xy} & I_{xx} \\ I_{yy} & I_{xy} \end{bmatrix}\begin{Bmatrix} \sin\alpha \\ \cos\alpha \end{Bmatrix} \quad \Rightarrow \quad \frac{E}{\rho}\begin{Bmatrix} \sin\alpha \\ \cos\alpha \end{Bmatrix} = \begin{bmatrix} I_{xy} & I_{xx} \\ I_{yy} & I_{xy} \end{bmatrix}^{-1}\begin{Bmatrix} M_x \\ M_y \end{Bmatrix} \tag{4-22}$$

$$\frac{E}{\rho}\begin{Bmatrix} \sin\alpha \\ \cos\alpha \end{Bmatrix} = \frac{1}{I_{xx}I_{yy} - I_{xy}^2}\begin{bmatrix} -I_{xy} & I_{xx} \\ I_{yy} & -I_{xy} \end{bmatrix}\begin{Bmatrix} M_x \\ M_y \end{Bmatrix} \tag{4-23}$$

Now, using Eq. (4-17) bending stress at any point on the cross-section is given by,

$$\sigma_z = \frac{(M_y I_{xx} - M_x I_{xy})}{I_{xx}I_{yy} - I_{xy}^2} x + \frac{(M_x I_{yy} - M_y I_{xy})}{I_{xx}I_{yy} - I_{xy}^2} y \tag{4-24}$$

It is noted that x and y are the distances taken from section centriodal axes to the point.

4.4.2 Calculation of Actual Design Load on Skin-Stringer Panel

Using Eq. (4-24), the bending stress in the skin and stringer elements can be calculated by knowing the airfoil section properties. Hence, the total load acting on the skin-stringer panel becomes [20],

$$Q = A_{sk}\sigma_{sk} + A_{st}\sigma_{st} \tag{4-25}$$

It is noted that, different panels will share different magnitude of bending stress (either compressive or tensile) depending on their relative positions with respect to the centriodal axes of the section. For a panel on the upper wing cover, the axial load intensity can be calculated as,

$$N = \frac{Q}{b_s} \tag{4-26}$$

Stage-II repeats the optimization process using new values of N for all n_u upper panels and using new values of tensile bending stress for all n_l lower panels to obtain the new optimum dimensions. This completes the final design of the wing-box at a section. The process of Stage-I and Stage-II is repeated to design the wing-box for Section A and Section B defined earlier and thus completely define the tapered wing section as showed in Figure 4-5. As explained earlier, the design of front and rear spar web thickness and their corresponding upper and lower web cap dimensions are not included here. Hence, reasonable dimensions are assumed to completely define the wing-box.

4.5 SHEAR FLOW IN TAPERED WING SECTION

In airplane wing and fuselage structures, the common case is a beam of non-uniform section in the flange (stringer) direction. The present tapered wing section (Figure 4-5) under consideration is also a beam with non-uniform cross-section. In cases

where the change in cross-sectional area is fairly well distributed between the various flange members, the shear flow results as given by the solution for beams of constant moment of inertia are not much in error. For beams where this is not the case, shear flow results may be considerably different from the actual shear flows [3].

Figure 4-16 shows a single cell distributed flange beam. Consider the beam acts as a cantilever beam with the bending moment existing at section (A) being greater than that at section (B) and that the moment produces compression on the upper surfaces. By using the flexural stress equations, the bending stress on each stringer can be found, which if multiplied by the stringer area gives the stringer axial load. Thus, at beam section (B), p_1, p_2, p_3 etc. represent the axial loads due to bending moment M. Bending moment at section (A) is $M+\Delta M$, and hence the stringer axial loads at section (A) will be $p_1+\Delta\ p_1, p_2+\Delta\ p_2, p_3+\Delta\ p_3$ etc. These stringer axial loads are shown in Figure 4-16.

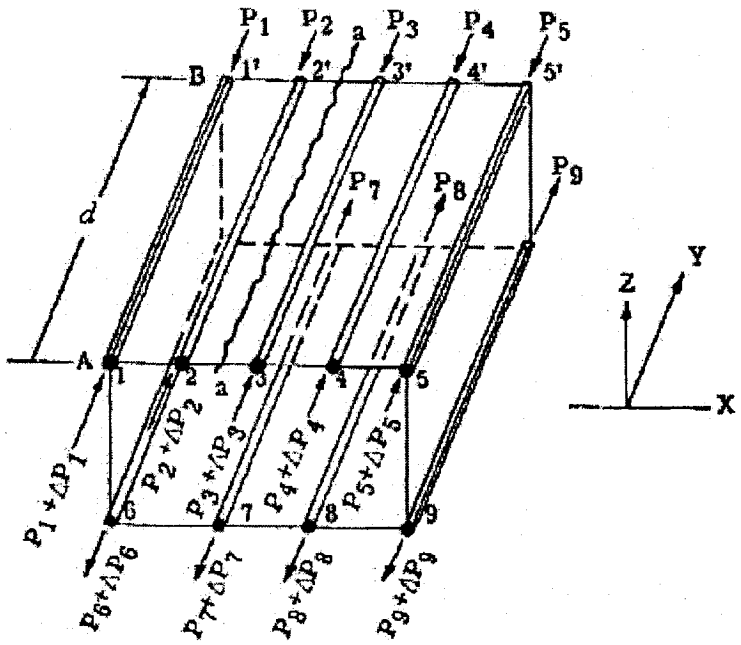

Figure 4-16: Non-uniform beam cross section [3]

Now, imagine the upper sheet panel 2-2'-3'-3 is cut along the line (a-a). Free body diagram of stringer number (3) is shown in Figure 4-17(a). Let q_y be the average shear flow per inch over the distance '*d*' on the sheet edge bb. It has been assumed positive relative to sense along y axis. For equilibrium of this free body,

$$\sum F_y = 0, \text{ hence } \Delta p_3 + q_y d = 0 \tag{4-27}$$

where $q_y = -\Delta p_3 / d$.

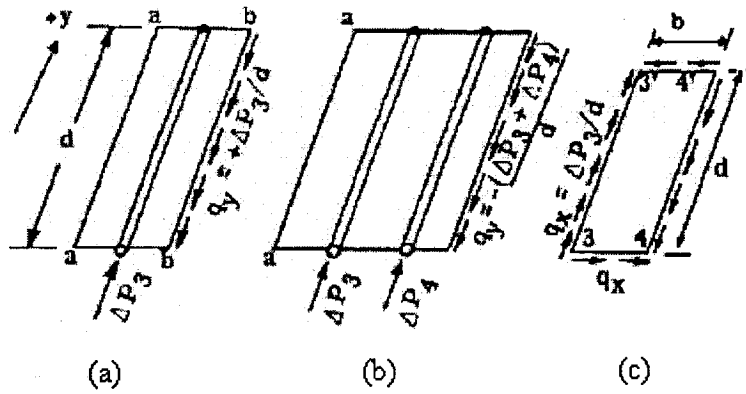

Figure 4-17: Free body diagram of panels [3]

Free body diagram including two stringers (3 and 4) is shown in Figure 4-17(b). Again writing equilibrium in y direction gives,

$$\sum F_y = 0 \text{ where } \Delta p_3 + \Delta p_4 + q_y d = 0 \text{ or } q_y = -(\Delta p_3 + \Delta p_4)/d \tag{4-28}$$

Therefore, starting at any place where the value of q_y is known, the change in the average shear flow at other section equals,

$$q_y = -\sum \frac{\Delta p}{d} \tag{4-29}$$

Figure 4-17(c) shows sheet panel (3-3'-4'-4) isolated as a free body. Taking moments about corner 4' and equating to zero for equilibrium,

$$\sum M_{4'} = \frac{d(\Delta p_3)b}{d} - q_x bd \text{ where } q_x = \Delta p_3 / d \qquad (4\text{-}30)$$

Thus, for rectangular sheet panels between flange members, the shear flow q_x or q_z equals the average shear flow q_y.

4.5.1 Elastic Axis of a Wing

The elastic axis of a wing is defined as the axis about which rotation will occur when the wing is loaded in pure torsion [6]. The shear center of a wing cross-section is defined as the point at which the resultant shear load must act to produce a wing deflection with no rotation. The shear force applied at shear center deflects the wing in translation, but causes no rotation of the cross section about a span wise axis. If the wing is an elastic structure, then the shear center of a cross-section must lie on the elastic axis. Practical wings deviate slightly from conditions of elasticity because the skin wrinkles and becomes ineffective in resisting compression loads but, for practical purposes, the elastic axis may be assumed to coincide with the line joining the shear centers of the various cross-sections. The shear center of a cross-section may be calculated by finding the position of the resultant shear force which yields a zero twist angle. The shear center location depends on the distribution of the flange areas and the thickness of the shear webs.

4.5.2 Margin of Safety for Combined Compression, Bending and Shear Load

The calculation of shear flow around the wing-box at a section is necessary if the design of a wing panel is to be done for a multiple load case of combined compression and torsion loads. At a wing section, all the loads are applied on the elastic axis of the

wing. As explained earlier, elastic axis is the locus of shear centers of the section in the spanwise direction of the wing.

For a closed section of the wing-box, it is assumed that a section wall is cut at the center of front spar web, thus making shear flow value 'zero' at that point. Starting from this point, the shear flow around the section is calculated using Eq. (4-29). It should be noted that the shear flow values found here are the average values between Section A and Section B of the wing section defined in Figure 4-5. The moment produced by the shear flow (q_y) on the skin between two adjacent stringers is equal in to the magnitude of q_y times double the enclosed area formed by drawing lines from the moment center (centroid of the section) and their end points [3,6]. Taking moment of all forces both external (M_y) and internal (M_s and M_f) about centroid of the section gives,

$$M_g = M_s + M_f + M_y \tag{4-31}$$

Here, M_s is the total moment produced by the internal shear flow. M_f is the total moment produced by the flange loads about the centroid (since the flange members are usually inclined at an angle to the beam section, their components contribute to the rotation of the section). M_y is the moment produced by the external loads acting on the section about its centroid calculated as,

$$M_y = M_{qc} + V_z e \tag{4-32}$$

where M_{qc} is the pitching moment about quarter chord point on the airfoil section. V_z is the shear force in the vertical direction on the section and 'e' is the distance between the quarter chord point and the centroid of the section. Thus, for equilibrium of the section,

the moment M_g should be applied in the opposite direction to internal shear flow. This moment is applied as a constant shear flow around the section, whose magnitude is,

$$q = -\frac{M_g}{2A_s} \tag{4-33}$$

where A_s is the enclosed area of the wing-box. Adding this constant shear flow to that of the transverse shear, we obtain the final shear flow around the section. The shear stress acting on the skin of any panel can be obtained as,

$$f_s = \frac{q}{t_s} \tag{4-34}$$

Because of the bending moment, a different end compressive stress is produced in the panel cross-section. Hence, the total compressive stress is the sum of the compressive stress due to direct compression and due to bending. The total shear stress is the sum of transverse shear produced by transverse load and torsional shear produced by twisting loads.

The interaction equation for this kind of combined loading is given by [3],

$$R_c^{'} + (R_s^{'})^2 = 1 \text{ (>1, the panel buckles)} \tag{4-35}$$

$$\text{Margin of Safety (MOS)} = \frac{2}{R_c^{'} + \sqrt{(R_c^{'})^2 + 4(R_s^{'})^2}} - 1 \tag{4-36}$$

The first ratio is the compression stress ratio given by,

$$\text{Compression Stress Ratio} = R^{'}_c = \frac{f_c}{F_{c,cr}} \tag{4-37}$$

where f_c is obtained from the minimum of 3 loads calculated as explained in Chapter 2 and $F_{c,cr}$ is the critical compressive buckling stress in the skin given by,

$$F_{c,cr} = \frac{\eta_c \pi^2 k_c E}{12(1-\nu^2)} (\frac{t_s}{b_s})^2 \tag{4-38}$$

where η_c is the plasticity reduction factor, k_c is the buckling coefficient, ν is the Poisson's ratio, E Elastic Modulus, t_s is the thickness of skin and b_s is the width of the panel. The second ratio is the shear stress ratio given by,

$$\text{Shear Stress Ratio} = R'_s = \frac{f_s}{F_{s,Cr}} \tag{4-39}$$

where f_s is the shear stress in the skin obtained from Eq. (4-38) and $F_{s,cr}$ is the critical shear stress in the skin given by,

$$F_{s,cr} = \frac{\eta_s \pi^2 k_s E}{12(1-\nu^2)} (\frac{t_s}{b_s})^2 \tag{4-40}$$

where k_s is the shear constant. The margin of safety should always be greater than or equal to zero for the structure to be safe and sustain the applied loads. It is included as a constraint in optimization program for designing panels.

4.6 RESULTS AND CONCLUSIONS

Design optimization is tested on the tapered wing section defined by the airfoil sections at stations $\eta = 0.6854$ and $\eta = 0.7304$ as shown in Figure 4-5. The important dimensions of this tapered wing section are the dimensions of skin-stringer panels that make up the wing-box. It is noted that the stringers considered here are Z-type with equal flanges on both upper and lower wing skin of the wing-box. The length of the section (essentially the length of the panel) is $L = 20.8153$ *in.* As explained in section 4.3, the design in done in two Stages and the results are presented for the two Stages separately. Before presenting the results, the details of the sections at two stations are given below:

(A) Details of Section at Station $\eta = 0.6854$

Width of the wing-box, $c_s = 36.0869\ in$

Average height of the wing-box, $h_s = 8.5646\ in$

Shear force, $SF = 7439\ lb$

Bending moment, $M = 0.4886e6\ lb\text{-}in$ (about x^*-axis)

Pitching Moment about quarter chord, $M_{qc} = -1.0628e5\ lb\text{-}in$ (about y^*-axis)

(B) Details of Section at Station $\eta = 0.7304$

Width of the wing-box, $c_s = 34.2809\ in$

Average height of the wing-box, $h_s = 8.1513\ in$

Shear force, $SF = 6132\ lb$

Bending moment, $M = 0.3474e6\ lb\text{-}in$ (about x^*-axis)

Pitching Moment about quarter chord = $-0.8789e5\ lb\text{-}in$ (about y^*-axis)

The drag force and the moment about the about z^*-axis are assumed to be zero.

For the design of compression panels, the skin and stringer are assumed to be made of same material with material properties as below: $\sigma_{cy} = 75000 psi$ (allowable compressive yield stress); $E = 10.5e6 psi$ (modulus of elasticity in compression); $m = 23$ (material characteristic index). For the design of tension panels (lower wing panels), the skin and stringer are assumed to be made of same material with material properties of $E = 10.3e6 psi$ (modulus of elasticity in tension); $\nu = 0.3$ (Poisson's Ratio).

All the lower panels are assumed to have an initial half crack of length of $a = 0.025\ in$ at the center of the skin. The values for Paris's constants are taken as $C_p = 1e\text{-}12$

and m_p=3. The Fracture Toughness value for aluminium is taken as, $K_{IC} = 26\,ksi - in^{1/2}$. An adhesive material of thickness equal to that of the skin (t_s), over a width equal to that of the upper flange width (b_a) is used to attach the stringer to the skin. The shear modulus of adhesive used is taken as 87000 *psi*.

The results are calculated separately for single and multiple load cases. But, for design of lower wing panels, only single load case for a Mode-I failure is considered neglecting the shear loading.

4.6.1 Results for Stage-I

Axial compressive load intensity acting on airfoil section defined at station $\eta = 0.6854$, obtained using Eq. (4-7) is N = 1508 *lb/in*. It is noted that this value is for cruise condition. This cruise load is multiplied by a factor 2.5 to make it 2.5g maneuver case load. An additional Factor of safety of 1.5 is also applied to get the actual design load, $N = 5928$ *lb/in*.

Upper panel dimensions before load re-distribution for single load case:

$t_s = 0.13$; $b_s = 4.14$

$$n_u = \frac{c_s}{b_s} = 36.0869/4.14 = 8.7166 \approx 9 \text{ (rounded to nearest integer)}$$

The effective tensile stress acting on the lower panel is calculated as $\sigma_t = 30400\,psi$.

Lower panel dimensions before load re-distribution:

$t_s = 0.10$; $b_s = 4.60$

$$n_l = \frac{c_s}{b_s} = 36.0869/4.60 = 7.8450 \approx 8 \text{ (rounded to nearest integer)}$$

As explained in section 4.3, the first stringer is placed at a distance $b_s/2$ from the front spar on both upper and lower skin. The next stringer is placed at b_s from here and continued to reach rear spar using the same stringer pitch. So, from the above calculations, 9 stringers (1-9) are needed on upper skin and another 8 on lower skin (10-17) as shown in Figure 4-18.

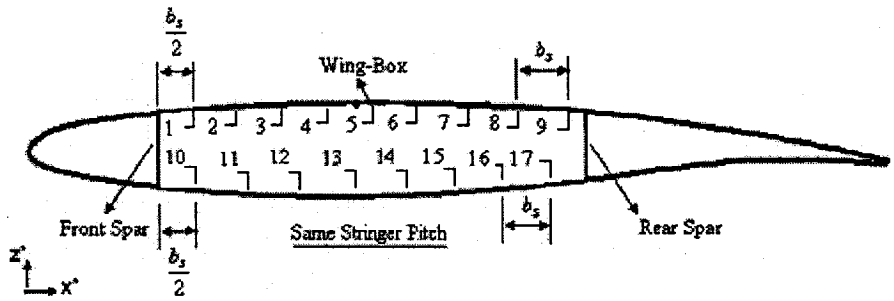

Figure 4-18: Arrangement of stringers on the wing-box of section defined at station $\eta = 0.6854$ before load re-distribution

Similarly, design axial load intensity at station $\eta = 0.7304$ is $N = 4663$ *lb/in.*

Upper panel dimensions before load re-distribution for single load case:

$t_s = 0.11$ *in*; $b_s = 4.06$ *in*

$$n_u = \frac{c_s}{b_s} = 34.2809/4.06 = 8.4436 \approx 8 \text{ (rounded to nearest integer)}$$

The effective tensile stress acting on the lower panel is calculated as $\sigma_t = 28261\,psi$.

Lower panel dimensions before load re-distribution:

$t_s = 0.09$ *in*; $b_s = 4.58$ *in*

$$n_l = \frac{c_s}{b_s} = 34.2809/4.58 = 7.4849 \approx 7 \text{ (rounded to nearest integer)}$$

The stringers are arranged similar to the previous section and the final arrangement (1-8 stringers on upper skin and 9-15 on lower skin) is shown in Figure 4-19.

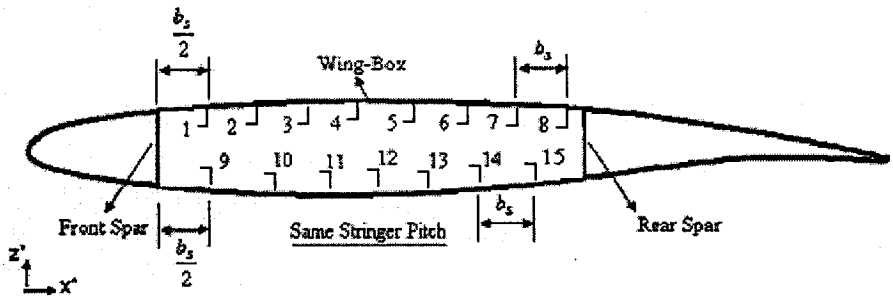

Figure 4-19: Arrangement of stringers on the wing-box of section defined at station $\eta = 0.7304$ before load re-distribution

4.6.2 Results for Stage-II

The actual load acting on each of these panels is calculated as explained in section 4.4.2. Table 4-4 and 4-5 show the actual values of the design loads (N for upper panels and σ_t for lower panels) acting on the panels for sections defined at stations $\eta = 0.6854$ and $\eta = 0.7304$, respectively. The new optimum dimensions calculated for all the upper and lower wing panels are tabulated as below. Tables 4-6 and 4-7 have the new values of design variables for upper and lower panels, respectively corresponding to the section defined at station $\eta = 0.6854$. Tables 4-8 and 4-9 contain the new values for design variables of upper and lower panels, respectively corresponding to the section defined at station $\eta = 0.7304$.

Table 4-4: Actual values of the design loads after load re-distribution acting on the panels arranged on section at $\eta = 0.6854$

Stringer#	1	2	3	4	5	6	7	8	9
N (*lb/in*)	5158	5540	5776	5870	5828	5655	5354	4932	4393
Stringer#	10	11	12	13	14	15	16	17	-
σ_t (*psi*)	30306	34779	38008	39901	40368	39319	36661	32306	-

Table 4-5: Actual values of the design loads after load re-distribution acting on the panels arranged on section at $\eta = 0.7304$

Stringer#	1	2	3	4	5	6	7	8
$N\,(lb/in)$	4149	4468	4666	4747	4717	4578	4336	3993
Stringer#	9	10	11	12	13	14	15	-
$\sigma_t\,(psi)$	29824	33583	35969	36880	36216	33877	29704	-

Table 4-6: Upper panel dimensions after load re-distribution for section defined at station $\eta = 0.6854$

Stringer#	1	2	3	4	5	6	7	8	9
$t_s\,(in)$	0.12	0.12	0.12	0.125	0.125	0.12	0.12	0.11	0.11
$b_s\,(in)$	4.09	4.14	4.16	4.18	4.18	4.12	4.10	4.05	3.92

Table 4-7: Lower panel dimensions after load re-distribution for section defined at station $\eta = 0.6854$

Stringer#	10	11	12	13	14	15	16	17
$t_s\,(in)$	0.10	0.108	0.11	0.11	0.11	0.11	0.11	0.10
$b_s\,(in)$	4.68	4.72	4.78	4.81	4.81	4.81	4.77	4.68

Table 4-8: Upper panel dimensions after load re-distribution for section defined at station $\eta = 0.7304$

Stringer#	1	2	3	4	5	6	7	8
$t_s\,(in)$	0.11	0.11	0.12	0.12	0.12	0.12	0.11	0.11
$b_s\,(in)$	3.97	3.99	4.07	4.08	4.07	4.06	3.97	3.92

Table 4-9: Lower panel dimensions after load re-distribution for section defined at station $\eta = 0.7304$

Stringer#	9	10	11	12	13	14	15
$t_s\,(in)$	0.09	0.09	0.09	0.09	0.09	0.09	0.09
$b_s\,(in)$	4.58	4.60	4.62	4.65	4.63	4.60	4.58

Since the stringers 9 and 17 appear near to the rear spar and that the upper and lower web caps on the rear spar can give enough support, these stringers can be eliminated on the section defined at $\eta = 0.6854$. When the stringers are re-arranged, the number of stringers needed to support the skin on upper and lower panels is less then the initial number of stringers obtained in Stage-I. Final arrangement of stringers on the wing-box of the section defined at station $\eta = 0.6854$ is shown in Figure 4-20. There is no change in the number of stringers at station $\eta = 0.7304$ before and after load re-distribution. Final arrangement of stringers on the wing-box of the section defined at station $\eta = 0.7304$ is shown in Figure 4-21. With the wing-box completely defined at two stations $\eta = 0.6854$ and $\eta = 0.7304$, the design of tapered wing section is completed. It is observed that the total mass of the wing-box of the section defined at station $\eta = 0.6854$ before load re-distribution (Stage-I) is found to be 25.9602 *lbs*.

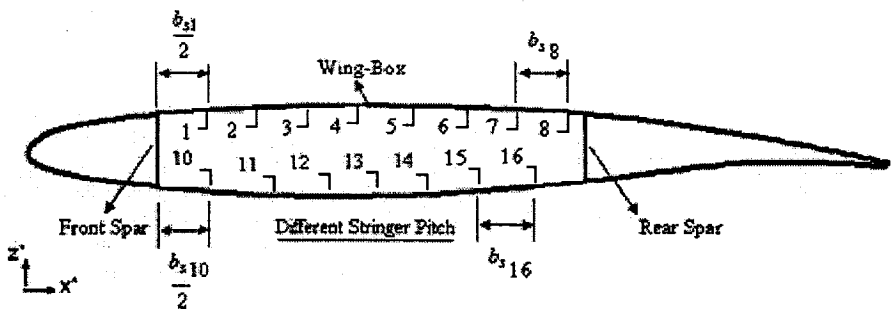

Figure 4-20: Arrangement of stringers on the wing-box of section defined at station $\eta = 0.6854$ after load re-distribution

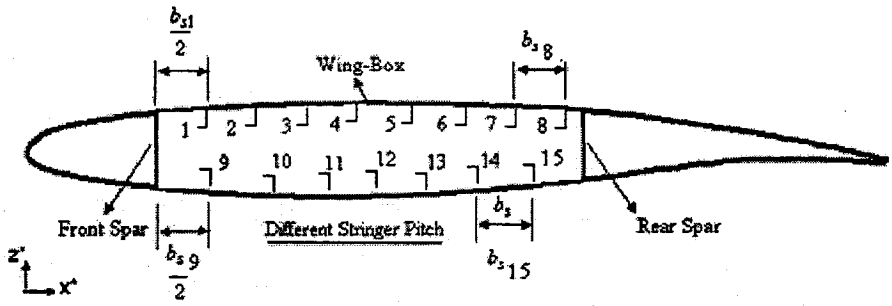

Figure 4-21: Arrangement of stringers on the wing-box of section defined at station $\eta = 0.7304$ after load re-distribution

After load re-distribution (i.e. Stage-II), it is found that the mass of the wing-box is 23.0835 *lbs* resulting in saving considerable amount of mass. Similarly, at station $\eta = 0.7304$, the mass of the wing-box before load re-distribution is 20.1077 *lbs*, while the mass of the wing-box after load re-distribution is 19.6692 *lbs* showing a significant saving in the mass.

It can be concluded from the above results that the above defined methodology works well to design preliminary wing-box structure effectively.

4.6.3 Design Optimization for Multiple Load Case

The shear flow values around the section defined at station $\eta = 0.6854$ are obtained using the procedure explained in section 4.5 and are shown in Figure 4-22. Now, the value of shear flow on a panel becomes an input to the optimization problem. From the values obtained for single load case, Stage-I optimization program is recalled to calculate the new optimum dimensions for multiple load case.

Margin of safety is changed according to Eq. (4-36) to include the effect of multiple loading on the panel. The new dimensions for upper panels for the section defined at $\eta = 0.6854$ are tabulated in Table 4-10.

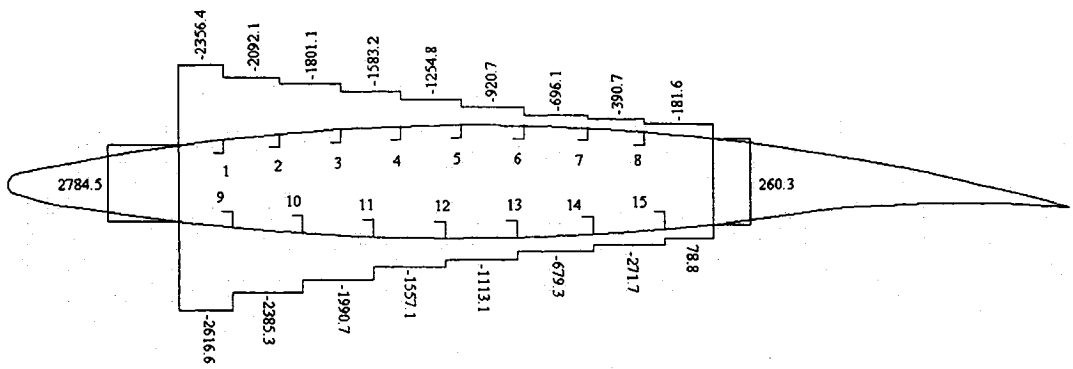

Figure 4-22: Shear Flow values around the section defined at $\eta = 0.6854$

It can be observed that the optimization converged to the same optimum values for the design variables. Hence, it can be concluded that the effect of shear loading is very small on the design of these panels.

Table 4-10: Upper panel dimensions multiple load case for section defined at $\eta = 0.6854$

Stringer#	1	2	3	4	5	6	7	8
$t_s\,(in)$	0.122	0.122	0.122	0.125	0.125	0.12	0.12	0.11
$b_s\,(in)$	4.08	4.14	4.16	4.18	4.18	4.12	4.10	4.05

CHAPTER 5

CONCLUSIONS AND RECOMMENDATIONS FOR THE FUTURE WORK

5.1 CONCLUSIONS

Although the need for developing and integrating various design modules to form an effective MDO process has been studied, the present work emphasizes more on structural design optimization of an aircraft wing-box. The most important conclusions and contributions from the current work are listed as follows:

1. An effective optimization routine has been developed to design a compressive skin-stringer panel for a minimum mass while guarding against important failures modes such as; crippling stress, column buckling, up-bending at center span and compression in skin, down bending at supports, compression in stringer outstanding flange, inter-rivet buckling and beam column eccentricity.
2. An optimization routine has been developed to design a lower skin-stringer panel subjected to tensile load. Damage tolerance analysis principles are implemented successfully in the. The Boundary Element Method is combined with the method of compatibility deformations to analyze the stress distributions in cracked finite sheets reinforced by bonded stiffeners.
3. The above optimization routines have been successfully used to design a wing-box at any specific station of a DLR-F6 scaled model aircraft. A good preliminary design of wing-box saving considerable amount of mass was obtained by implementing the two stage design process. The design of upper panels for case of multiple loading was also done successfully.

5.2 RECOMMENDATIONS FOR THE FUTURE WORK

Although most of the important aspects have been covered in this thesis work in designing a preliminary wing-box, other important and interesting subjects for the future work are identified as follows:

1. Although the design of a lower wing panel for simple case of single straight crack is a good start, it can be extended to design for a case of multiple cracks. Instead of using adhesive material to join stringer with skin, it would be interesting to design by replacing adhesive material with rivets (fasteners).
2. The drag force can also be included while generating the design load curves.
3. As the dimensions for spars and their corresponding web caps are taken with reasonable assumptions, the design can be refined by taking actual dimensions for them.
4. This design process can be repeated at different stations along the wing semi-span to design a complete preliminary wing-box.

REFERENCES

[1]. Niu, M., "*Airframe structural design*", Conmilit Press Ltd., 1993.

[2]. Niu, M., "*Airframe stress analysis and sizing*", Conmilit Press Ltd., 1997.

[3]. Bruhn, E. F., "*Analysis and design of flight vehicle structures*", Jacobs & Associates Inc., June 1973.

[4]. Megson, T. H., "*Aircraft structures for engineering students*", John Wiley & Sons, Inc., 1999.

[5]. Sun, C. T., "*Mechanics of aircraft structures*", John Wiley & Sons, Inc., 1998.

[6]. Peery, D. J., and Azar, J. J., "*Aircraft structures*", McGraw Hill, 1982.

[7]. Schuhmacher, G., Murra, I. and Wang, L., "*Multidisciplinary design optimization of a regional aircraft wing box*", Copyright with Fairchild Dornier, Germany, Published with permission by AIAA.

[8]. Falco, S. A. and De Faria, A. R., "*Optimization of a simple aircraft wing*", A Technical Report presented in association with FAPESP, Brazil.

[9]. Piperni, P., Abdo, M. and Kafyeke, F., "*The application of multi-disciplinary optimization technologies to the design of a business jet*", 10th AIAA/ISSMO Multi-Disciplinary Analysis and Optimization Conference, New York, August 2004.

[10]. Abdo, M., Piperni, P., Isikveren, A. T. and Kafyeke, F., "*Optimization of business jet*", CASI & Canadian Aeronautics Annual General Meeting, Aircraft Design & Development Symposium, 2005

[11]. Niles, A. S., "*Tests of flat panels with four types of stiffeners*", NACA Report No.882, February 1943.

[12]. Rossman, C. A., Bartone, L. M. and Dobrowski, C. V., "*Compressive strength of flat panels with Z-section stiffeners*", NACA Report No.4B03, February 1944.

[13]. Butler, R. and Williams, W., "*Optimum design using VICONOPT, a buckling and strength constraint program for prismatic assemblies of anisotropic plates*", Journal of Computers & Structures, vol.43, no.4, pp.699-708, 1992.

[14]. Butler, R., Tyler, A. and Cao, W., "*Optimum design and evaluation of stiffened panels with practical loading*", Journal of Computers & Structures, vol.52, no.6, pp.1107-1118, 1994.

[15]. Bushnell, D., "*Minimum weight design of a stiffened panel VIA PANDA1 and evaluation of the optimized panel VIA STAGS*", Journal of Computers & Structures, vol.50, no.4, pp.569-602, 1994.

[16]. Butler, R., "*Optimum design of composite stiffened wing panels - a parametric study*", Aeronautical Journal, paper no.2012, May 1995.

[17]. Butler, R., "*Sequential use of conceptual MDO and panel sizing methods for aircraft wing design*", The Aeronautical Journal, paper no.2422, August 1999.

[18]. Veen, S. V., "*Optimizing new aluminum alloys for aerospace through computer simulations*" Copyright with Pechiney Aerospace, Published with permission by AIAA, no.1851, 2003.

[19]. Veen, S. V., "*Monolithic airframe structure: materials and methods for reduced cost, reduced weight and improved damage tolerance*", Copyright with Pechiney Aerospace, Published with permission by AIAA, no.1457, 2003.

[20]. Abdo, M., Piperni, P. and Kafyeke, F., "*Conceptual design of stringer stiffened compression panels*", CASI Institute 50th AGM and Conference 16th Aerospace Structures and Materials Symposium, Montreal, April 2003.

[21]. Chintapalli, S., Sedaghati, R., Li, J. and Abdo, M., "*Minimum mass design of stringer-stiffened compression panels under compressive axial load*", 6th WCSMO, Rio de Janeiro, May 2005.

[22]. Gill, P. E., "*Practical optimization*", Academic Press, 1981.

[23]. Young, W. C., "*Roark's formulae for stress & strain*", McGraw Hill, 1989.

[24]. Broek, D., "*Elementary engineering fracture mechanics*", Kluwer Academic Publications, 1986.

[25]. Salgado, N. K., "*Boundary element methods for damage tolerance design of aircraft structures*", Computational Mechanics Publications, 1998.

[26]. Brebbia, C. A. and Dominguez, J., "*Boundary elements: An introduction course*", McGraw Hill, 1992.

[27]. Ameen, M., "*Boundary element analysis, Theory and programming*", CRC Press, 2001.

[28]. Cruse, T. A., "*Boundary element analysis in computational fracture mechanics*", Kluwer Academic Publications, 1988.

[29]. Dowrick, G., Cartwright, D. J. and Rooke, D. P., "*The effect of repair patches on the stress distribution in a cracked sheet*", Proceedings of the 2nd International Conference on Numerical Methods in Fracture Mechanics, pp.763-775, 1980.

[30]. Dowrick, G., "*Stress intensity factors for cracks in patched and orthogonally stiffened sheets*", Ph.D Thesis, Southampton University, 1987.

[31]. Young, A., Cartwright, D. J. and Rooke, D. P., "*The boundary element method for analyzing repair patches on cracked finite sheets*", Aeronautical Journal, December 1988.

[32]. Young, A., "*Analysis of bonded repair patches on cracked thin sheets*", Ph.D Thesis, Southampton University, 1988

[33]. Dowrick, G., Cartwright, D. J. and Rooke, D. P., "*Boundary effects for a reinforced cracked sheet using the boundary element method*", Journal of Theoretical and Applied Fracture Mechanics, vol.12, pp.251-260, 1990.

[34]. Utukuri, M. and Cartwright, D. J., "*Stress intensity factors for a crack near finite boundaries in multiply stiffened sheets*", Journal of Theoretical and Applied Fracture Mechanics, vol.15, pp.257-266, 1991.

[35]. Young, A., Rooke, D. P. and Cartwright, D. J., "A*nalysis of patched and stiffened cracked panels using the boundary element method*", International Journal of Solids and Structures, vol.29, no.17, pp.2201-2216, 1992.

[36]. Erdogan, F., "*On the stress distribution in plates with collinear cuts under arbitrary loads*", Proceedings of the 4th U.S National Congress on Applied Mathematics, pp. 547-53, 1962.

[37]. Salgado, N. K. and Aliabadi, M. H., "*The boundary element analysis of cracked stiffened sheets, reinforced by adhesively bonded patches*", International Journal of Numerical Methods in Engineering, vol.42, pp.195-217, 1998.

[38]. Dirgantara, T. and Aliabadi, M. H., "*Crack growth analysis of plates loaded by bending and tension using dual boundary element method*", International Journal of Fracture, vol.105, pp.27-47, 2000.

[39]. Rooke, D. P. and Cartwright, D. J., "*Compendium of stress intensity factors*", 1976.

[40]. Stroud, A. H., "*Gaussian quadrature formulas*", Prentice Hall, 1966.

[41]. "*http://aaac.larc.nasa.gov/tsab/cfdlarc/aiaa-dpw*", 3rd AIAA CFD Drag Prediction Workshop, San Francisco, 2006.

[42]. "*http://www.grc.nasa.gov/WWW/K-12/airplane/short.html*"

[43]. Anderson, J. D., "*Fundamentals of aerodynamics*", McGraw Hill, 2000.

[44]. MATLAB User Guide, Version 7.0, 2004

[45]. MSC.PATRAN User Guide, Version 2005R2, 2005

APPENDIX

The fundamental equations for an isotropic material of Poisson's ratio ν and tensile modulus E_{sk} are given below. [$k = 3-\nu/1+\nu$ and Shear Modulus $G_{sk} = E/2(1+\nu)$]

The complex variables of field point and source point corresponding to the points x and x_0, respectively are represented as,

$$z = x_1 + ix_2,\ z_0 = x_{01} + ix_{02} \tag{A1}$$

where $i^2 = -1$. The complex parameter $S_j\ (j = 1,2)$ is defined by

$$S_j = \frac{1}{2\pi(1+k)}(\delta_{1j} + i\delta_{2j}) \tag{A2}$$

represents the vector force $(j = 1,2)$ per unit thickness in the fundamental solutions. A superimposed bar will be used to denote the complex conjugation ($\bar{z} = x_1 - ix_2$).

The functions U_{ji} and Y_{ji} are of the form,

$$U_{j1} + iU_{j2} = \frac{1}{2G_{sk}} D_j(z,\bar{z};z_0,\overline{z_0})$$

$$Y_{j1} + iY_{j2} = -i\left\{(1+k)\Omega_j(z;z_0,\overline{z_0}) - D_j(z,\bar{z};z_0,\overline{z_0})\right\} \tag{A3}$$

The Kelvin fundamental solutions are given by,

$$\Omega_j^{\infty}(z;z_0) = -S_j \log(z - z_0)$$

$$D_j^{\infty}(z,\bar{z};z_0,\overline{z_0}) = -kS_j \log|z - z_0|^2 + \overline{S_j}\left(\frac{z - z_0}{\bar{z} - \overline{z_0}}\right) \tag{A4}$$

The fundamental solution for a crack situated at $\{-a \le x_1 \le +a, x_2 = 0\}$ involves terms Ω_j and D_j given by,

$$\Omega_j(z;z_0,\overline{z_0}) = \Omega_j^{\infty}(z,z_0) + \Omega_j^{c}(z;z_0,\overline{z_0}) \tag{A5}$$

$$D_j(z,\bar{z};z_0,\overline{z_0}) = D_j^{\infty}(z,\bar{z};z_0,\overline{z_0}) + k\,\Omega_j^{c}(z;z_0,\overline{z_0}) - \Omega_j^{c}(\bar{z};z_0,\overline{z_0}) - (z-\bar{z})\overline{\Omega_j^{c'}(z;z_0,\overline{z_0})}$$

where,

$$\Omega_j^{c}(\bar{z};z_0,\overline{z_0}) = -\frac{1}{2}S_j\left[kN_1(z,\overline{z_0}) - N_1(z,z_0)\right] - \frac{1}{2}\overline{S_j}(\overline{z_0} - z_0)N_2(z,\overline{z_0})$$

$$\overline{\Omega_j^{c'}(z;z_0,\overline{z_0})} = \frac{\partial}{\partial z}\Omega_j(z;z_0,\overline{z_0})$$

$$= -\frac{1}{2}(z^2-a^2)^{-1/2}\left\{-\frac{1}{2}S_j\left[kM_1(z,\overline{z_0})-M_1(z,z_0)\right]+\overline{S_j}(\overline{z_0}-z_0)M_2(z,\overline{z_0})\right\} \tag{A6}$$

$$N_1(z,z_0) = \log\left[\frac{2(zz_0-a^2+(z^2-a^2)^{1/2}(z_0^2-a^2)^{1/2}}{(z+(z^2-a^2)^{1/2})(z_0+(z_0^2-a^2)^{1/2})}\right]$$

$$N_2(z,z_0) = (z_0^2-a^2)^{-1/2}M_1(z,z_0)$$

$$M_1(z,z_0) = \frac{(z^2-a^2)^{1/2}-(z_0^2-a^2)^{1/2}}{z-z_0}-1$$

$$M_2(z,z_0) = \left[M_1(z,z_0)+1-z_0(z_0^2-a^2)^{-1/2}\right]/(z-z_0) \tag{A7}$$

The functions G_{kji} and Z_{kji} are of the form,

$$G_{1j1}+iG_{1j2} = \frac{1}{2G_{sk}}\left(\frac{\partial}{\partial z_0}+\frac{\partial}{\partial \overline{z_0}}\right)D_j(z,\bar{z};z_0,\overline{z_0})$$

$$G_{2j1}+iG_{2j2} = \frac{i}{2G_{sk}}\left(\frac{\partial}{\partial z_0}-\frac{\partial}{\partial \overline{z_0}}\right)D_j(z,\bar{z};z_0,\overline{z_0})$$

$$Z_{1j1}+iZ_{1j2} = i\left\{(1+k)\left(\frac{\partial}{\partial z_0}+\frac{\partial}{\partial \overline{z_0}}\right)\Omega_j(z;z_0,\overline{z_0})-2G\left[G_{1j1}+iG_{1j2}\right]\right\}$$

$$Z_{2j1}+iZ_{2j2} = i\left\{(1+k)i\left(\frac{\partial}{\partial z_0}-\frac{\partial}{\partial \overline{z_0}}\right)\Omega_j(z;z_0,\overline{z_0})-2G\left[G_{1j1}+iG_{1j2}\right]\right\} \tag{A8}$$

and the derivatives of the two fundamental solutions (A4) and (A5) are given by

$$\frac{\partial D_j^{\infty}}{\partial z_0} = \frac{kS_j}{z-z_0}-\frac{\overline{S_j}}{\bar{z}-\overline{z_0}};\ \frac{\partial D_j^{\infty}}{\partial \overline{z_0}} = \frac{kS_j}{\bar{z}-\overline{z_0}}+\frac{\overline{S_j}(z-z_0)}{(\bar{z}-\overline{z_0})^2};\ \frac{\partial \Omega_j^{\infty}}{\partial z_0} = \frac{S_j}{z-z_0};\ \frac{\partial \Omega_j^{\infty}}{\partial \overline{z_0}} = 0$$

$$\frac{\partial D_j}{\partial z_0} = k\psi_1(z;z_0,\overline{z_0})-\psi_1(\bar{z};z_0,\overline{z_0})-(z-\bar{z})\overline{\psi_2(z;z_0,\overline{z_0})}$$

$$\frac{\partial D_j}{\partial \overline{z_0}} = k\psi_3(z;z_0,\overline{z_0})-\psi_3(\bar{z};z_0,\overline{z_0})-(z-\bar{z})\overline{\psi_4(z;z_0,\overline{z_0})}$$

$$\frac{\partial \Omega_j}{\partial z_0} = \psi_1(z;z_0,\overline{z_0});\ \frac{\partial \Omega_j}{\partial \overline{z_0}} = \psi_3(z;z_0,\overline{z_0}) \tag{A9}$$

where,

$$\psi_1(z;z_0,\overline{z_0}) = -\frac{1}{2}\left\{S_j Q_1(z,z_0) + \overline{S_j} N_2(z,\overline{z_0})\right\}$$

$$\psi_2(z;z_0,\overline{z_0}) = \frac{1}{2}(z^2-a^2)^{-1/2}\left\{S_j M_2(z,z_0) + \overline{S_j} M_2(z,\overline{z_0})\right\}$$

$$\psi_3(z;z_0,\overline{z_0}) = -\frac{1}{2}\left\{kS_j Q_1(z,\overline{z_0}) + \overline{S_j}\left[N_2(z,\overline{z_0}) + (\overline{z_0}-z_0)Q_2(z,\overline{z_0})\right]\right\}$$

$$\psi_4(z;z_0,\overline{z_0}) = -\frac{1}{2}(z^2-a^2)^{-1/2}\left\{kS_j M_2(z,\overline{z_0}) + \overline{S_j}\left[M_2(z,\overline{z_0}) + (\overline{z_0}-z_0)P_2(z,\overline{z_0})\right]\right\} \tag{A10}$$

$$P_2(z,z_0) = \left[2M_2(z,z_0) + a^2(z_0^2-a^2)^{-3/2}\right]/(z-z_0)$$

$$Q_1(z,z_0) = (z_0^2-a^2)^{-1/2} M_1(z,z_0) \qquad \text{(A11)}$$

$$Q_1(z,z_0) = \left\{M_2(z,z_0) - z_0(z_0^2-a^2)^{-1}[M_1(z,z_0)+1]\right\}/(z_0^2-a^2)^{1/2}$$

The kernels $G^*_{kji}(x,\pm a)$ and $Z^*_{kji}(x,\pm a)$ required to calculate the stress intensity factors in Eq. (3-57) are related to four functions $\psi^*_n(z,\pm a)$ $(n=1,2,3,4)$ in the same way that the stress kernels G_{kji} and Z_{kji} involve the four functions $\psi_n(z;z_0,\overline{z_0})$ $(n=1,2,3,4)$ in Eq (A9). The terms ψ^*_n are of the form,

$$\psi^*_1(z,\pm a) = -\frac{1}{2}\left(\frac{\pi}{a}\right)^{1/2}(S_j+\overline{S_j})\psi(z,\pm a)$$

$$\psi^*_2(z,\pm a) = -\frac{1}{2}\left(\frac{\pi}{a}\right)^{1/2}(S_j+\overline{S_j})\psi'(z,\pm a)$$

$$\psi^*_3(z,\pm a) = \frac{1}{2}\left(\frac{\pi}{a}\right)^{1/2}(k\overline{S_j}+S_j)\psi(z,\pm a)$$

$$\psi^*_3(z,\pm a) = \frac{1}{2}\left(\frac{\pi}{a}\right)^{1/2}(k\overline{S_j}+S_j)\psi'(z,\pm a) \tag{A12}$$

where,

$$\psi(z,\pm a) = \left(\frac{z\pm a}{z\mp a}\right)^{1/2} - 1 \qquad \psi'(z,\pm a) = \frac{\mp a}{(z\mp a)(z^2-a^2)^{1/2}} \tag{A13}$$